NASA TN D-915

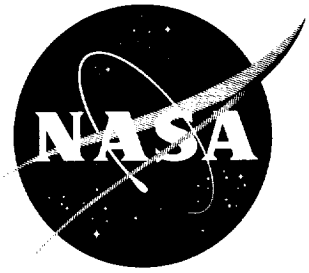

TECHNICAL NOTE

D-915

INVESTIGATION OF INTERFERENCE OF A DEFLECTED JET WITH FREE STREAM AND GROUND ON AERODYNAMIC CHARACTERISTICS OF A SEMISPAN DELTA-WING VTOL MODEL

By Kenneth P. Spreemann

Langley Research Center
Langley Field, Va.

NATIONAL AERONAUTICS AND SPACE ADMINISTRATION

WASHINGTON August 1961

NATIONAL AERONAUTICS AND SPACE ADMINISTRATION

TECHNICAL NOTE D-915

INVESTIGATION OF INTERFERENCE OF A DEFLECTED JET WITH FREE STREAM AND GROUND ON AERODYNAMIC CHARACTERISTICS OF A SEMISPAN DELTA-WING VTOL MODEL

By Kenneth P. Spreemann

SUMMARY

An investigation of the mutual interference effects of the ground, wing, deflected jet stream, and free stream of a semispan delta-wing VTOL model at zero and low forward speeds has been conducted in the 17-foot test section of the Langley 300-MPH 7- by 10-foot tunnel. The model consisted of two interchangeable semispan clipped delta wings, a simplified fuselage, and a high-pressure jet for simulation of a jet exhaust. Attached to the wing behind the jet were various sets of vanes for deflecting the jet stream to different turning angles.

The effect of ground proximity gave the normally expected losses in lift at zero and very low forward speeds (up to about 60 or 80 knots for the assumed wing loading of 100 lb/sq ft); at higher forward speeds ground effects were favorable.

At low forward speeds, out of ground effect, the model encountered large losses in lift and large nose-up pitching moments with the model at low angles of attack and the jet deflected 90° or 75° (the angles required for VTOL performance and very low forward speeds). Rotating the model to higher angles of attack and deflecting the jet back to lower angles eliminated these losses in lift. Moving the jet rearward with respect to the wing reduced the losses in lift and the nose-up moments at all speeds within the range of this investigation.

INTRODUCTION

Much interest has been shown in VTOL aircraft which use the vertically directed thrust for take-off and landing. A few recent investigations have described and given some characteristics of configurations

that could be used for this purpose (refs. 1, 2, and 3). Some of these investigations reported on proposals that have in common the object of keeping the fuselage horizontal while taking off or landing and accelerating up to full forward flight speed. One method of achieving horizontal-attitude VTOL performance would be a nozzle or series of vanes to deflect the jet stream downward for take-off and landing and subsequently program the jet rearward for forward flight up to speeds where the wing aerodynamic lift would support the aircraft.

One serious problem is the jet-induced down load within ground effect, as has been shown for example in references 3 and 4. Also reference 5 indicates that the interference effects at low forward speeds away from the ground can be important. The present investigation was undertaken to investigate this problem in more detail.

L
1
4
6
6

SYMBOLS

The positive senses of forces, moments, and angles are indicated in figure 1(a) for the static tests and in figure 1(b) for the wind-tunnel tests.

A	aspect ratio, $\frac{b^2}{S}$
b	wing span, ft
c	local wing chord, ft
$\bar{c}$	mean aerodynamic chord, $\frac{2}{S}\int_0^{b/2} c^2 dy$, ft
C_D	drag coefficient, $\frac{\text{Drag}}{qS}$
C_L	lift coefficient, $\frac{\text{Lift}}{qS}$
C_m	pitching-moment coefficient, $\frac{\text{Pitching moment}}{qS\bar{c}}$
C_T	thrust coefficient, $\frac{F}{qS}$
F	resultant force from static tests outside of ground effect, lb

F_h	resultant force from static tests within ground effect, lb
F_X	longitudinal force from tunnel tests, Thrust - Drag, lb
F'_X	longitudinal force from static tests, lb
ΔF_X	increment in longitudinal force due to interference, lb
g	acceleration due to gravity, ft/sec^2
h	height of moment reference center above ground board, ft
L	lift from tunnel tests, lb
L'	lift from static tests, lb
ΔL	increment in lift due to interference, lb
M	pitching moment from tunnel tests, ft-lb
M'	pitching moment from static tests outside of ground effect, ft-lb
M'_h	pitching moment from static tests within ground effect, ft-lb
ΔM	increment in pitching moment due to interference, ft-lb
p_j	pressure in jet, lb/sq in.
p_o	atmospheric pressure, lb/sq in.
q	free-stream dynamic pressure, $\frac{1}{2}\rho V_\infty^2$, lb/sq ft
R	gas constant, 53.34, $\frac{\text{ft-lb}}{\text{lb}}/^oR$
S	wing area, sq ft
t	nozzle exit stagnation temperature, ^oR
T	measured thrust from nozzle without vanes, lb

T_{req} thrust required for steady level flight, lb

V airspeed, knots

V_j jet-exit velocity (assuming isentropic expansion from plenum chamber to free-stream static pressure), $\sqrt{\frac{2\gamma}{(\gamma-1)} Rtg \left[1 - \left(\frac{p_o}{p_j}\right)^{\frac{\gamma-1}{\gamma}}\right]}$, ft/sec

V_∞ free-stream velocity, ft/sec

W weight of assumed airplane, lb

y spanwise distance, ft

z distance of center line of thrust below moment reference center, ft

α angle of attack, deg

γ ratio of specific heat for air, 1.4

δ vane angle with respect to wing chord plane, deg

θ static turning angle (inclination of resultant force vector measured from longitudinal-force axis), $\tan^{-1} \frac{L'}{F'_X}$, deg

ρ mass density of air in free stream, slugs/cu ft

MODEL AND APPARATUS

Drawings of the two models with pertinent dimensions are presented in figure 2. Figure 2(a) is a drawing of the A = 3.00 model showing a typical vane location. A drawing of the A = 1.55 model with outboard body and horizontal tail is given in figure 2(b). Figure 3 shows

the geometry of the different sets of turning vanes employed. The geometric characteristics of the two models are as follows:

	A = 3.00 model	A = 1.55 model
Wing area (semispan), sq ft	1.102	0.906
Wing semispan, ft	1.286	0.836
Wing mean aerodynamic chord, ft	1.018	1.136
Wing taper ratio	0.143	0.443
Horizontal-tail area, sq ft		0.197

The reflection-plane VTOL models consisted of a simplified fuselage, a subsonic blowing nozzle, and various sets of turning vanes. These components were used interchangeably with both wings. The wings were simple planforms made from 1/2-in.-thick plate with the leading edges rounded and the trailing edges beveled as shown in figure 2. The A = 1.55 wing was made from a basic planform similar to the A = 3.00 wing by cutting off the wing tip section and mounting this section aft on a tip body to form an outboard-tail arrangement. (See fig. 2(b).)

In order to investigate the effects of changing the longitudinal location of the deflected jet with respect to the wing, the model was constructed so that the wing could be attached at several longitudinal positions with respect to the fuselage and vane assembly. As the wing was moved forward or rearward, the moment reference point was maintained at the same location relative to the fuselage and vane assembly.

The air to simulate the jet-engine exhaust was supplied to the plenum chamber through two flexible hoses connected to a tee so as to minimize pressure interference effects on the forces and moments of the model. The mass flow through the nozzle was measured by means of a standard sharp-edge orifice flowmeter. The jet-exit total pressure and velocity were measured by means of a pitot-static tube in the jet exit.

The ground was represented by a large sheet of plywood as shown in figure 1. The model lift, longitudinal force, and pitching moments were measured by a strain-gage balance. In the tunnel the model balance was mounted beneath the tunnel floor.

TESTS AND CORRECTIONS

The static tests were conducted in a large room in the Langley 7- by 10-Foot Tunnels Branch. The tunnel tests were conducted in the 17-foot test section of the 300-MPH 7- by 10-foot tunnel. The arrangement and calibration of this section are given in the appendix of

reference 6. The model thrust coefficient in the tunnel was varied by changing the jet-exit dynamic pressure or the free-stream dynamic pressure. The test Reynolds number, based on the wing mean aerodynamic chord and tunnel dynamic pressure, varied from 0.13×10^6 to 0.50×10^6.

Since the size of the models with respect to the tunnel size was very small, tunnel corrections to the data were estimated and found to be negligible and therefore were not applied to the data.

PRESENTATION OF RESULTS

The results of the investigation are presented in the following figures:

	Figure
Static data:	
Effect of vane angle	4
Effect of ground and pressure ratio	5
Effect of ground, vane angle, and center-of-gravity (c.g.) location	6, 7
Forward-speed data:	
Power-off characteristics	8
Power-on:	
Effect of thrust coefficient and turning angle -	
A = 3.00	9
A = 1.55	10
Effect of c.g. location -	
A = 3.00	11, 12
Effect of ground -	
A = 3.00	13, 14
A = 1.55	15, 16
Summary data	17 to 23

The basic data for the summary figures (figs. 17 to 23) were obtained from figures 9 to 16 and calculated for an assumed airplane wing loading of 100 lb/sq ft.

DISCUSSION

Static Data

In figure 4, which is basically a calibration of the vanes, it is seen that large losses in resultant force occurred with increases in vane angle. Most of these losses can be attributed to the poor aerodynamic shape of the vanes. Because of these losses all subsequent basic data have been based on the static resultant force from the flow out of the particular vane configuration under consideration. The large nose-up moments at the low turning angles are due to the resultant force not passing through the moment reference center of the model.

Figures 5 and 6 show the expected loss in resultant force as the model is brought close to the ground. The data at high deflection angles ($\theta = 90^\circ$ and 75°) show a tendency for recovery in resultant forces very near the ground. These same effects were experienced on another configuration which has been fully reported in reference 7.

From figure 7 it is seen that chordwise location of the turning vanes had little effect on the static thrust recovery or the pitching moments. Also, the jet pressure ratio had relatively small effects on the resultant force, turning angle, and pitching moment. (See figs. 4 and 5.)

Forward-Speed Data

Out of ground effect.- The basic power-off longitudinal coefficients of the two models tested out of ground effect are presented in figure 8. The basic power-on data presented in figures 9 to 16 are nondimensionalized by dividing by the resultant force F of the air exhausted from the vanes.

The data presented are the results as measured on the model and, inasmuch as the intake flow was not simulated, these data do not include the intake momentum drag. This drag is the exit mass flow multiplied by the free-stream velocity $\left(F_{X,\text{intake}} = mV_\infty\right)$. Since the thrust (turning losses removed) is the same mass flow multiplied by the jet velocity, the intake momentum drag is the thrust (resultant force) multiplied by the ratio of free-stream velocity to jet velocity; that is, $F_{X,\text{intake}} = F\frac{V_\infty}{V_j}$. The x-marks on the curves of figures 9 to 16 indicate the shift of the position of thrust-drag balance due to the intake momentum drag $\left(F_X/F = 0, \text{ which indicates steady level flight}\right)$.

For the static or hovering condition, the lift is equal to the thrust at zero angle of attack (L/T = 1.0 in fig. 9(a) for example). At forward speeds $\left(V_\infty/V_j > 0\right)$, however, the ratio of lift to resultant force (L/F) at zero angle of attack is less than 1.0 indicating an induced loss in lift. The losses in lift are even greater for the condition of thrust-drag equilibrium (as indicated by the x-marks on the curves of fig. 9(a)) because of the negative angles of attack required. Increasing forward speed also produced large nose-up pitching moments at zero angle of attack.

These losses in lift result in the thrust required for steady-level-flight transition becoming greater than the airplane weight for low angles of attack as shown in figure 17. Figure 17 also shows that by going to higher angles of attack (and deflecting the jet exhaust rearward to balance the thrust and drag), these losses in lift can be compensated for with wing lift.

Losses in lift and large nose-up pitching moments, at zero angle of attack, were also observed at low forward speeds on two buried-fan configurations. (See ref. 8.) Some explanation of the flow phenomena involved in these results has been obtained on a flat plate with a jet issuing vertically beneath it at low forward speeds. The pressure data obtained indicated large interference effects between the exiting jet and the free-stream flow which induce pressures on the lower surface of the plate. Positive pressures were generated in front of the jet and negative pressures behind the jet; however, the negative pressures outweighed the positive pressures and thus caused a loss in lift. Also, the combination of positive pressures ahead of the jet and the negative pressures behind the jet gave nose-up pitching moments. Similar pressures were also observed on a delta-wing configuration of reference 9.

The increments of lift, longitudinal force, and pitching moment induced on the present model by the effects of the jet have been extracted from the data of figure 9 by means of the following equations:

$$L = F \sin(\theta + \alpha) + C_L qS + \Delta L$$

$$F_X = F \cos(\theta + \alpha) - C_D qS + \Delta F_X$$

$$M = Fz \cos \theta + C_m qS\bar{c} + \Delta M$$

The quantity on the left-hand side of the equal sign represents the total measured force or moment (fig. 22). The first quantity on the right-hand side of the equal sign is the direct thrust contribution, the second term is the aerodynamic force or moment as determined from the power-off data of figure 8 and is presented in figure 21, and the third term is the interference increment.

The increments of lift, longitudinal force, and pitching moment due to jet interference are presented in figure 23 by use of the following expressions which were derived from the basic equations previously given:

$$\frac{\Delta L}{F} = \frac{L}{F} - \left[\sin(\theta + \alpha) + \frac{C_L qS}{F}\right]$$

$$\frac{\Delta F_X}{F} = \frac{F_X}{F} - \left[\cos(\theta + \alpha) - \frac{C_D qS}{F}\right]$$

$$\frac{\Delta M}{F\bar{c}} = \frac{M}{F\bar{c}} - \left(\frac{z \cos \theta}{\bar{c}} + \frac{C_m qS\bar{c}}{F\bar{c}}\right)$$

The results indicate that interference for this model on the lift and pitching moment was dependent primarily on the ratio of the free-stream velocity to the jet velocity and was relatively independent of the angle of attack. Also the interference effects on lift and pitching moment were reduced with decreases in the jet deflection angle θ.

The interference effects on the longitudinal force were somewhat erratic in comparison with those on the lift and pitching moment. At zero angle of attack there was a tendency for the drag $(-F_X)$ to increase with increases in forward speed, whereas at higher angles of attack, 10° and 20° for example, the drag was reduced with forward speed, and above some speeds thrust was obtained. Since θ for all tests is the measured jet deflection angle for the zero-forward-speed condition, the deflection angles at forward speed may be different from those measured statically. Thus changes in deflection angle and/or suction pressures behind the jet may account for the erratic interference effects on the longitudinal force associated with changes in angle of attack and forward speed.

By removing a large part of the lifting area from around the jet, the losses in lift and nose-up moments could be reduced. This was approximated in the present investigation by moving the jet exhaust rearward with respect to the wing (figs. 11 and 12); thus the surface area behind the jet was greatly reduced. The summary of these results is given in figure 18. With a deflection angle of 90° there were no significant changes in T_{req}/W in the practical speed range (0 to 40 knots) but with a deflection angle of 75° sizeable reductions in T_{req}/W were noted at a center-of-gravity location of $0.76\bar{c}$. Such a center-of-gravity location, of course, would be impractical in an airplane because of the problem of obtaining adequate longitudinal stability

in cruising flight. However, these data illustrate the need for a wing-jet configuration which does not have large surface areas behind the jet (perhaps a sweptback trailing edge could be considered).

Within ground effect.- Figures 13 to 16 present aerodynamic data at zero and low forward speeds for the two configurations tested within ground effect. These results are summarized in figures 19 and 20. At zero and very low forward speeds the usual losses in lift were experienced; with higher forward speeds (above 60 to 80 knots) the ground effects on lift became favorable, the most favorable effects being indicated for intermediate heights. Also, in general, as the ground was approached there was a reduction in the nose-up pitching moments at low forward speeds.

L
1
4
6
6

CONCLUSIONS

An investigation of the mutual interference effects of the ground, wing, deflected jet stream, and free stream in the static condition and at low forward speeds on a simple delta-wing VTOL model indicated the following conclusions:

1. The effect of ground proximity gave the normally expected losses in lift at zero and very low forward speeds (up to about 60 or 80 knots for the assumed wing loading of 100 lb/sq ft); at higher forward speeds ground effects were favorable.

2. At low forward speeds, out of ground effect, the model encountered large losses in lift and large nose-up pitching moments with the model at low angles of attack and the jet deflected 90° or 75° (the angles required for VTOL performance and very low forward speeds). These losses in lift and nose-up moments can be attributed primarily to the interaction of the exiting jet and the free-stream flow which induce pressures on the bottom of the wing and fuselage.

3. Rotating the model to higher angles of attack and deflecting the jet back to lower angles eliminated losses in lift.

4. Moving the jet rearward with respect to the wing reduced the losses in lift and the large nose-up moments at all speeds within the range of this investigation.

Langley Research Center,
National Aeronautics and Space Administration,
Langley Field, Va., May 8, 1961.

REFERENCES

1. Campbell, John P.: Research on VTOL and STOL Aircraft in the United States. Advances in Aero. Sci., vol. 2, Pergamon Press (New York), 1959, pp. 845-892.

2. O'Malley, James A., Jr., and Landphair, Lee C.: The X-14 VTOL Airplane - A Design Tool. Preprint 95B, SAE National Aeronautic Meeting (Los Angeles, Calif.), Sept. 29 - Oct. 4, 1958.

3. Newsom, William A., Jr.: Effect of Ground Proximity on Aerodynamic Characteristics of Two Horizontal-Attitude Jet Vertical-Take-Off-and-Landing Airplane Models. NASA TN D-419, 1960. (Supersedes NACA RM L57G16.)

4. Spreemann, Kenneth P., and Sherman, Irving R.: Effects of Ground Proximity on the Thrust of a Simple Downward-Directed Jet Beneath a Flat Surface. NACA TN 4407, 1958.

5. Williams, John: Some British Research on the Basic Aerodynamics of Powered Lift Systems. Jour. R.A.S., July 1960, pp. 413-437.

6. Kuhn, Richard E., and Hayes, William C., Jr.: Wind-Tunnel Investigation of Longitudinal Aerodynamic Characteristics of Three Propeller-Driven VTOL Configurations in the Transition Speed Range, Including Effects of Ground Proximity. NASA TN D-55, 1960.

7. Davenport, Edwin E., and Spreemann, Kenneth P.: Thrust Characteristics of Multiple Lifting Jets in Ground Proximity. NASA TN D-513, 1960.

8. Spreemann, Kenneth P.: Induced Interference Effects on Jet and Buried-Fan VTOL Configurations in Transition. NASA TN D-731, 1961.

9. Melbourne, W. H.: Experiments on a Delta Wing With Jet-Assisted Lift. ARC 21,968, May 1960.

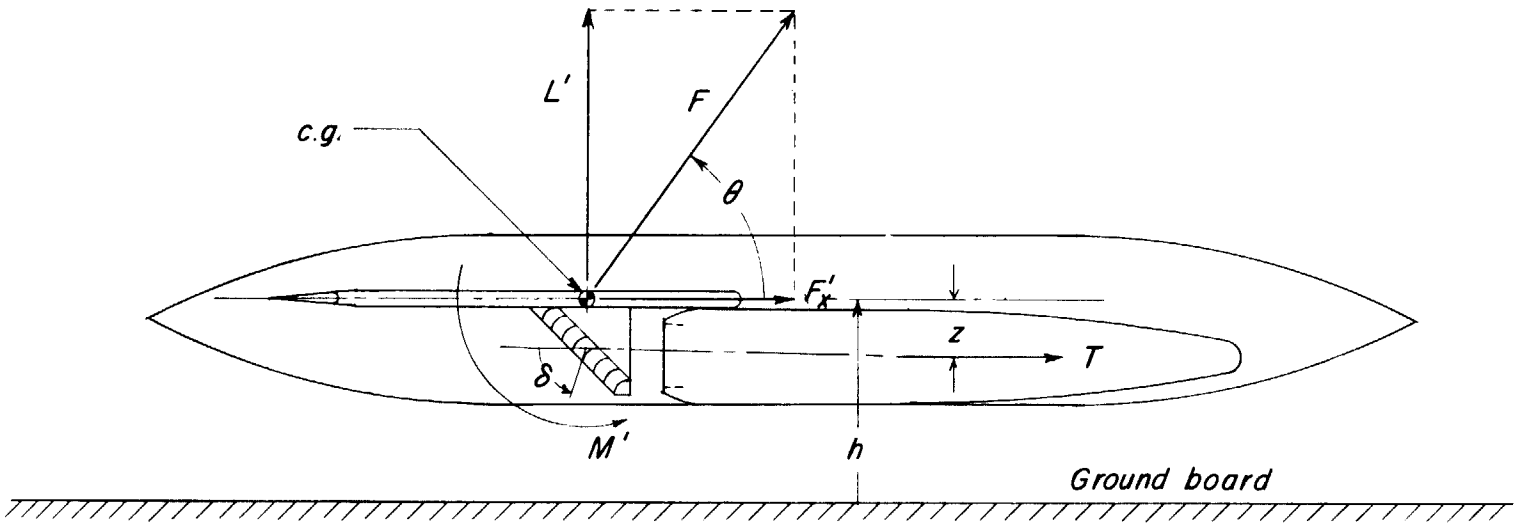

(a) Static tests.

Figure 1.- Conventions used to define positive senses of forces, moments, and angles.

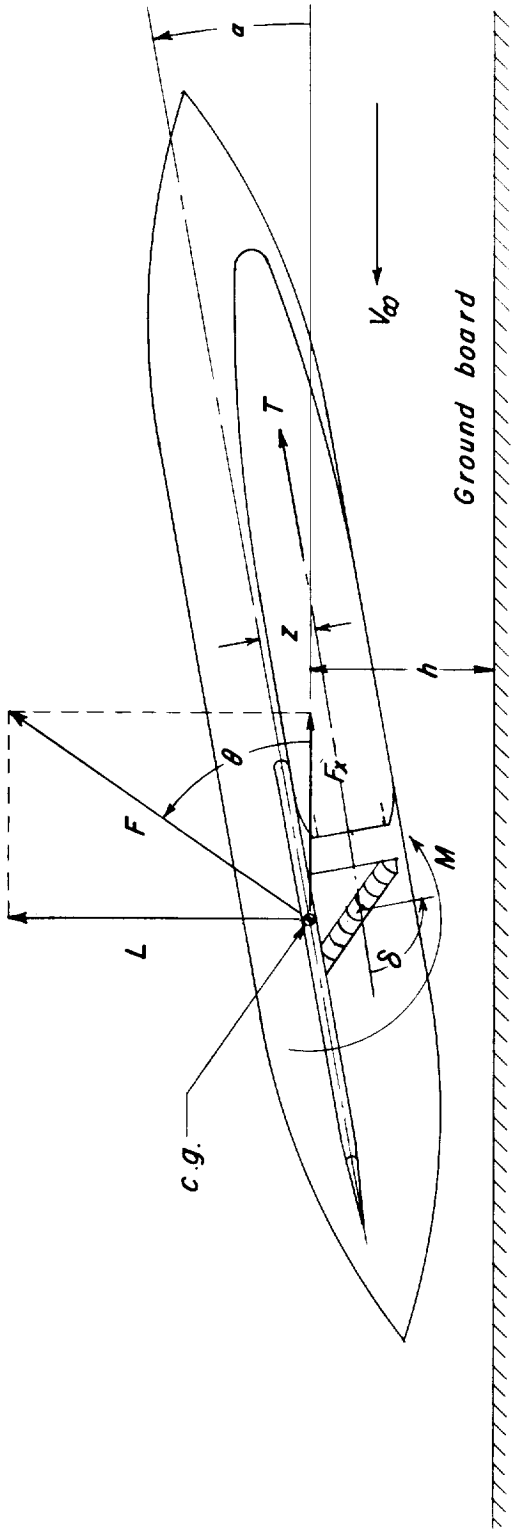

(b) Wind-tunnel tests.

Figure 1.- Concluded.

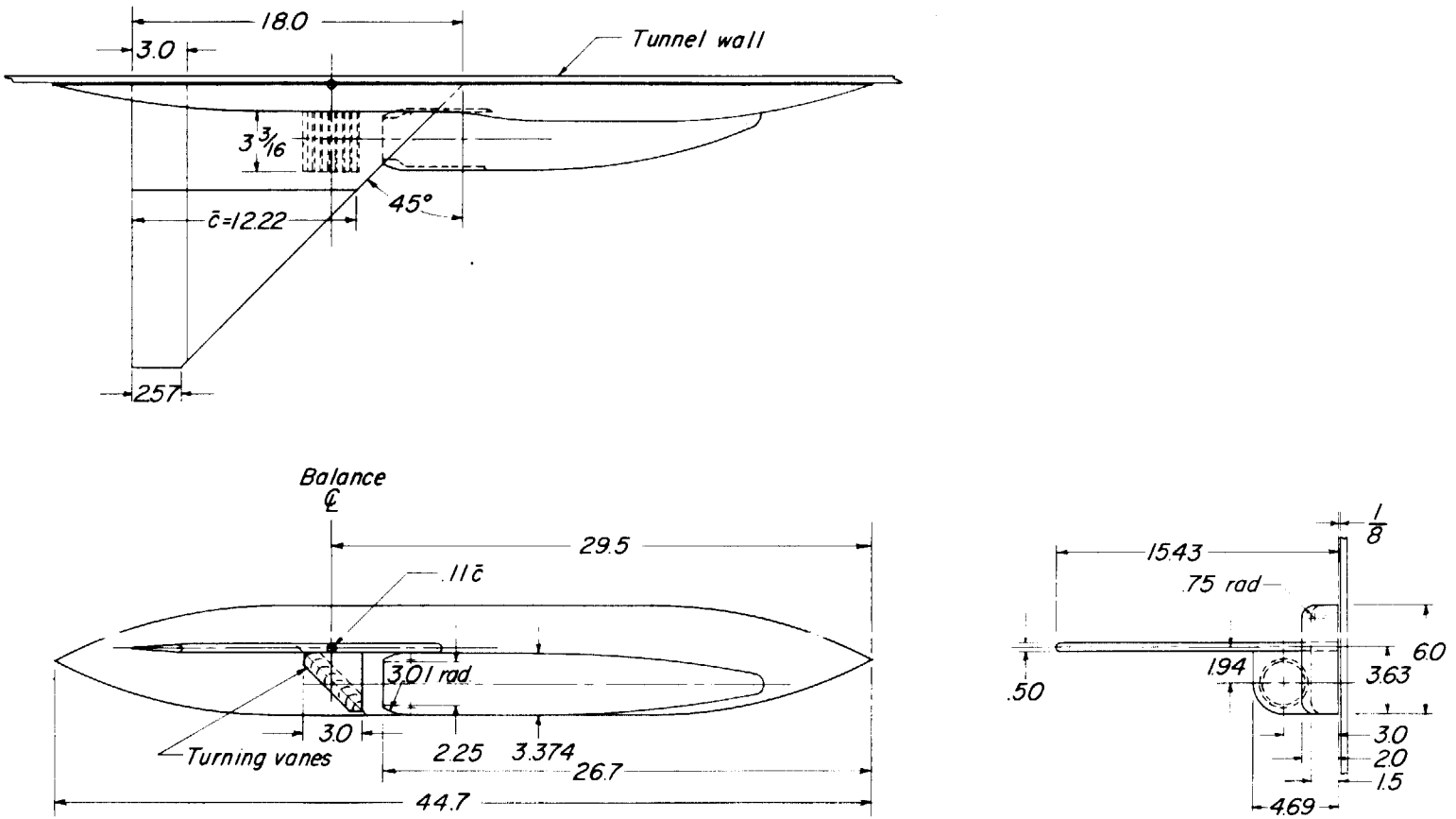

(a) A = 3.00 model showing location of turning vanes employed.

Figure 2.- Drawings of models. All dimensions in inches.

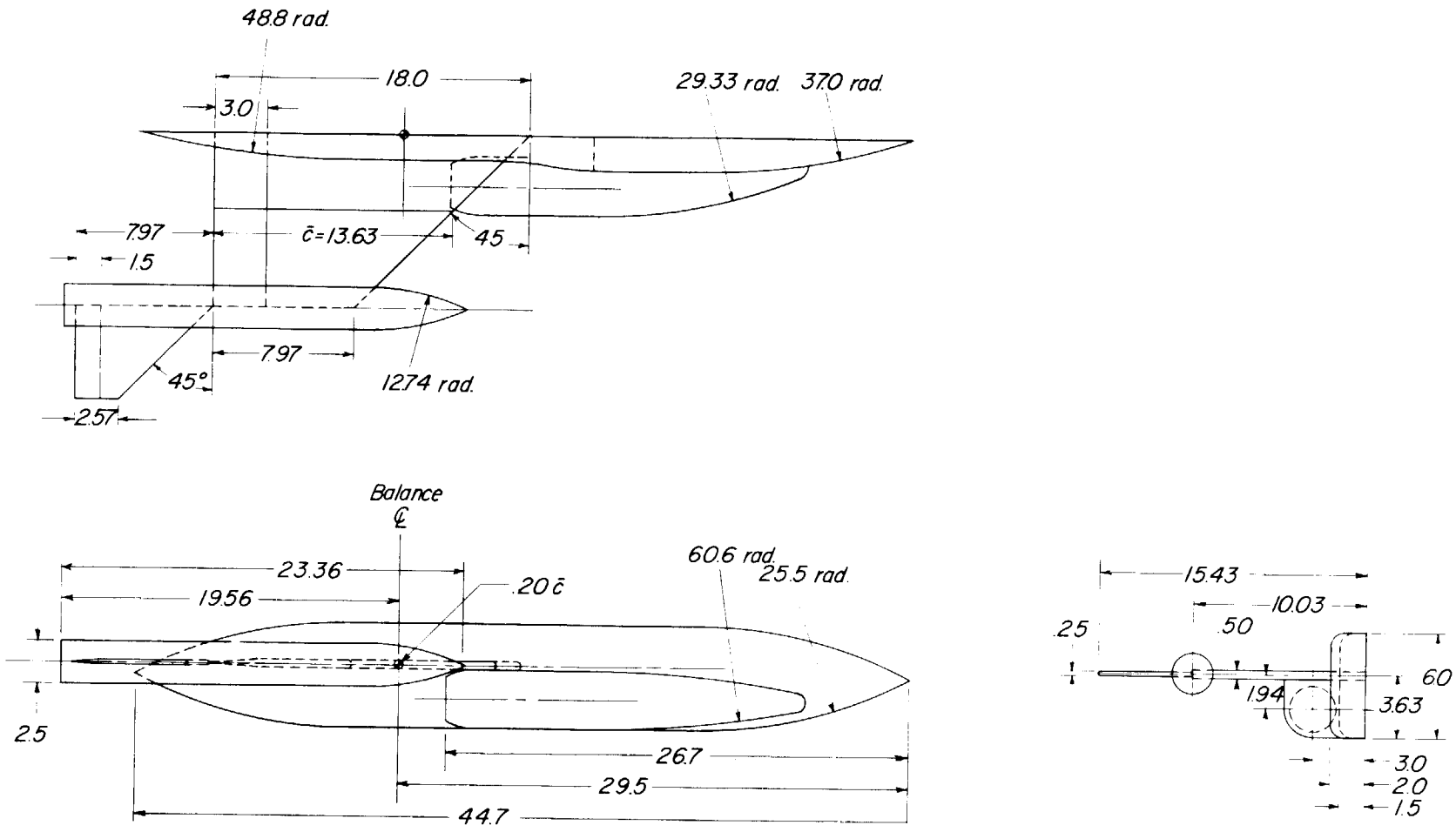

(b) A = 1.55 model with outboard body and tail.

Figure 2.- Concluded.

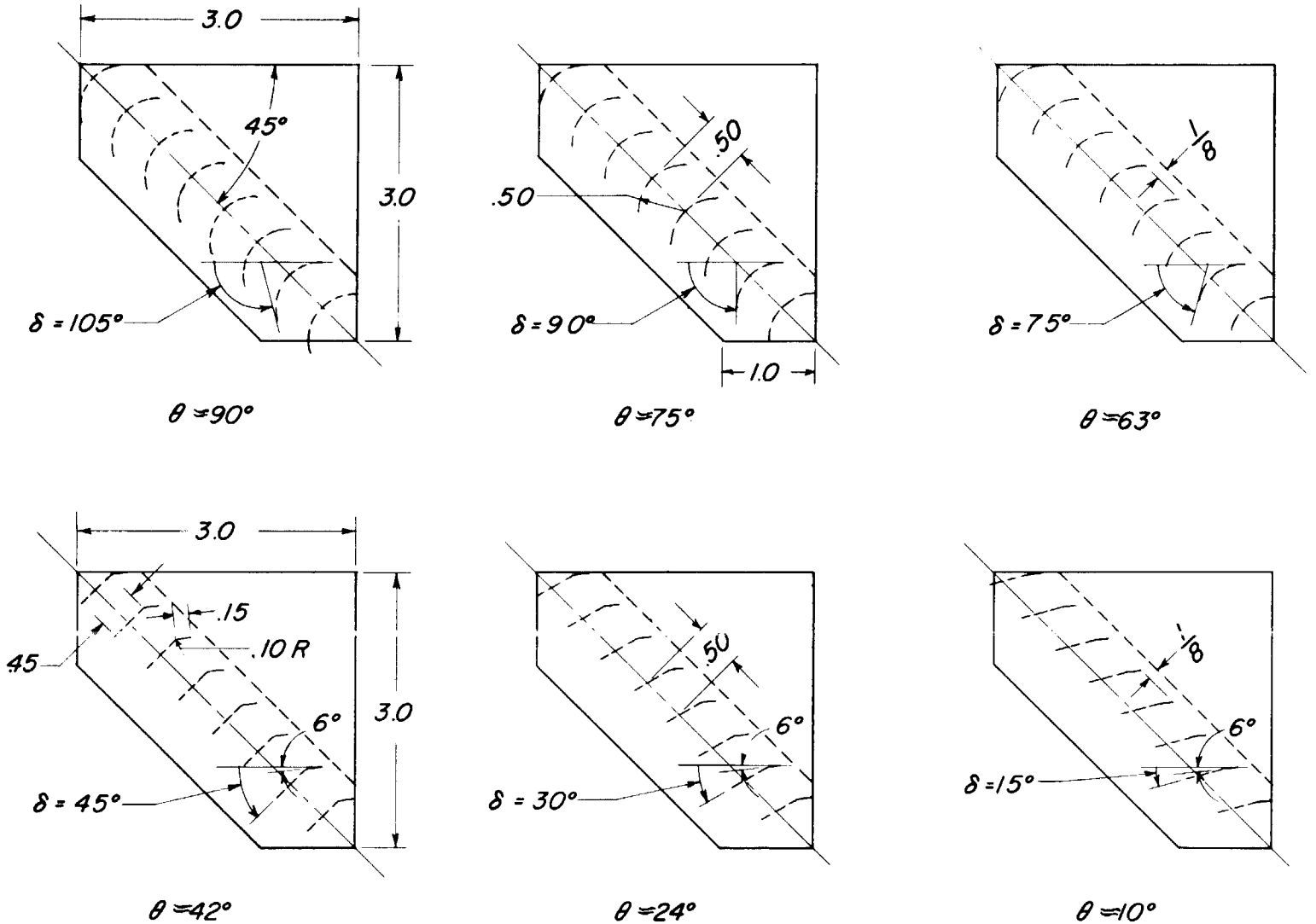

Figure 3.- Diagram of vanes employed. All dimensions in inches.

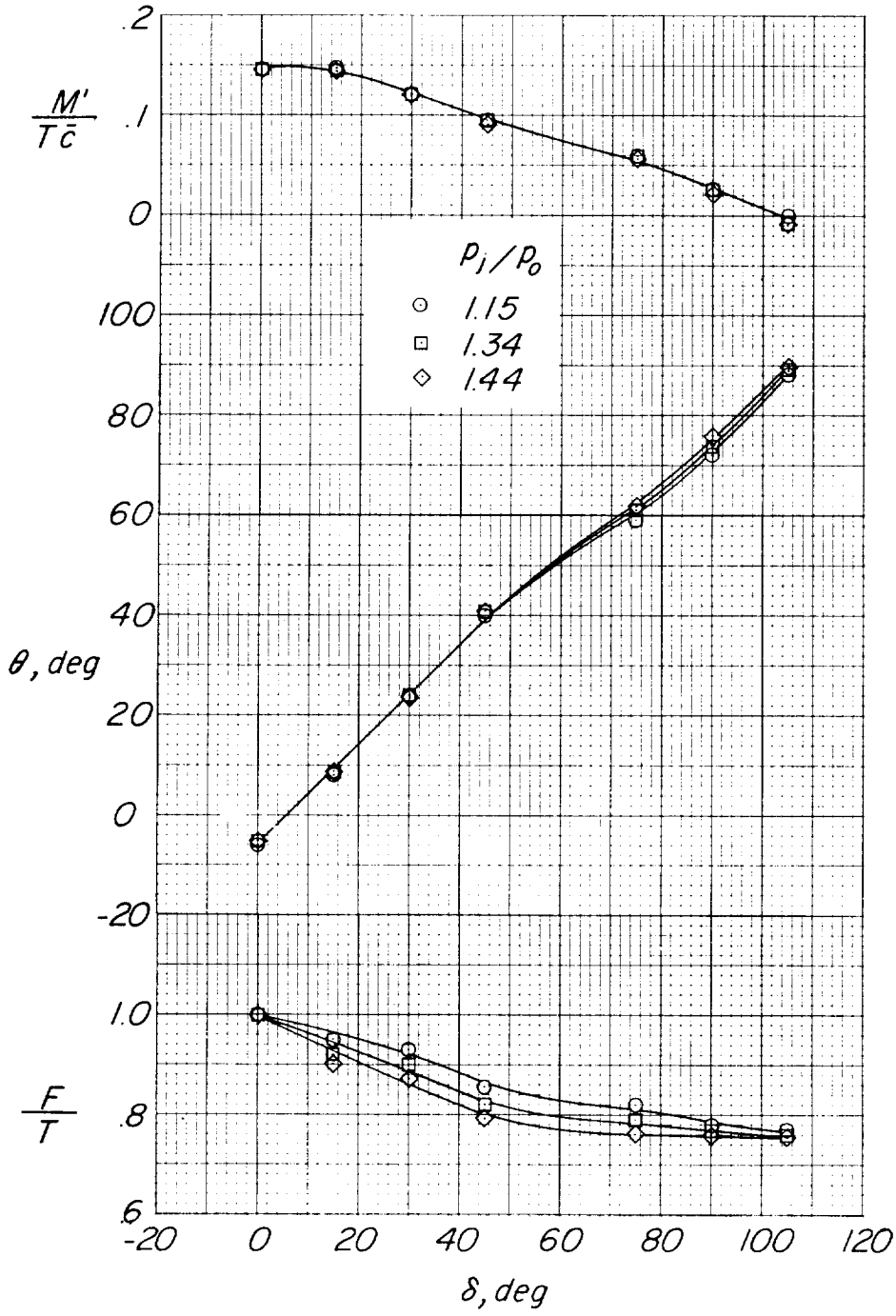

Figure 4.- Effect of vane angle on resultant force, turning angle, and pitching moment for three pressure ratios. A = 1.55; c.g. at 0.20$\bar{c}$; $C_T = \infty$.

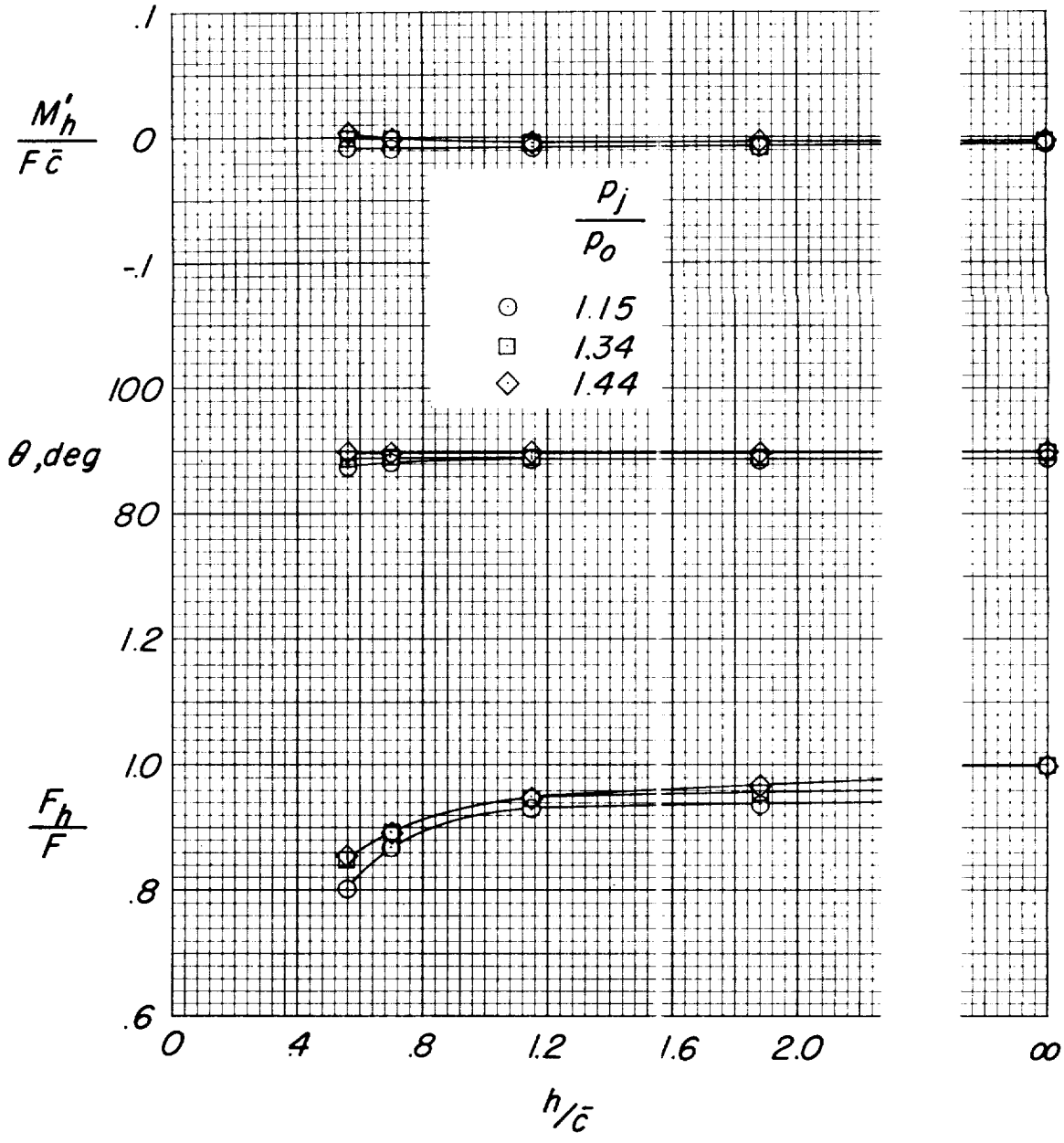

Figure 5.- Effect of height above the ground and pressure ratio on resultant force, turning angle, and pitching moment. A = 1.55; δ = 105°; c.g. at 0.20$\bar{c}$; $C_T = \infty$.

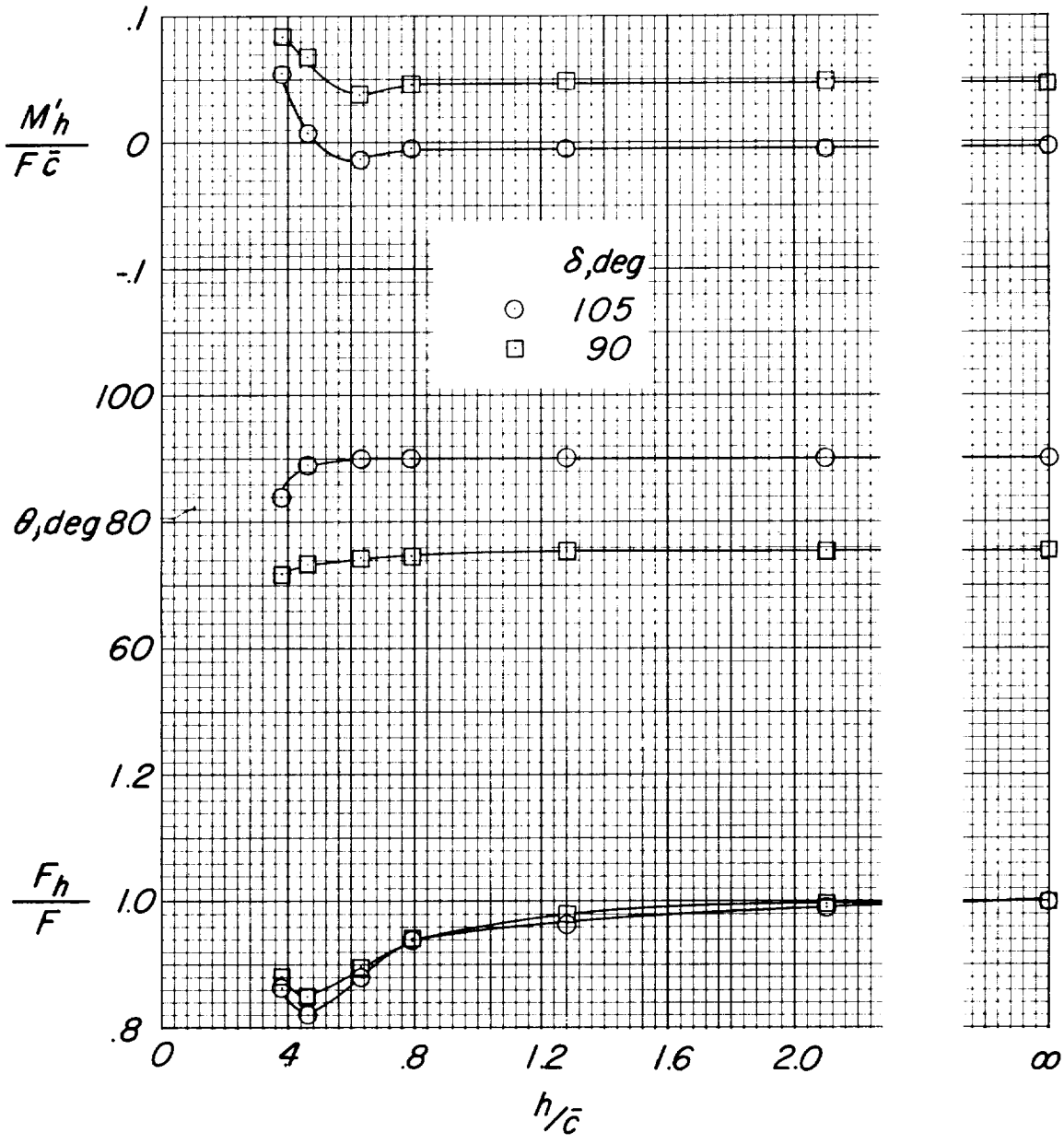

(a) c.g. at $0.11\bar{c}$.

Figure 6.- Effect of height above the ground on resultant force, turning angle, and pitching moment for different vane angles. A = 3.00; p_j/p_o = 1.44; C_T = ∞.

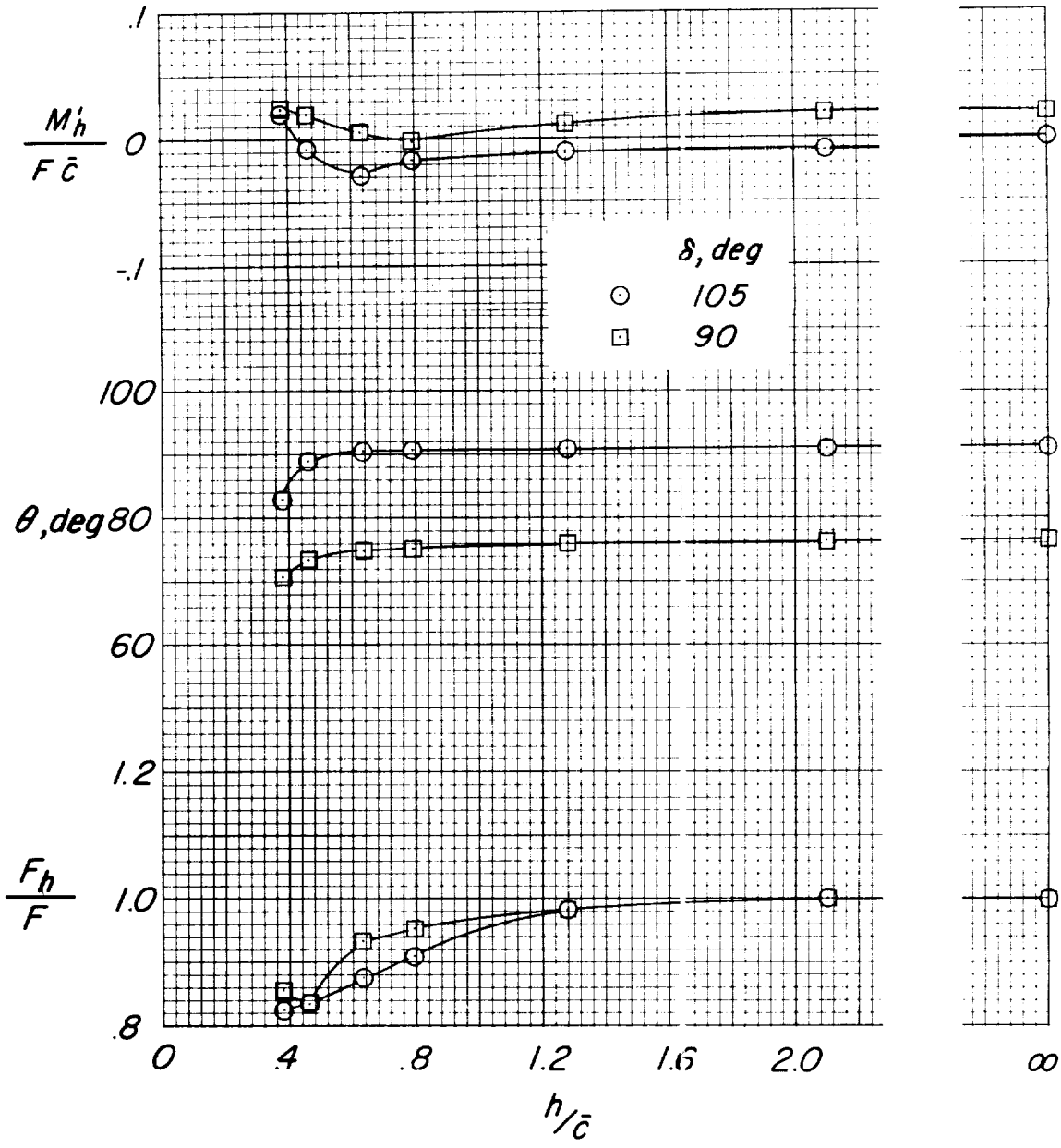

(b) c.g. at 0.35$\bar{c}$.

Figure 6.- Continued.

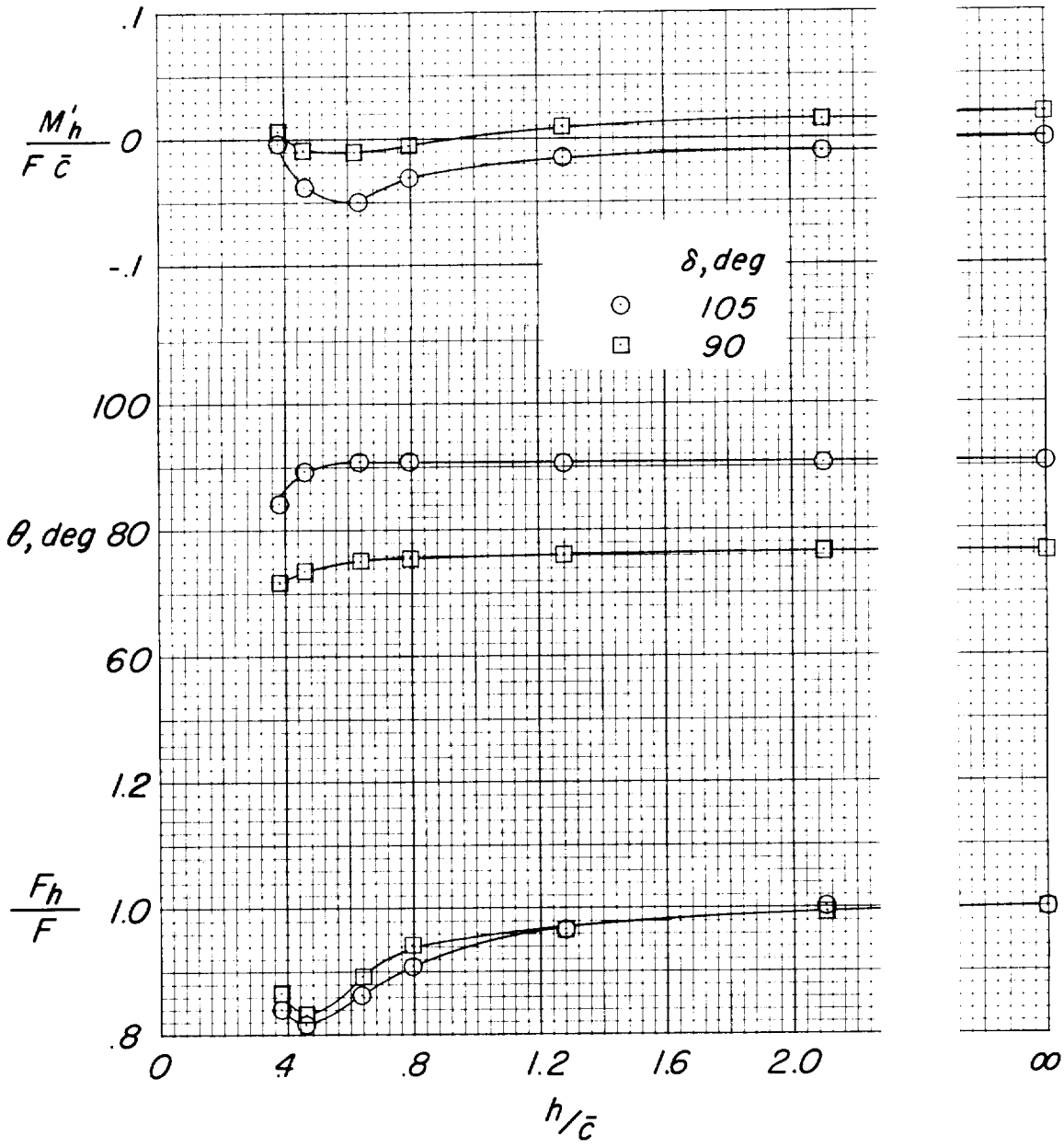

(c) c.g. at 0.58$\bar{c}$.

Figure 6.- Continued.

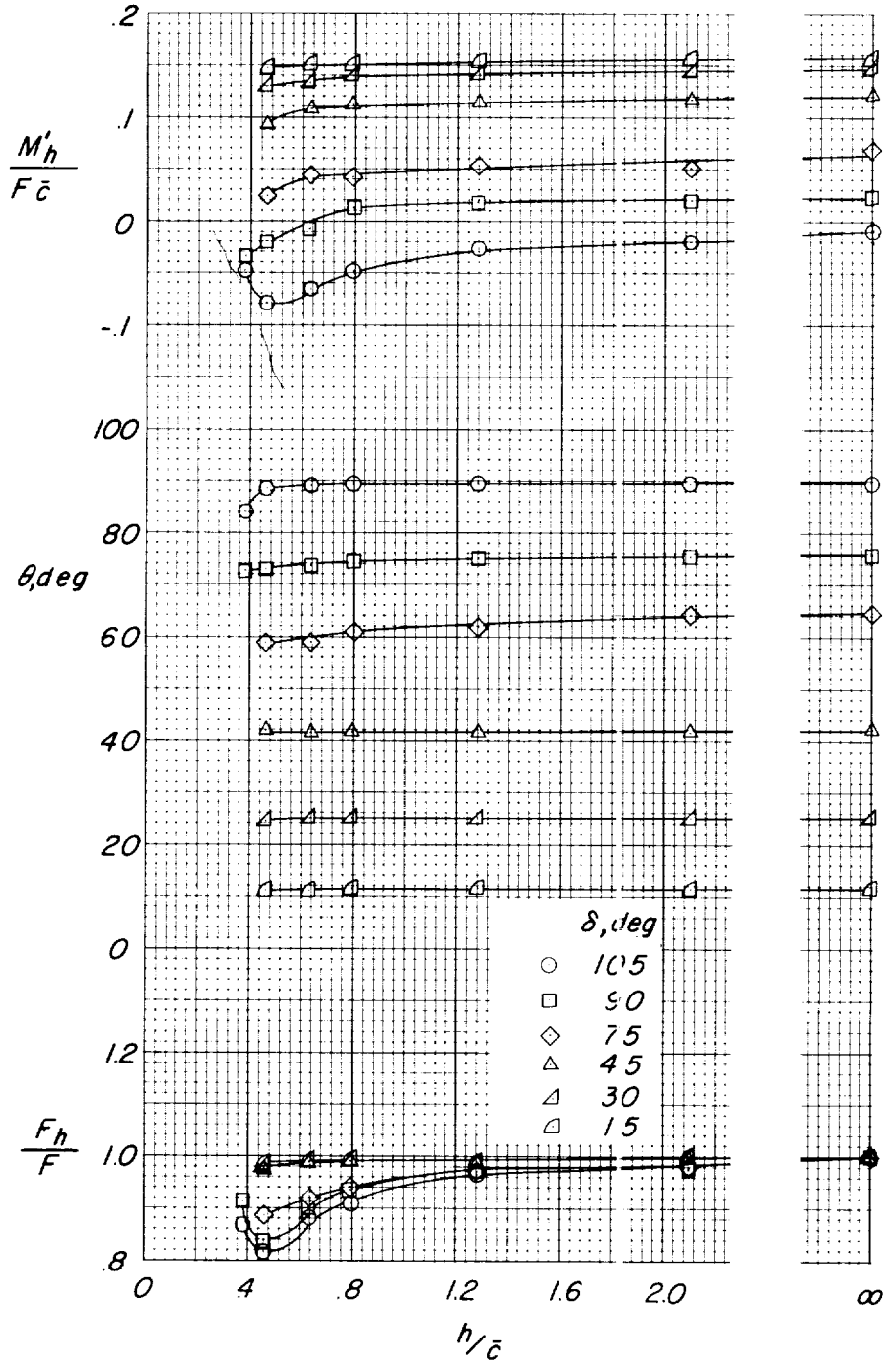

(d) c.g. at 0.76$\bar{c}$

Figure 6.- Concluded.

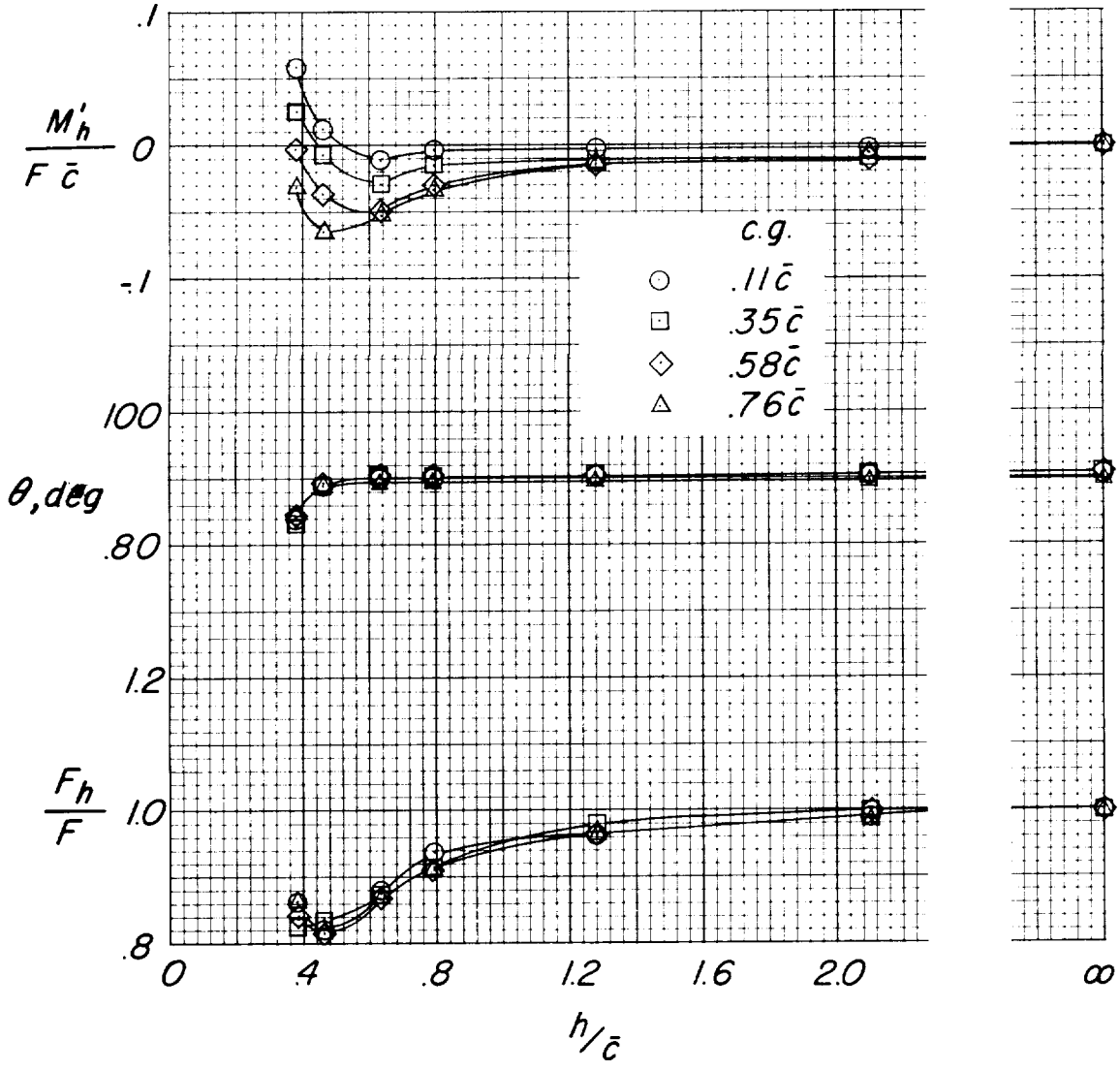

Figure 7.- Effect of height above the ground for different c.g. locations. A = 3.00; δ = 105°; p_j/p_o = 1.44; C_T = ∞.

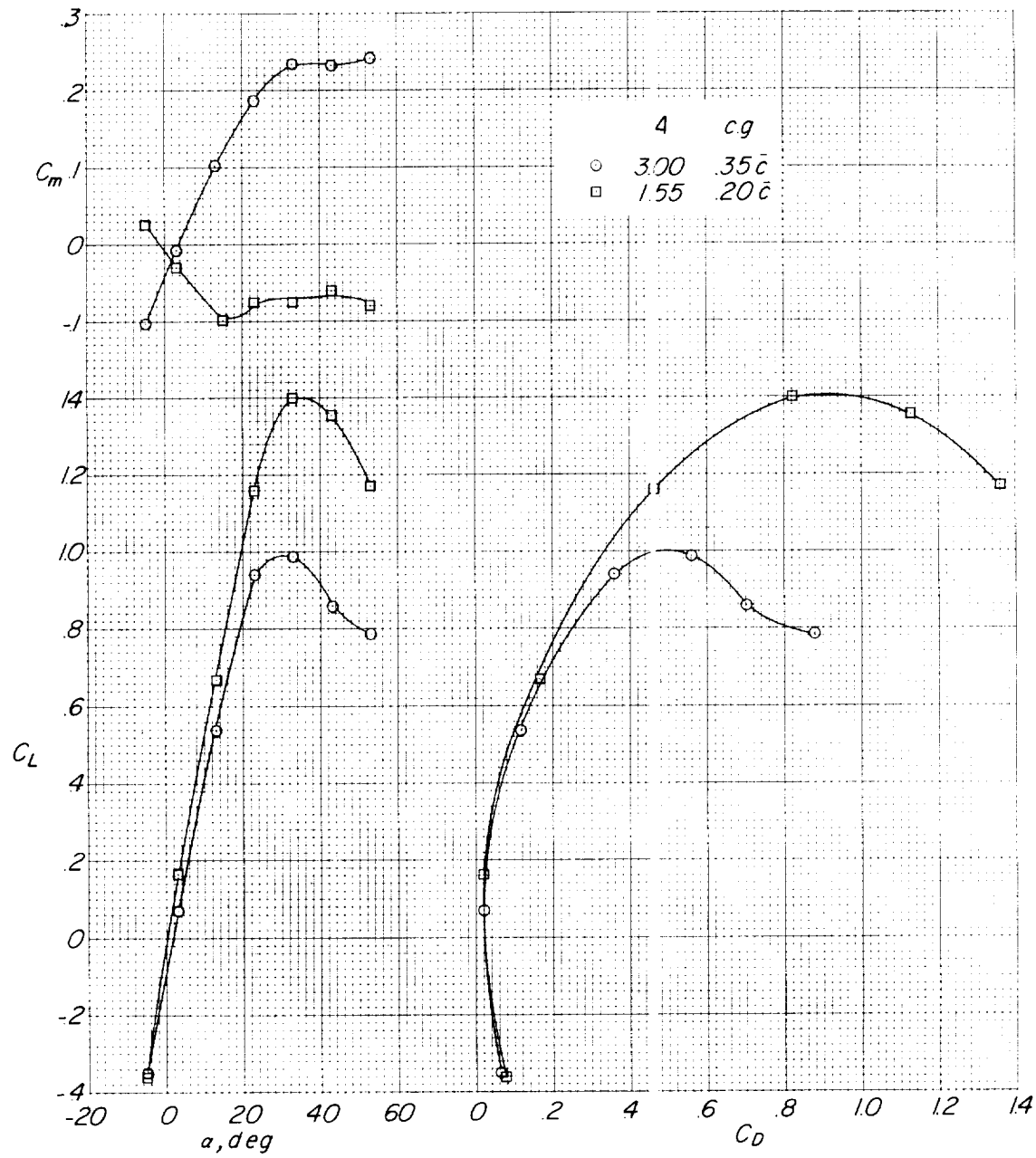

Figure 8.- Power-off characteristics of the two configurations tested. Vanes off; $C_T = 0$; $V_\infty/V_j = \infty$; $h/\bar{c} \approx \infty$.

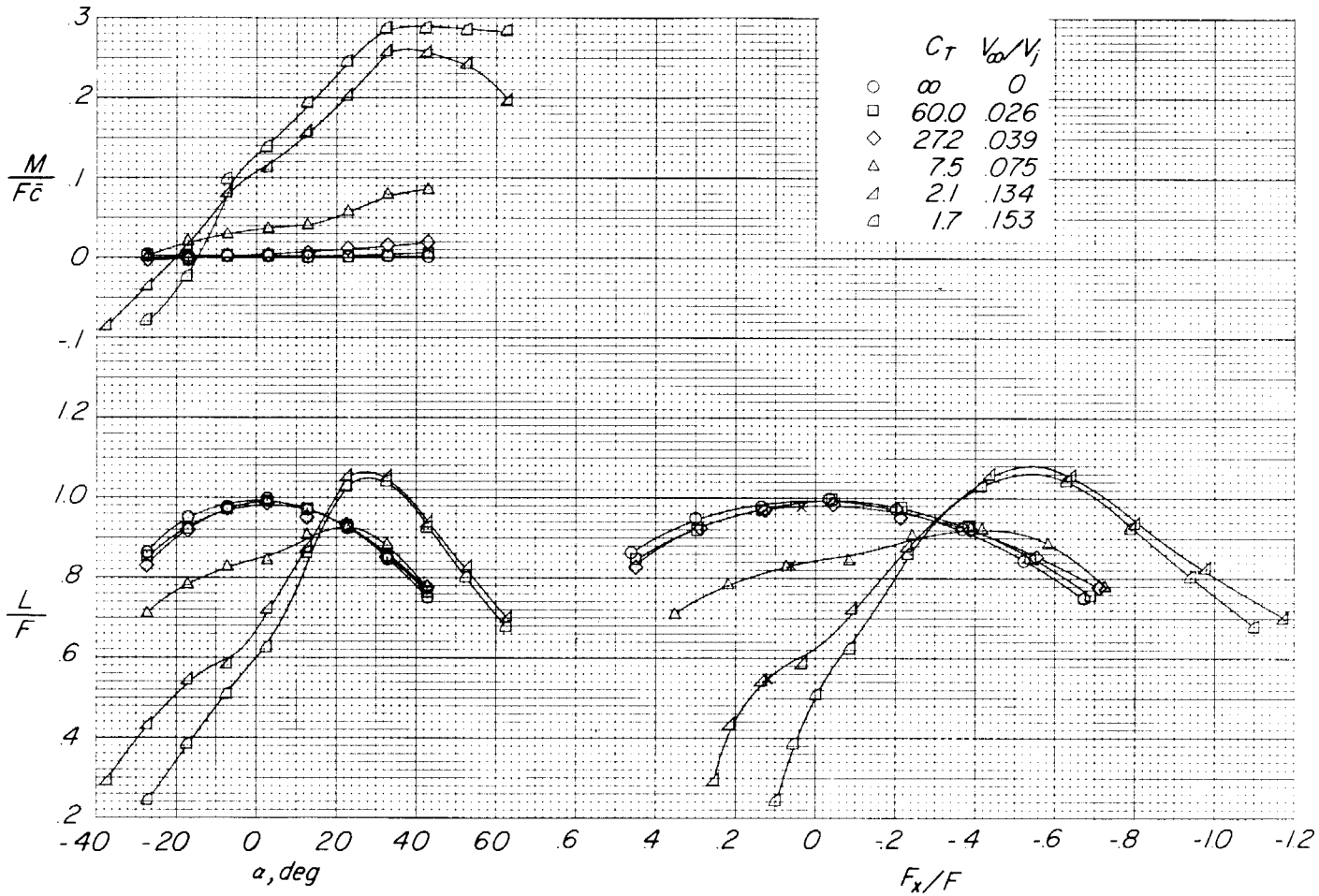

(a) $\theta \approx 90^\circ$.

Figure 9.- Effect of changes in thrust coefficient for various turning angles. A = 3.00; c.g. at 0.35$\bar{c}$; $h/\bar{c} \approx \infty$. (×-marks indicate condition of thrust-drag equilibrium.)

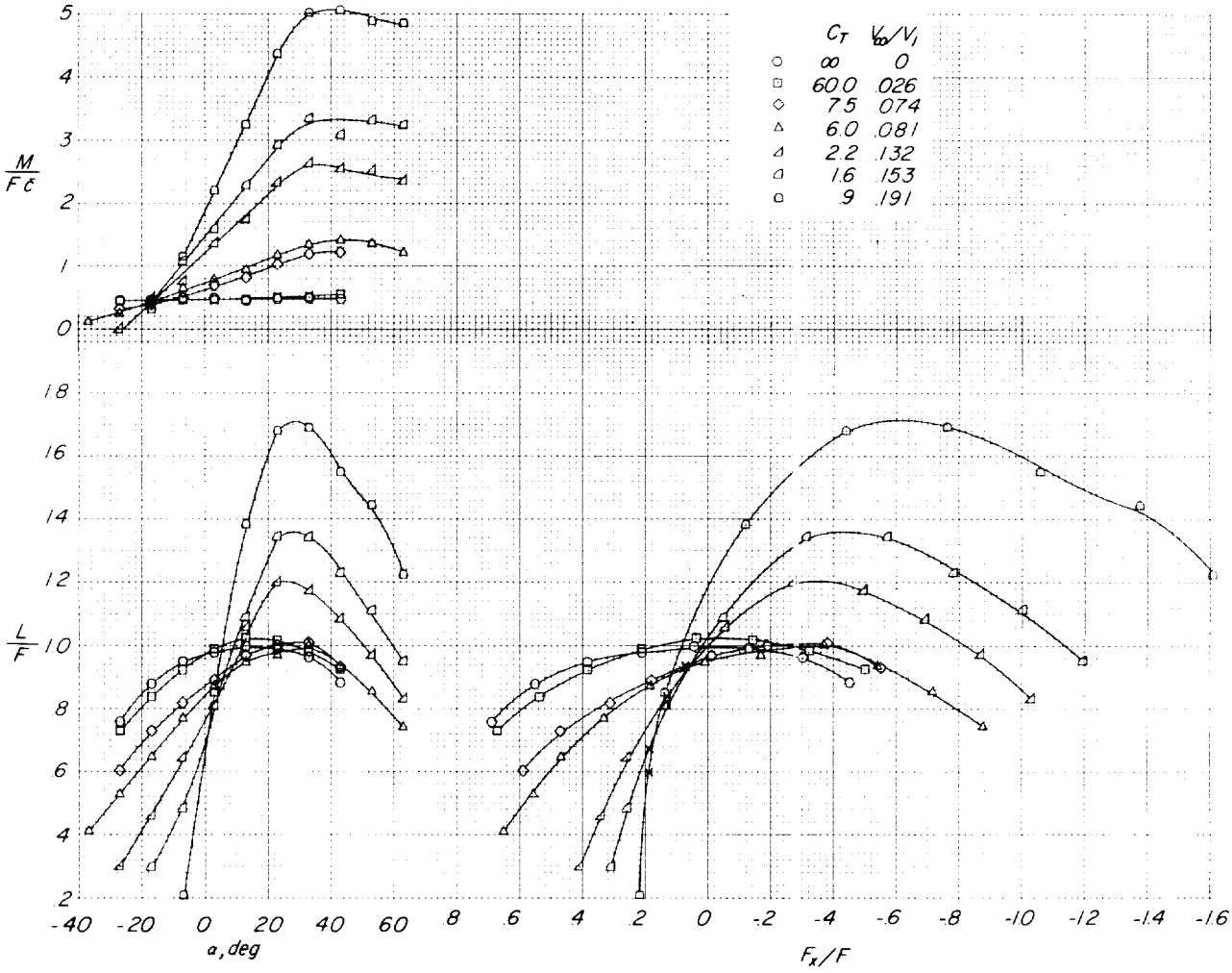

(b) $\theta \approx 75^\circ$.

Figure 9.- Continued.

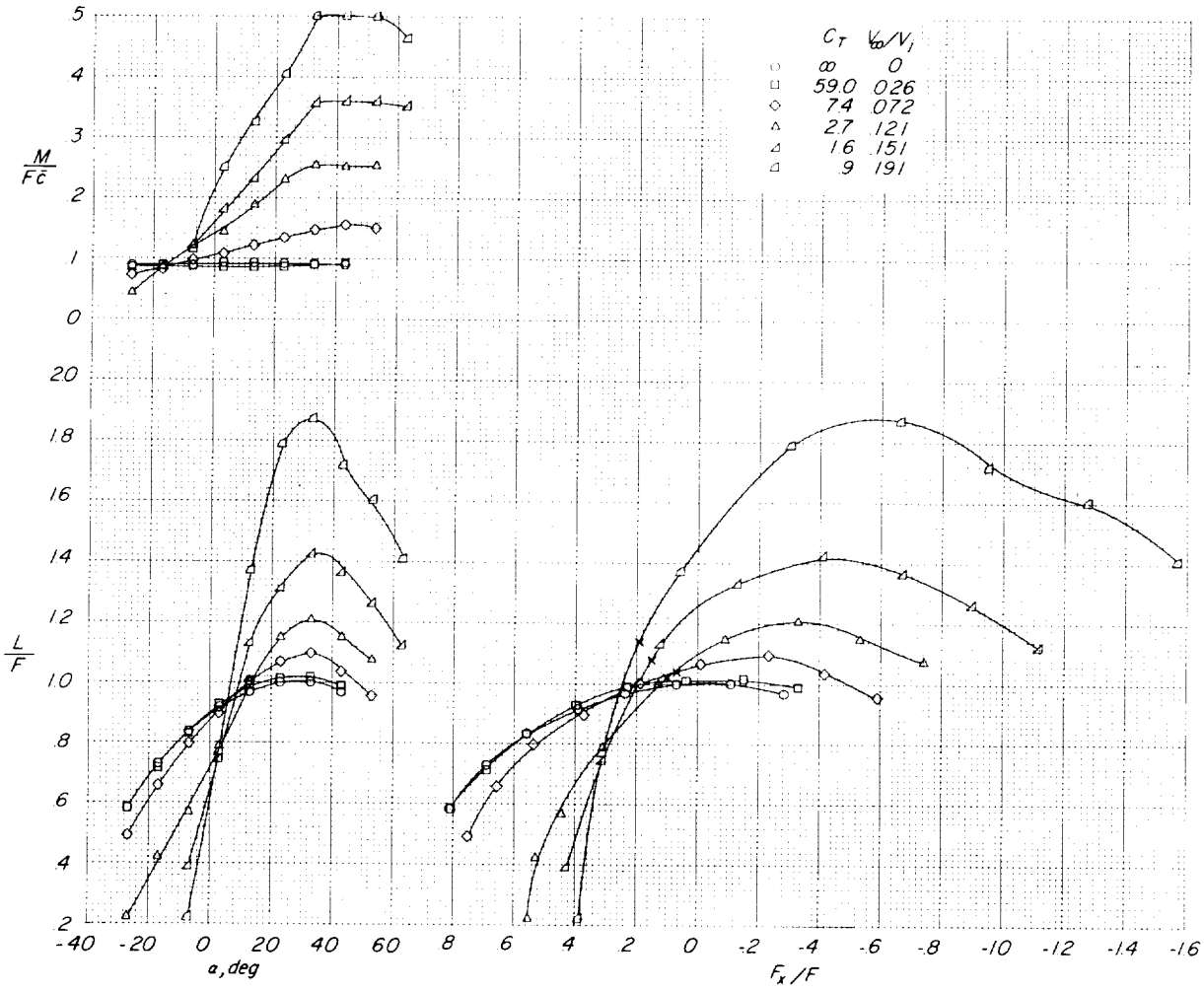

(c) $\theta \approx 62^\circ$.

Figure 9.- Continued.

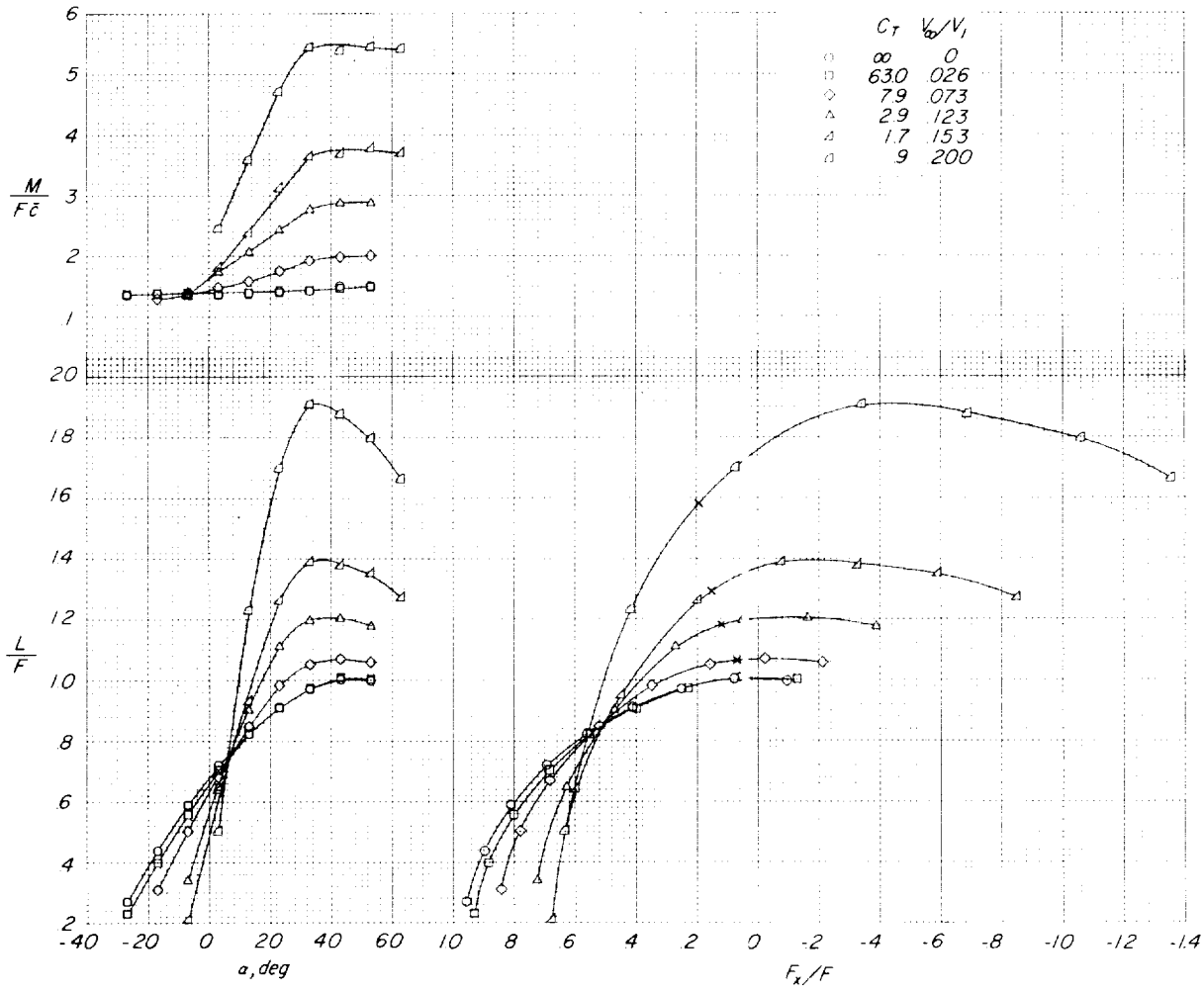

(d) $\theta \approx 42^\circ$.

Figure 9.- Continued.

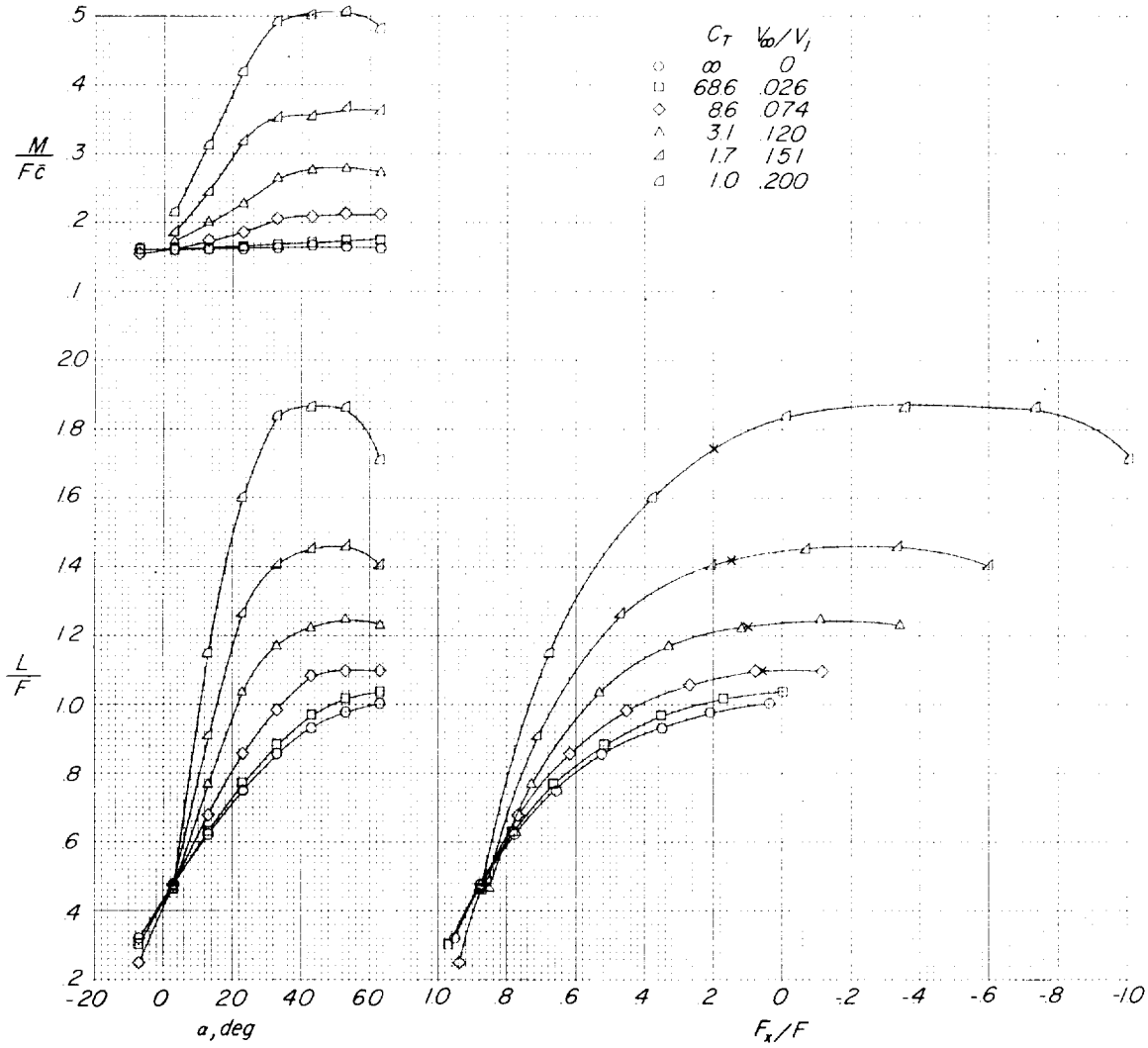

(e) $\theta \approx 25^\circ$.

Figure 9.- Continued.

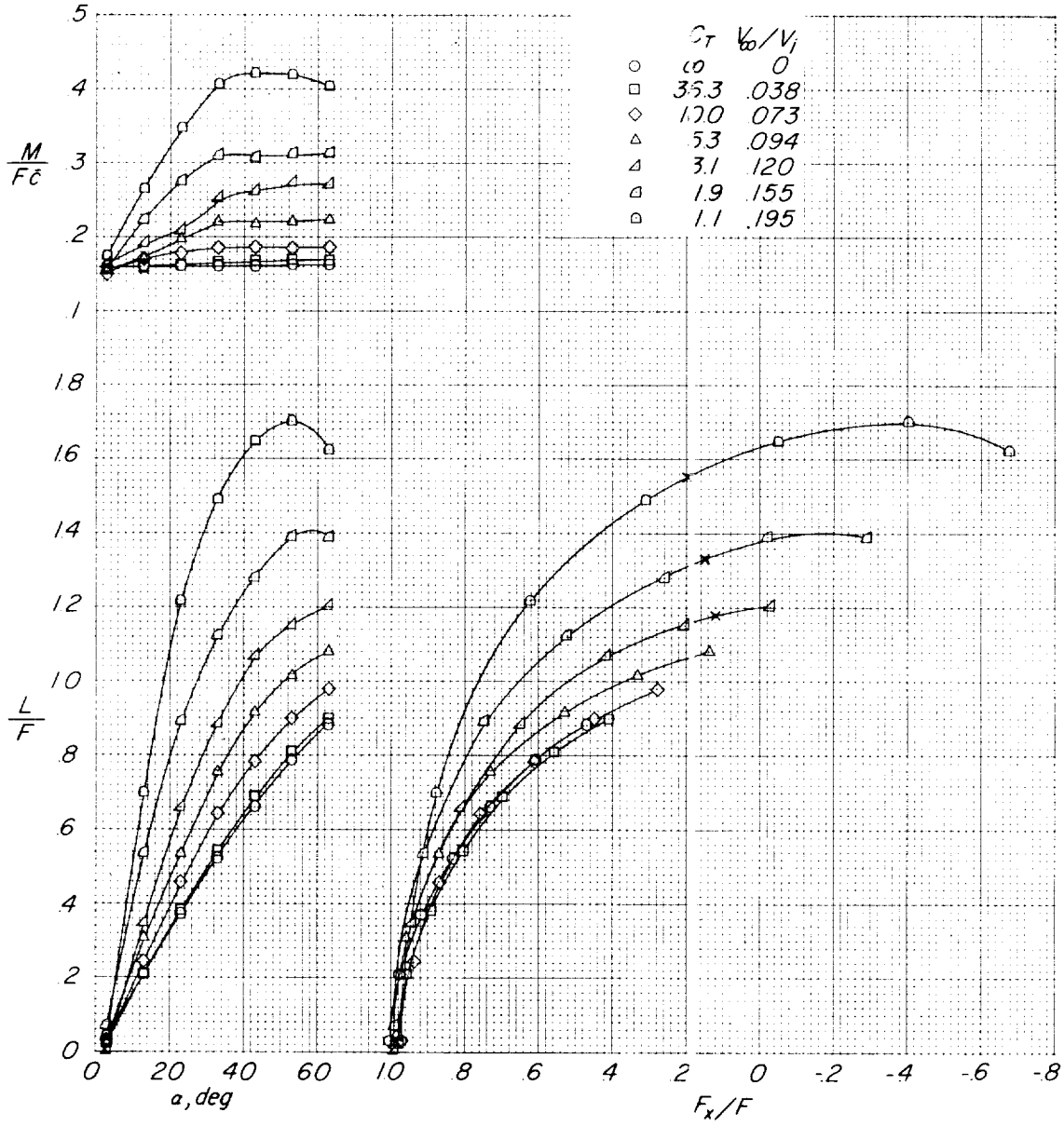

(f) $\theta \approx -5^\circ$.

Figure 9.- Concluded.

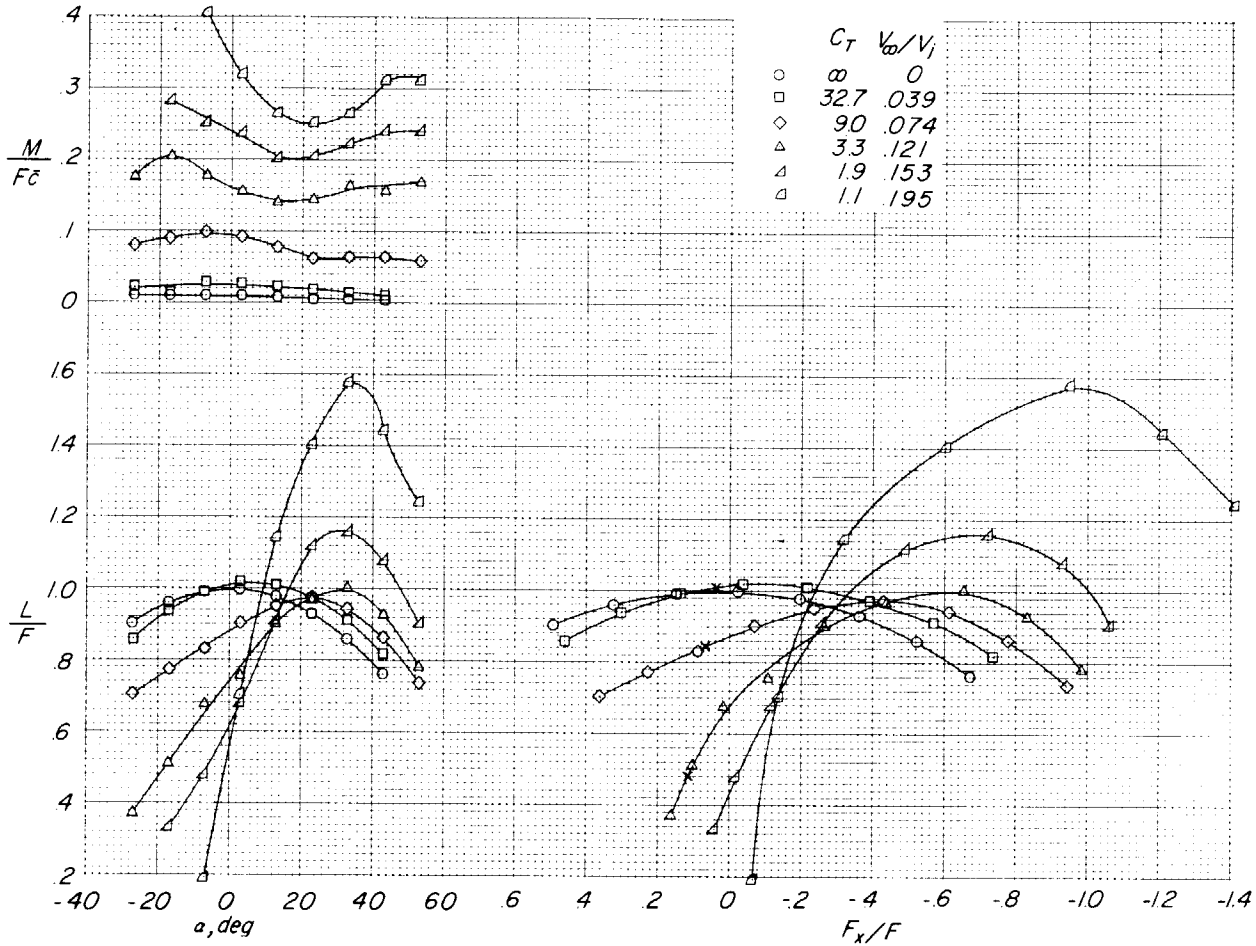

(a) $\theta \approx 90^\circ$.

Figure 10.- Effect of changes in thrust coefficient for various turning angles. A = 1.55; c.g. at .20$\bar{c}$; h/$\bar{c}$ ≈ ∞. (x-marks indicate condition of thrust-drag equilibrium.)

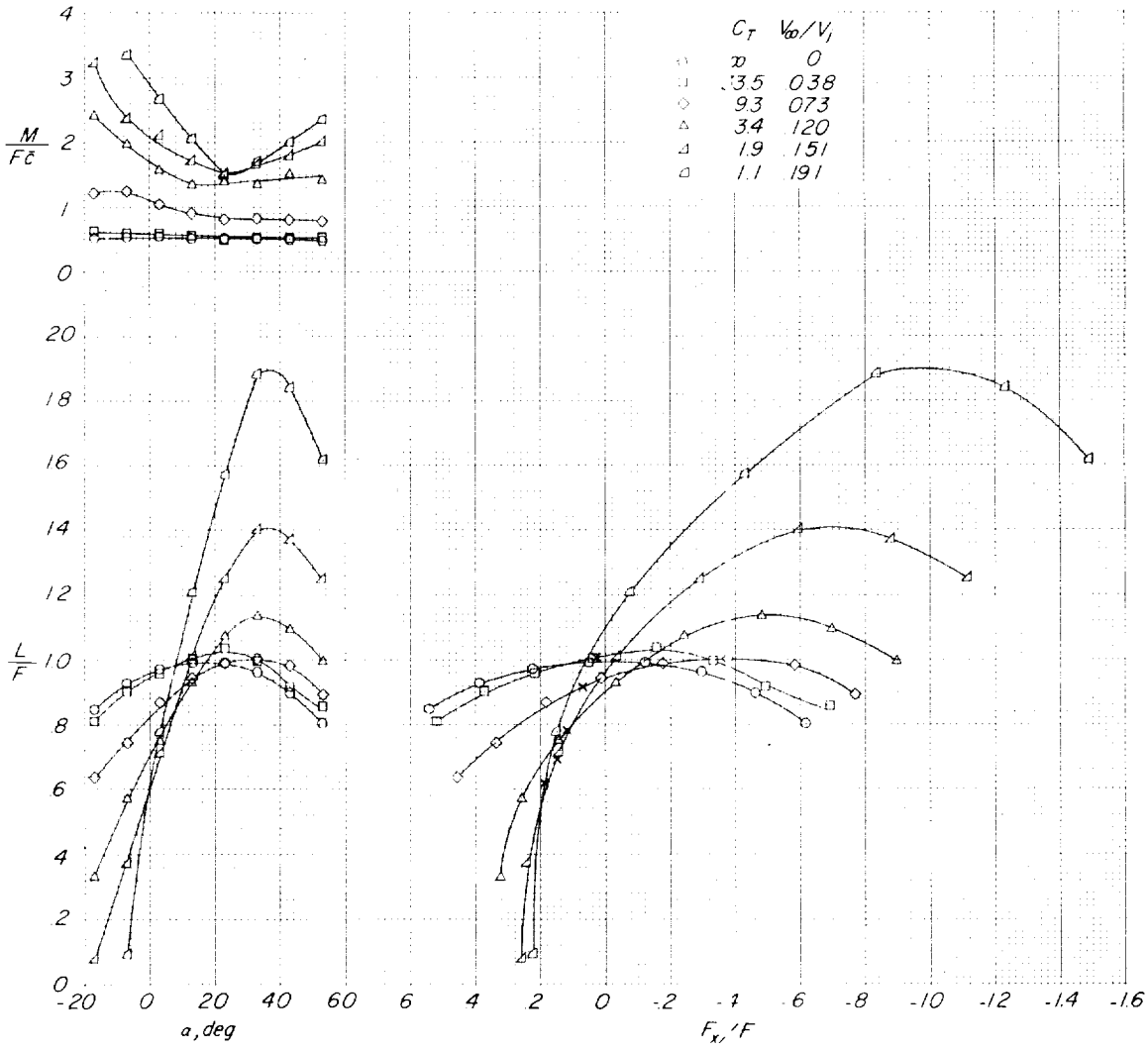

(b) $\theta \approx 74^{\circ}$.

Figure 10.- Continued.

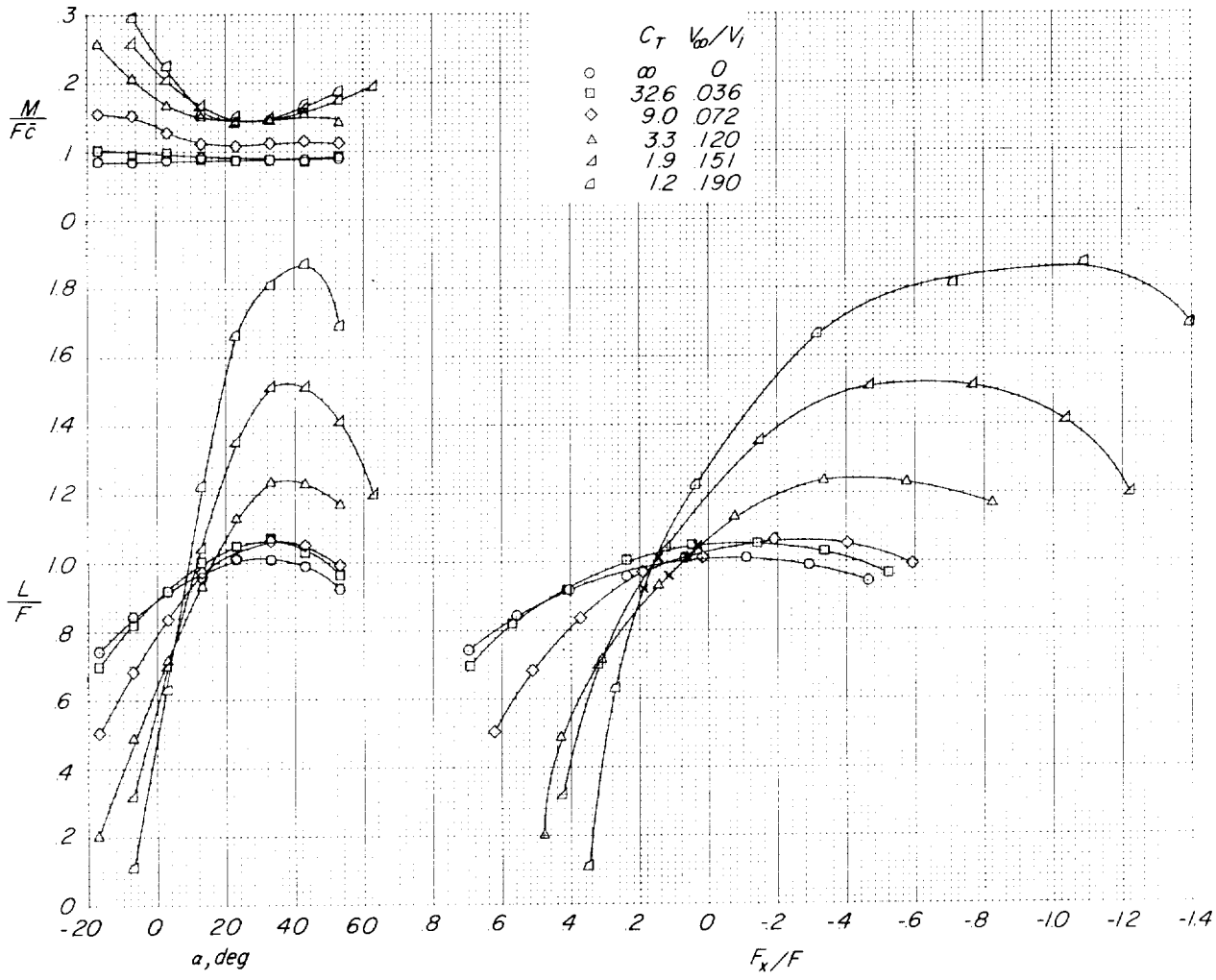

(c) $\theta \approx 64^\circ$.

Figure 10.- Continued.

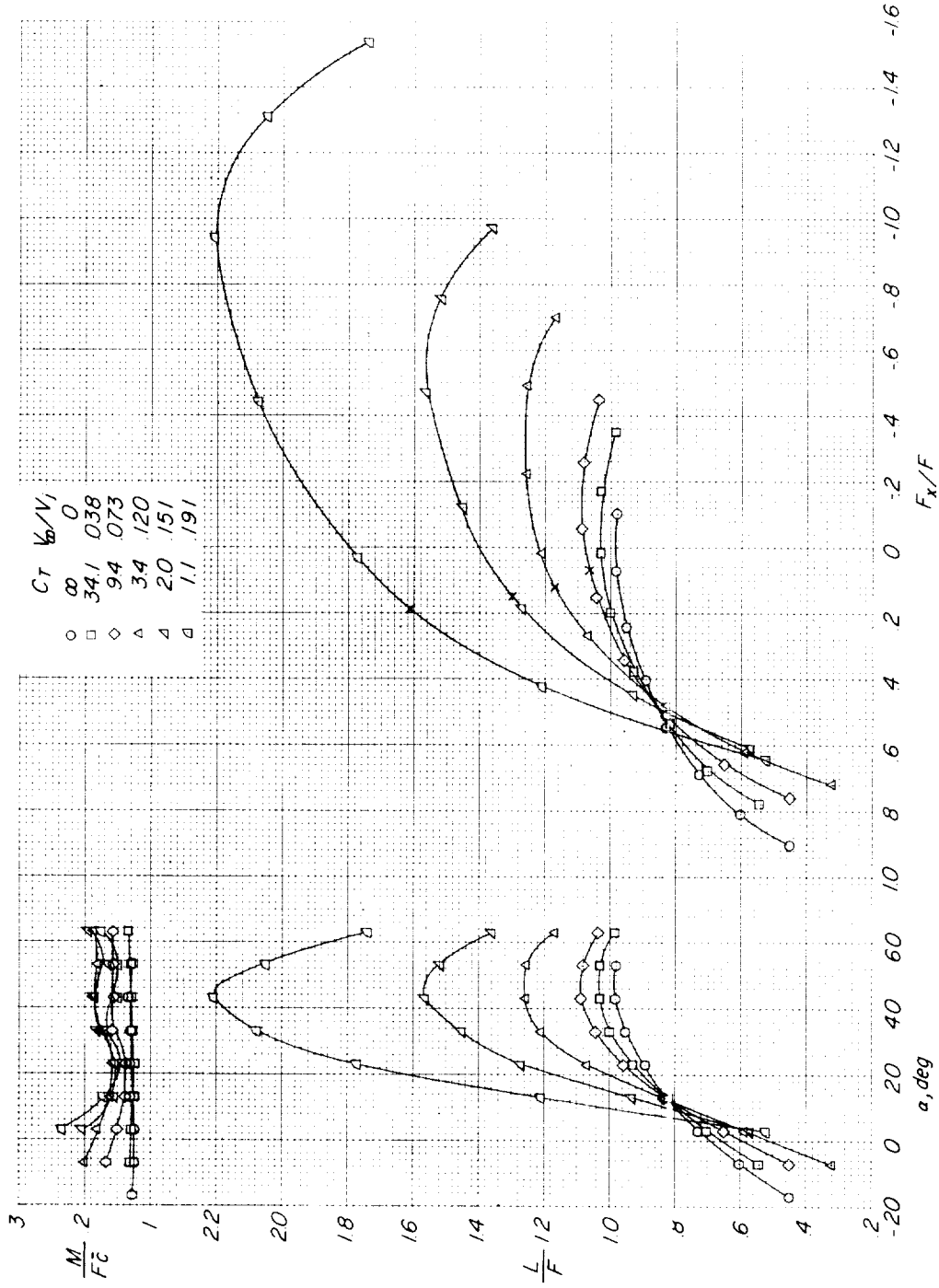

(d) $\theta \approx 42^{\circ}$.

Figure 10.- Continued.

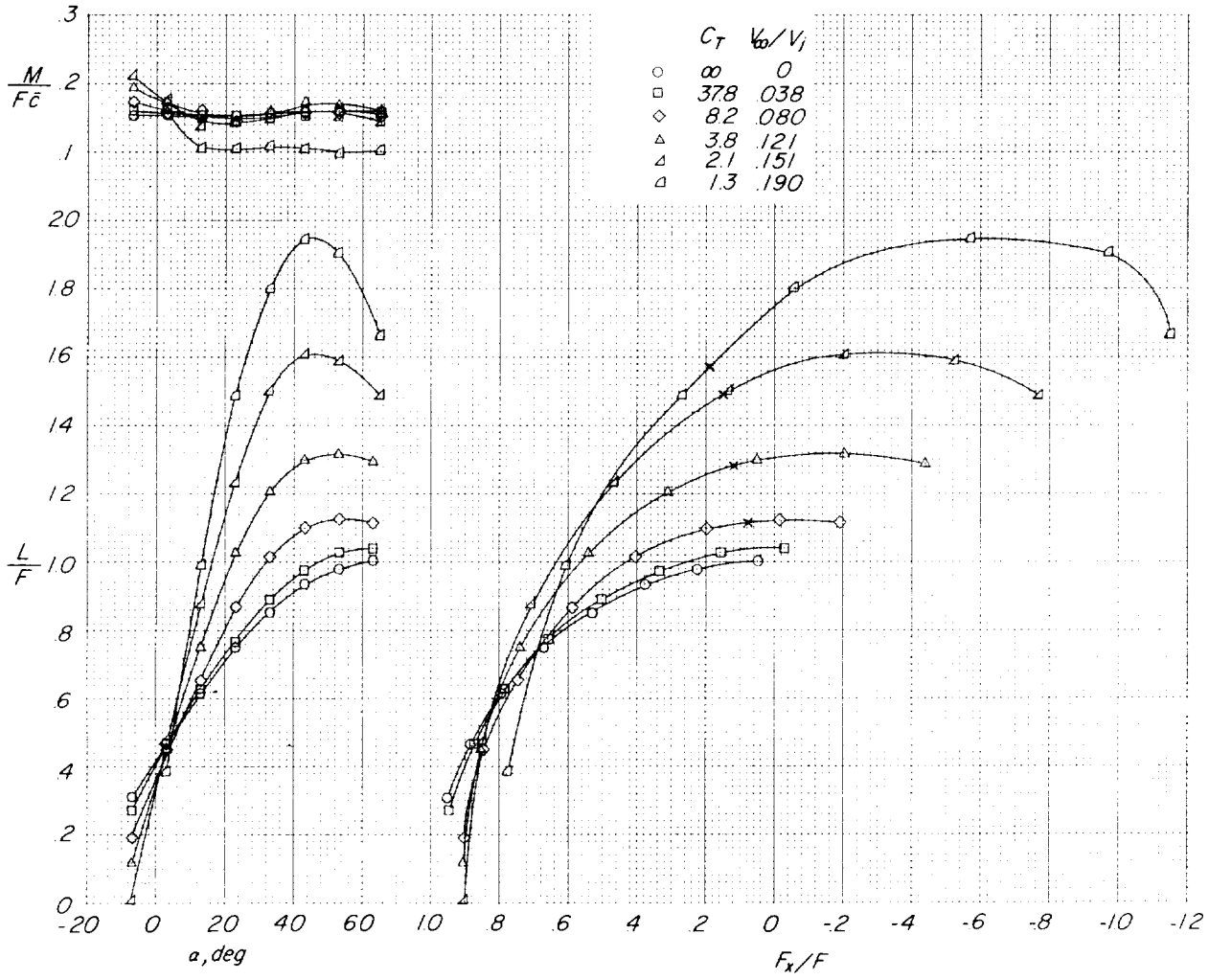

(e) $\theta \approx 24^\circ$.

Figure 10.- Continued.

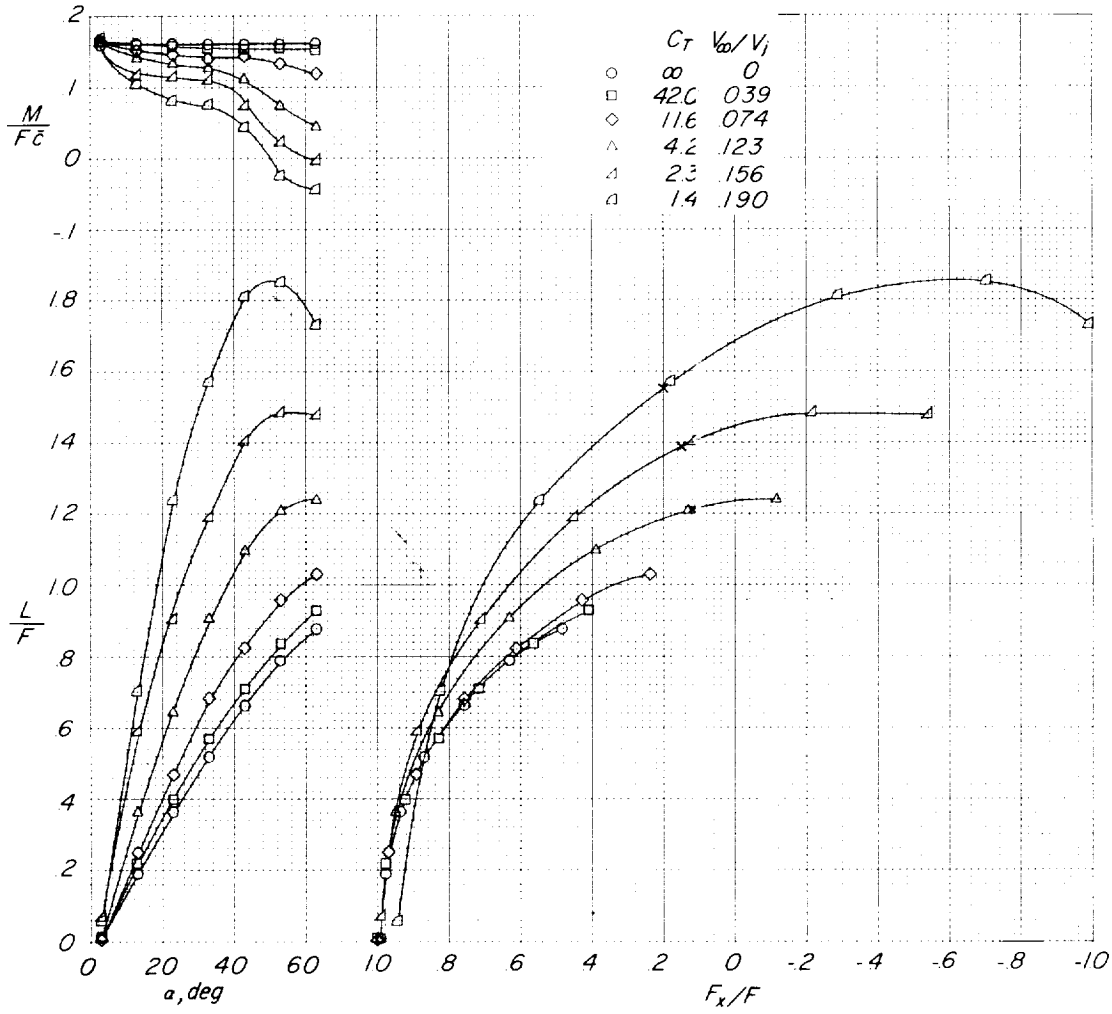

(f) $\theta \approx -5^\circ$.

Figure 10.- Concluded.

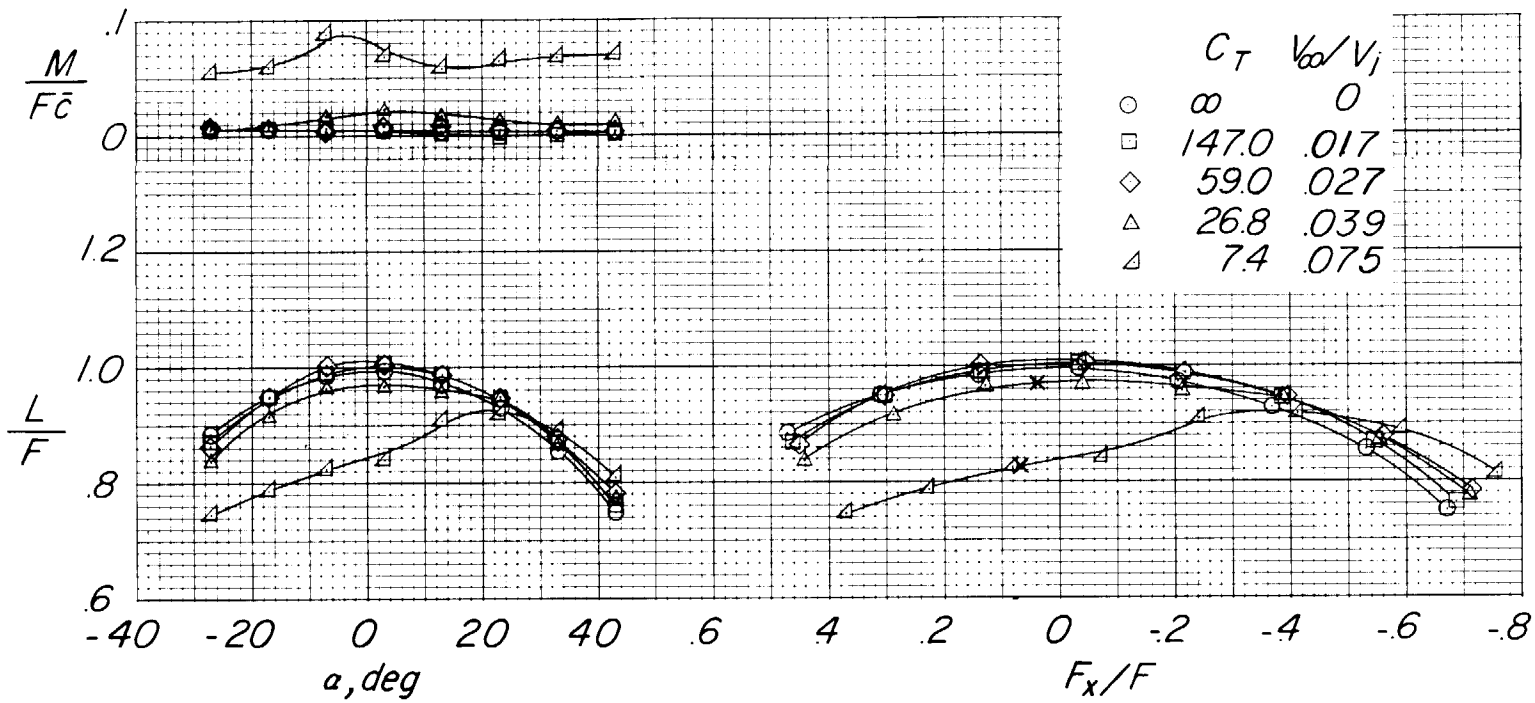

(a) c.g. at 0.11$\bar{c}$.

Figure 11.- Effect of changes in thrust coefficient for various c.g. locations. A = 3.00; $\theta \approx 90^{\circ}$; $h/\bar{c} \approx \infty$. (×-marks indicate condition of thrust-drag equilibrium.)

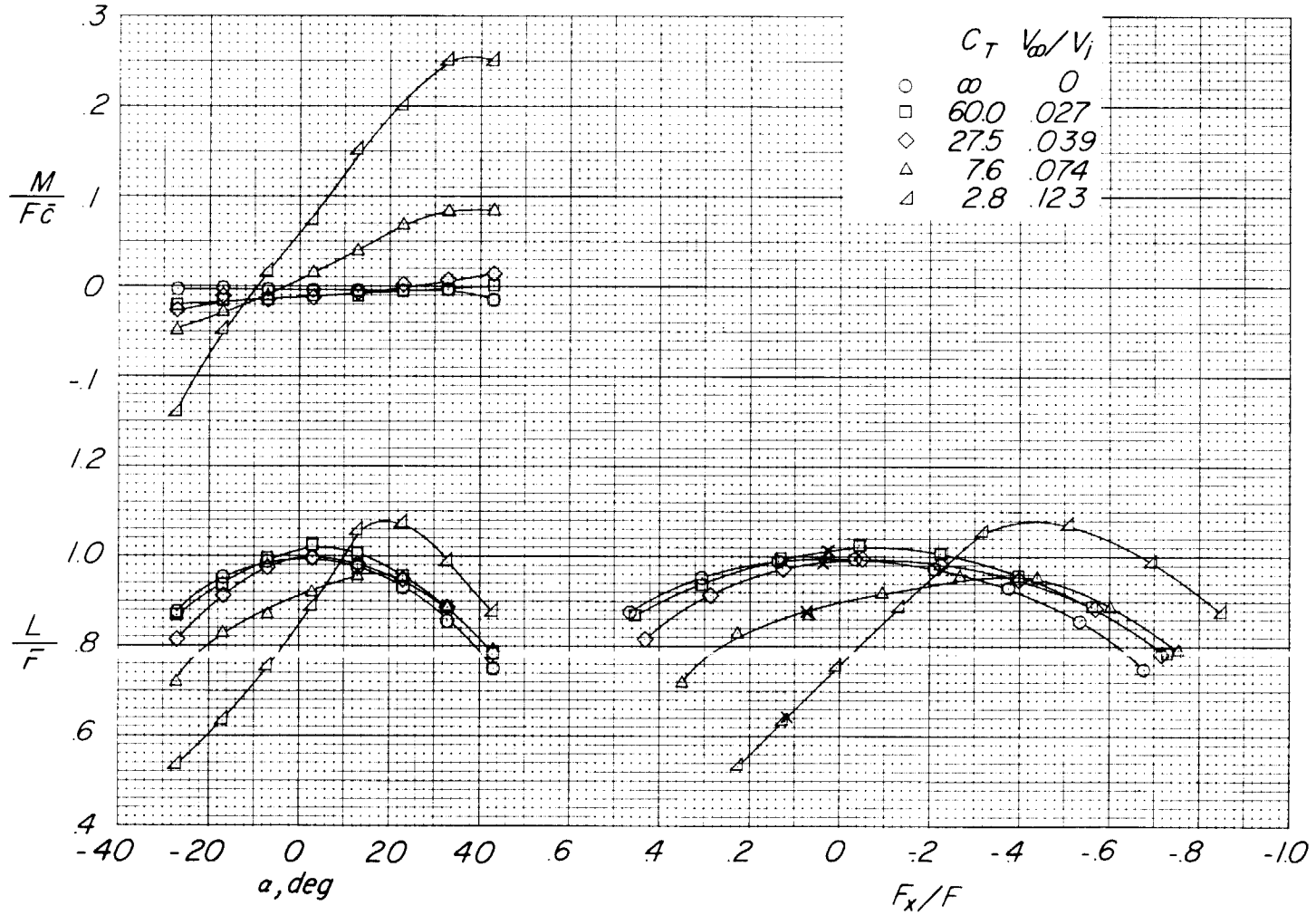

(b) c.g. at 0.58c̄.

Figure 11.- Continued.

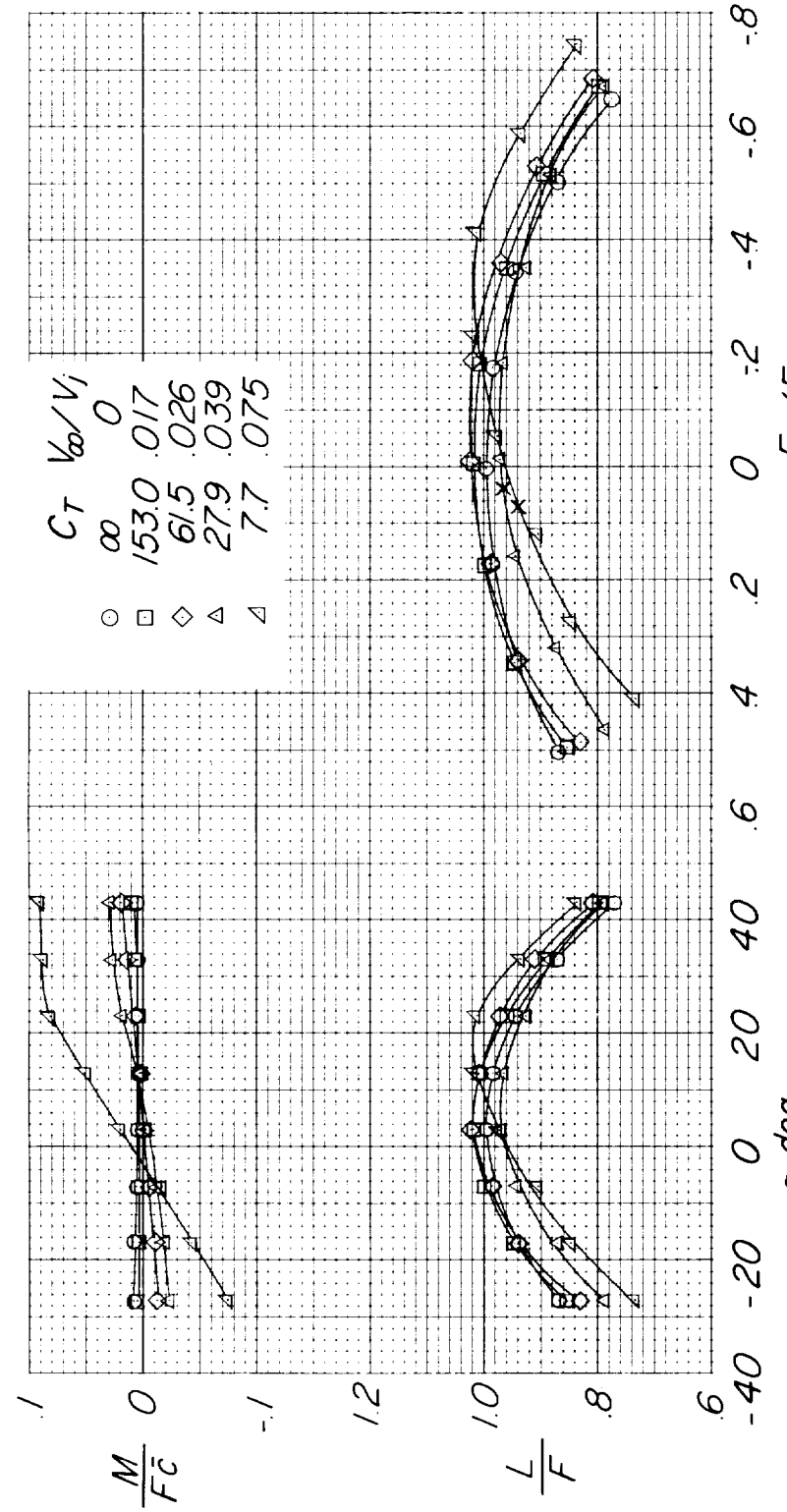

(c) c.g. at 0.76$\bar{c}$.

Figure 11.- Concluded.

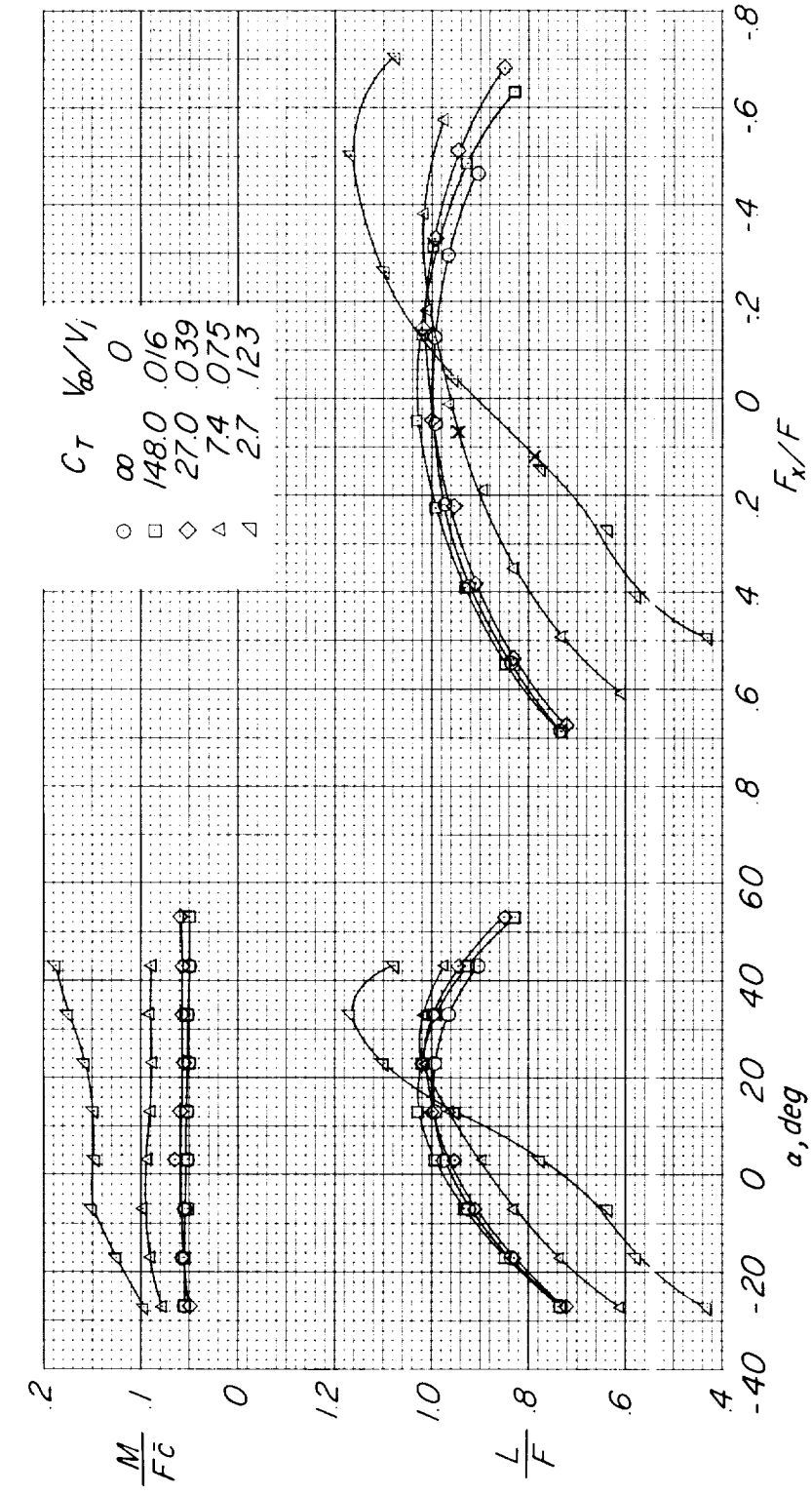

(a) c.g. at 0.11$\bar{c}$.

Figure 12.- Effect of changes in thrust coefficient for various c.g. locations. A = 3.00; $\theta \approx 75°$; $h/\bar{c} \approx \infty$. (x-marks indicate condition of thrust-drag equilibrium.)

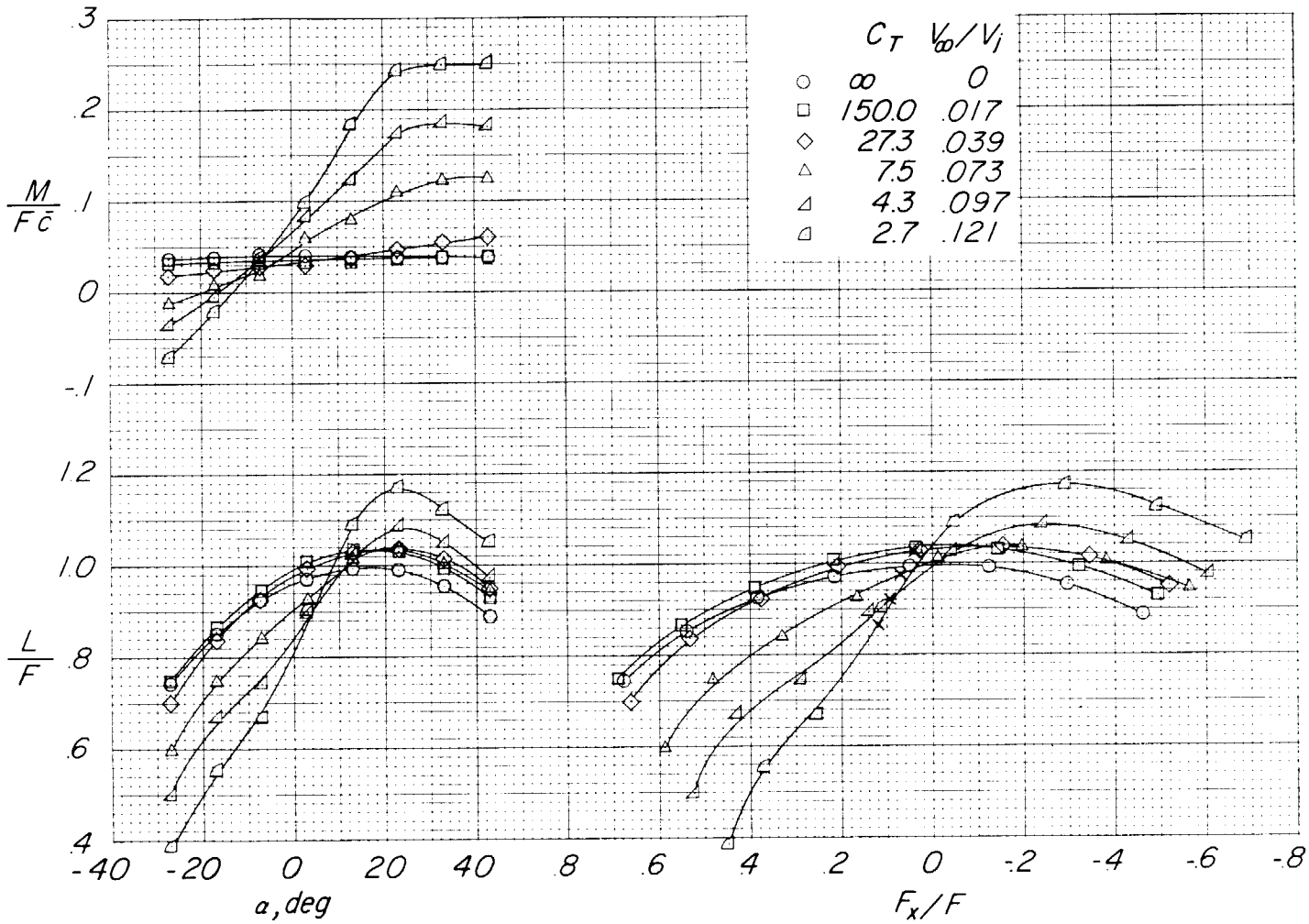

(b) c.g. at 0.58$\bar{c}$.

Figure 12.- Continued.

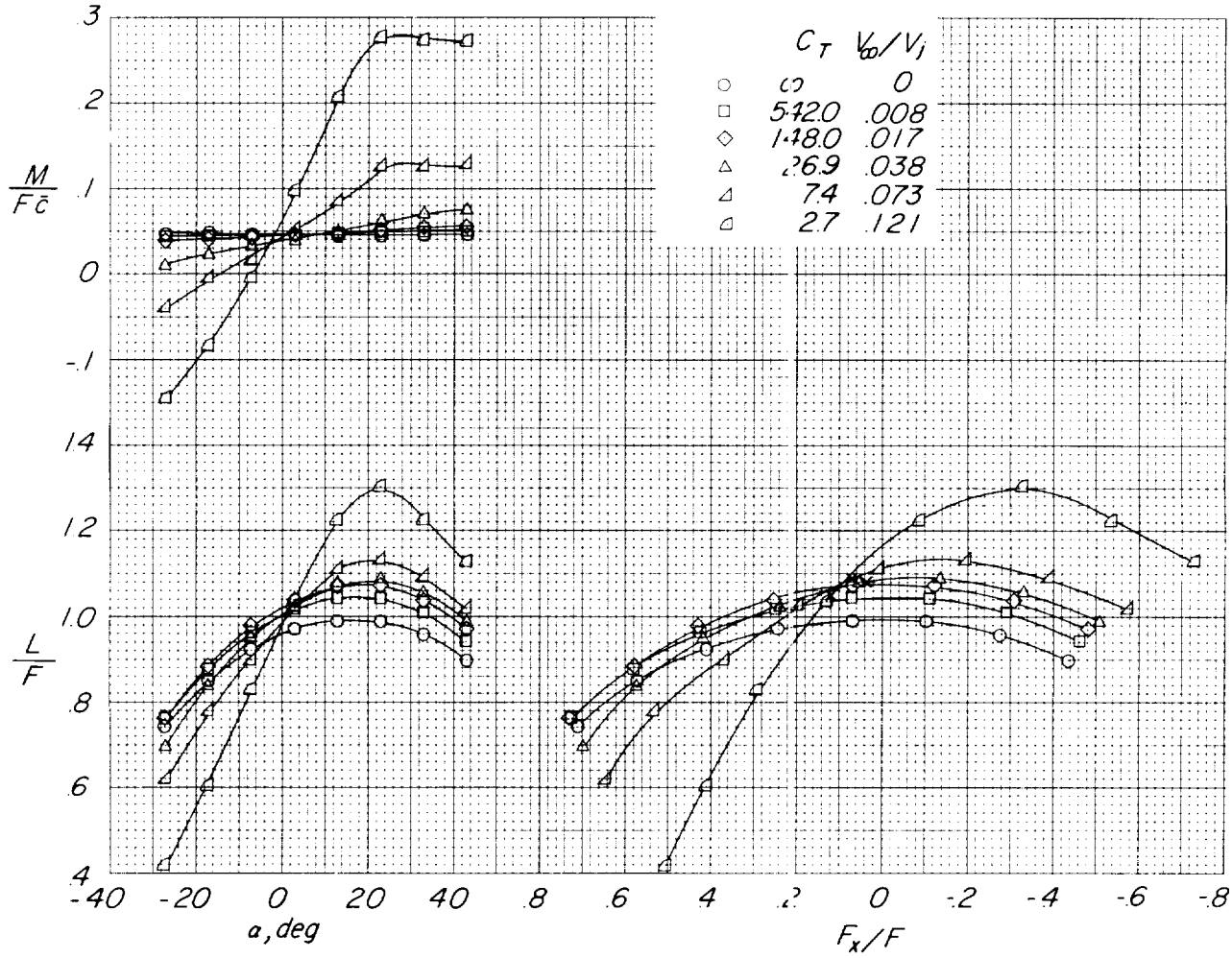

(c) c.g. at 0.76$\bar{c}$.

Figure 12.- Concluded.

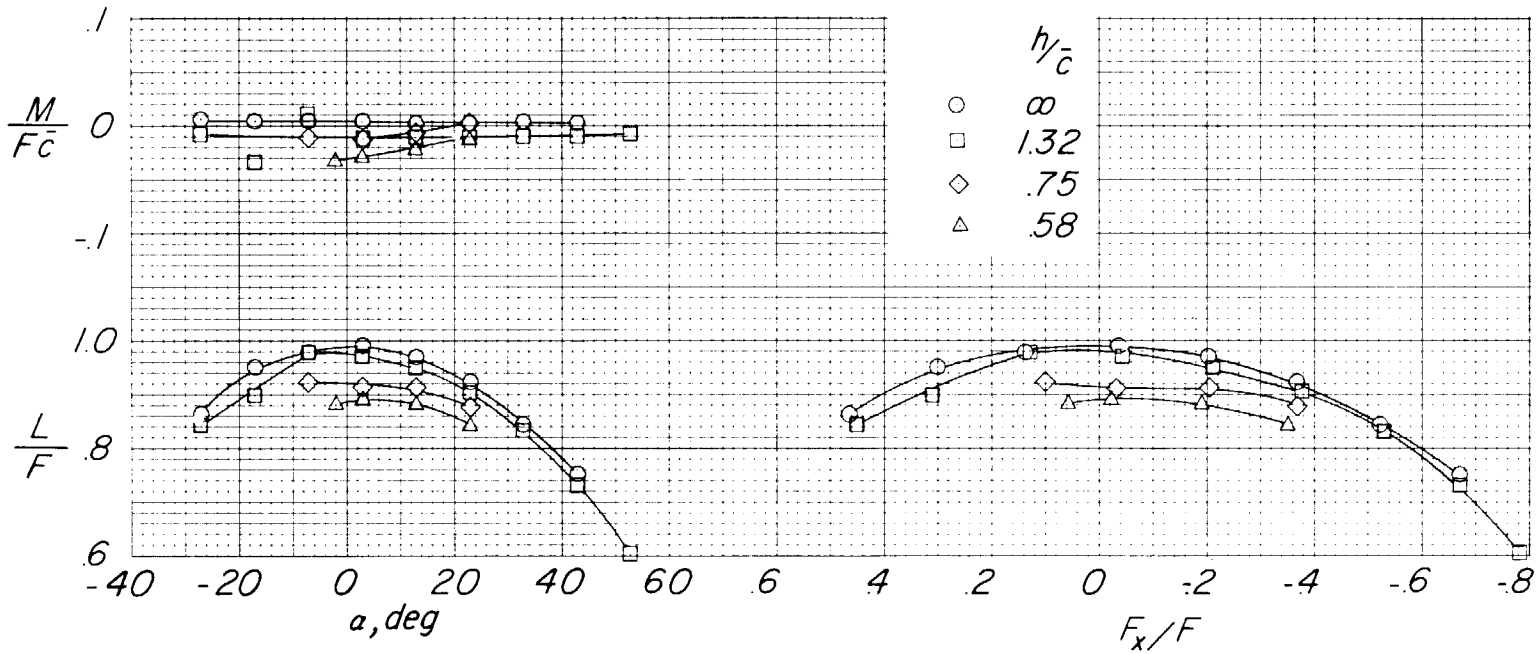

(a) $C_T = \infty$; $V_\infty/V_j = 0$.

Figure 13.- Effect of height above the ground for various thrust coefficients. A = 3.00; $\theta \approx 90^\circ$; c.g. at $0.35\bar{c}$. (x-marks indicate condition of thrust-drag equilibrium.)

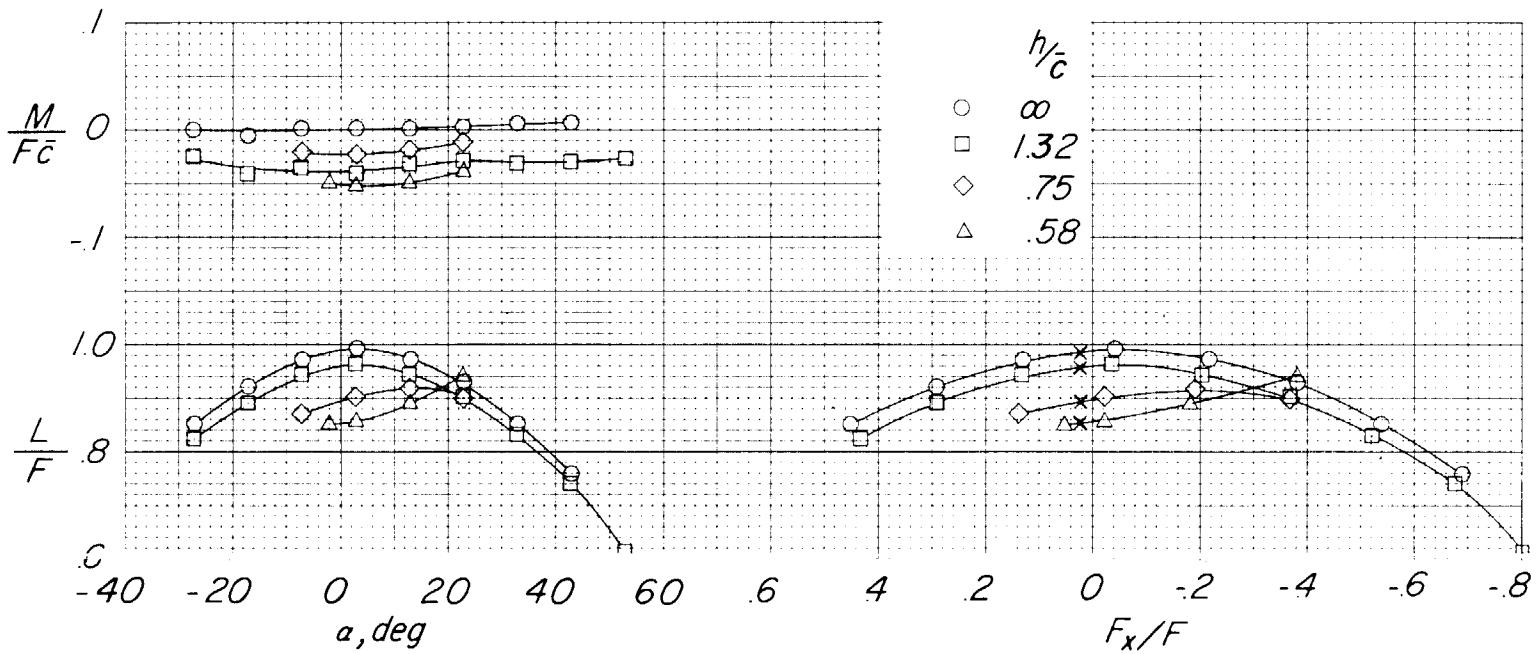

(b) $C_T = 60.0$; $V_\infty/V_j = 0.026$.

Figure 13.- Continued.

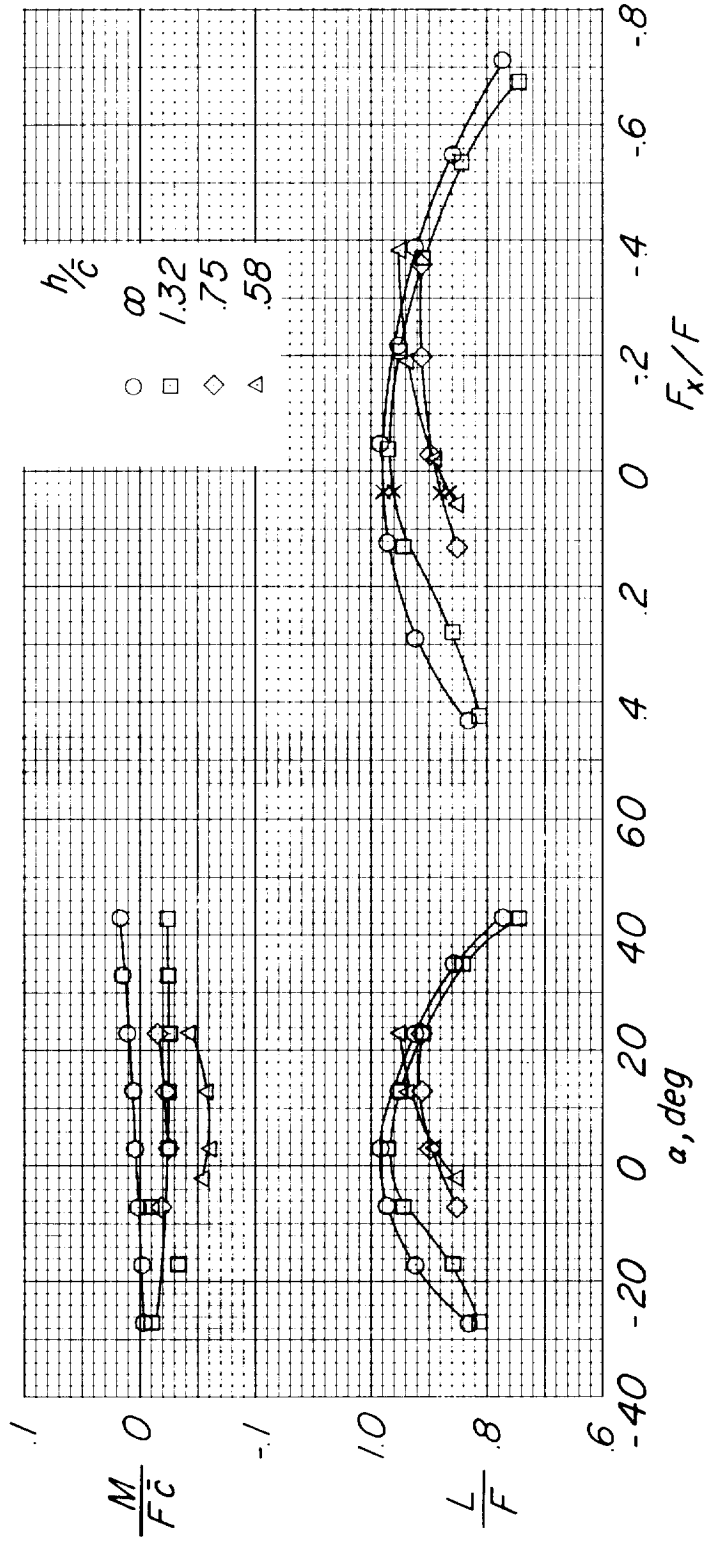

(c) $C_T = 27.2$; $V_\infty/V_j = 0.039$.

Figure 13.- Continued.

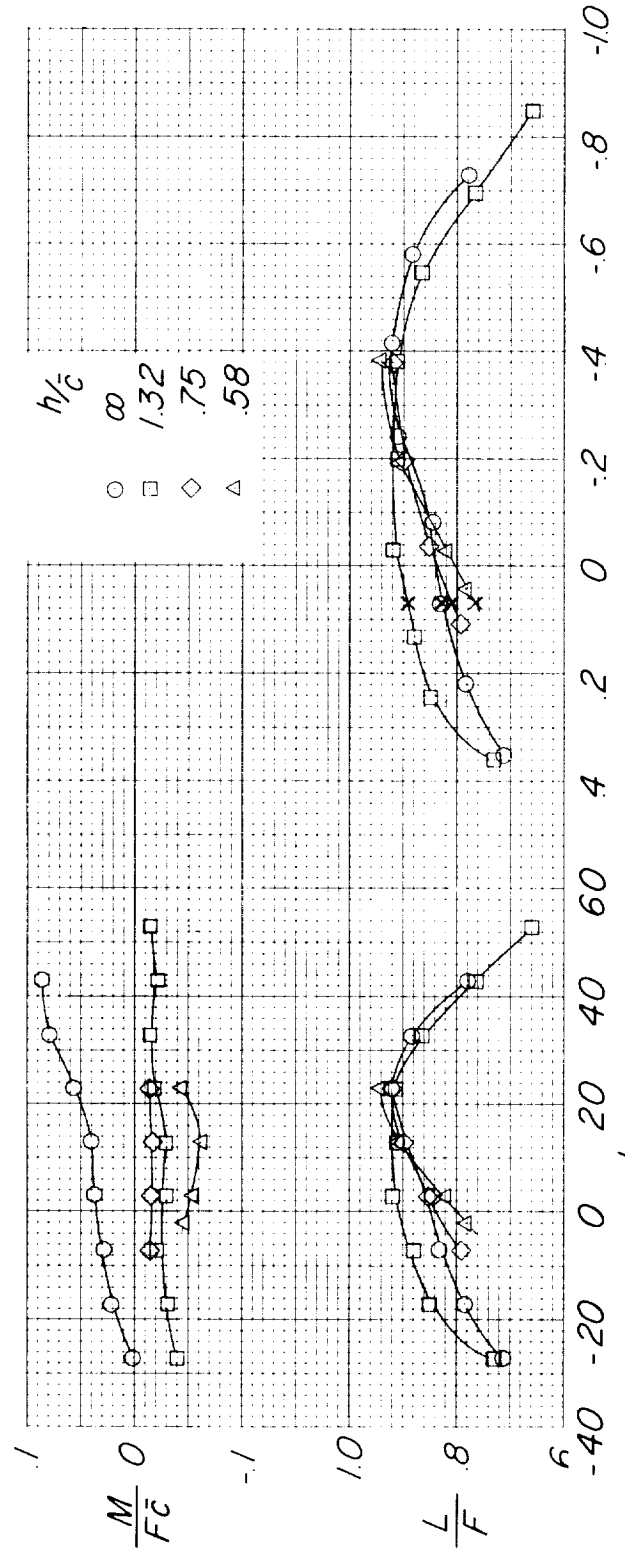

(d) $C_T = 7.5$; $V_\infty/V_j = 0.074$.

Figure 13.- Continued.

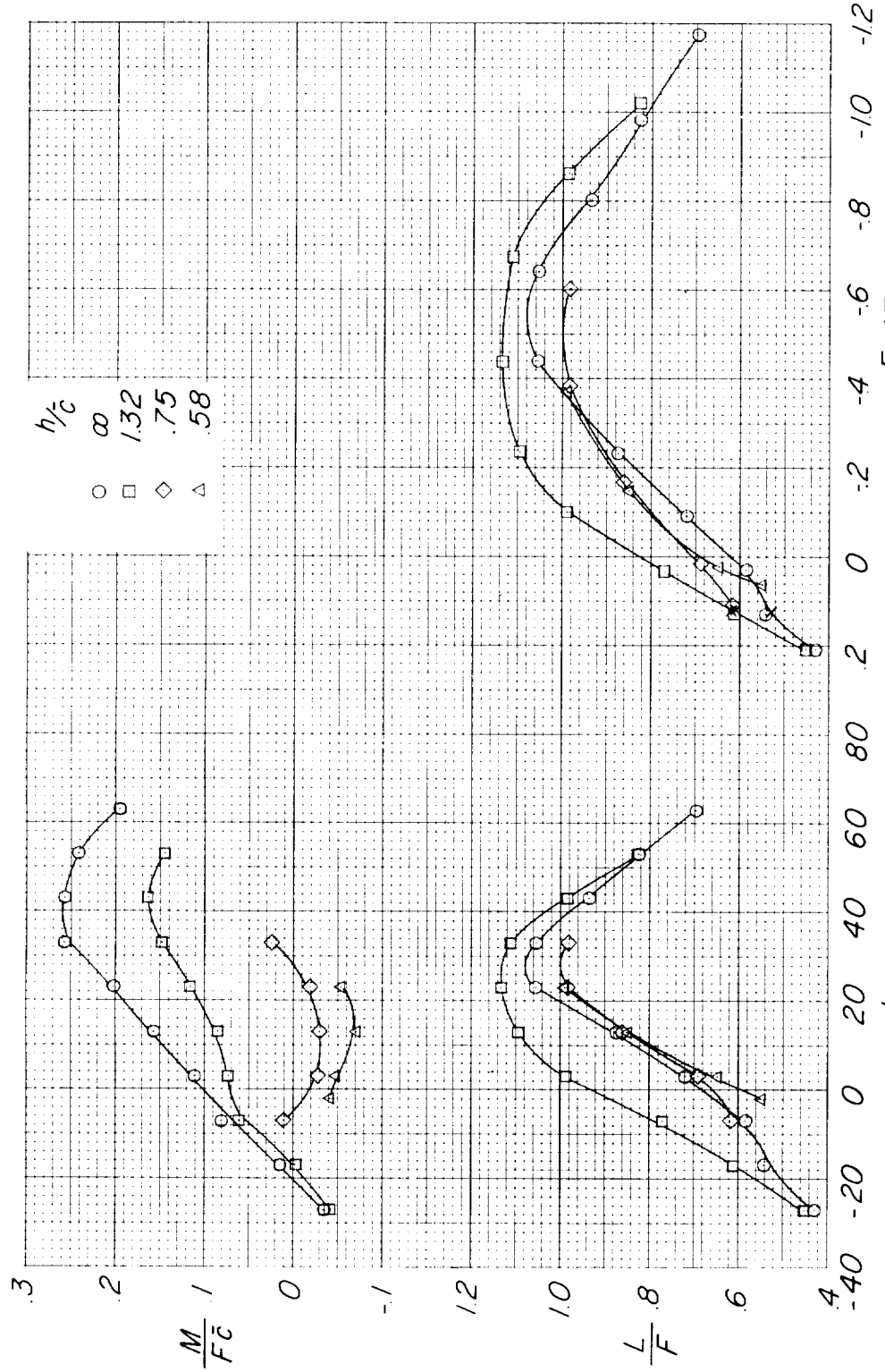

(e) $C_T = 2.1$; $V_\infty/V_j = 0.135$.

Figure 13.- Continued.

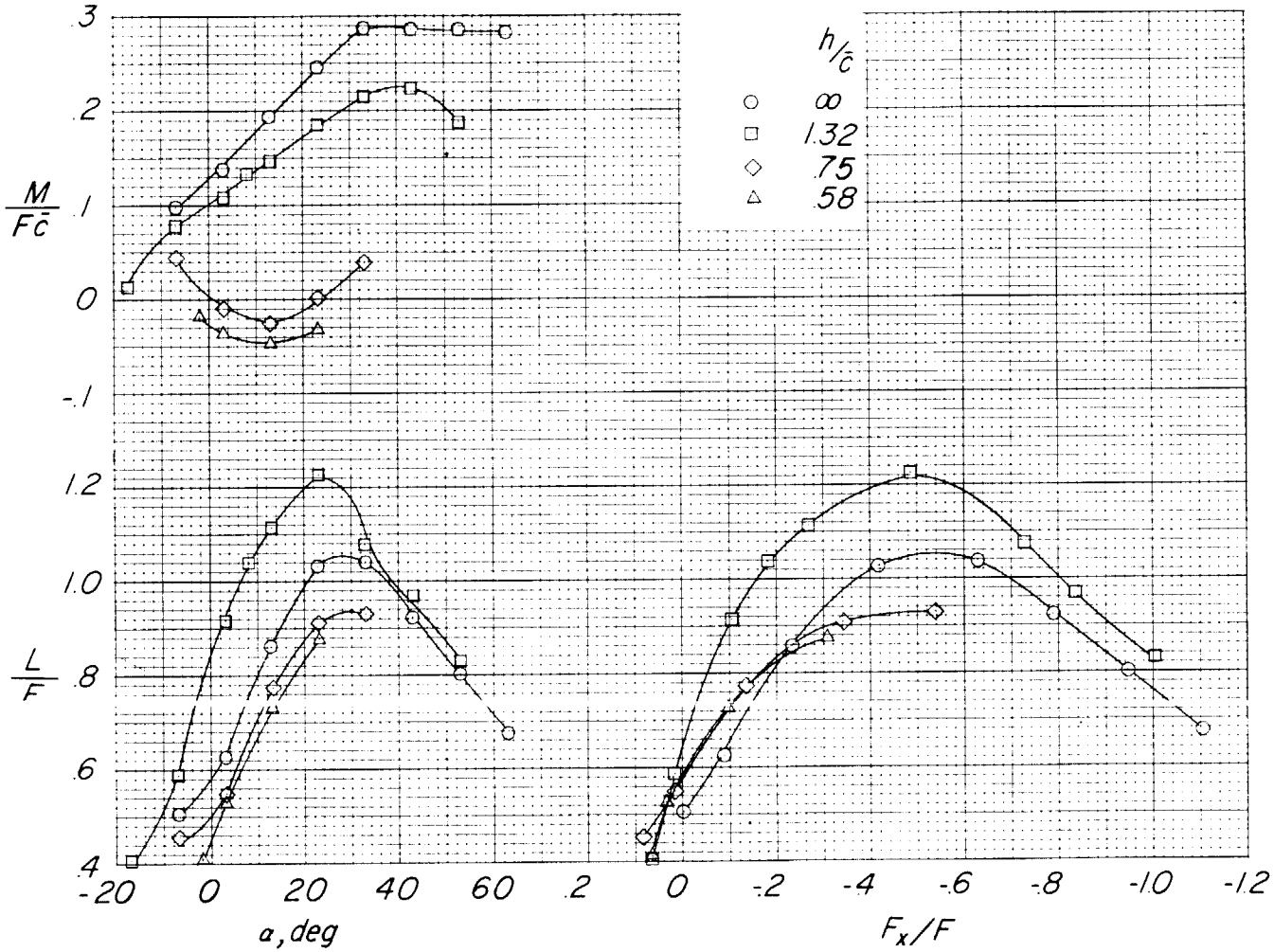

(f) $C_T = 1.7$; $V_\infty/V_j = 0.154$.

Figure 13.- Concluded.

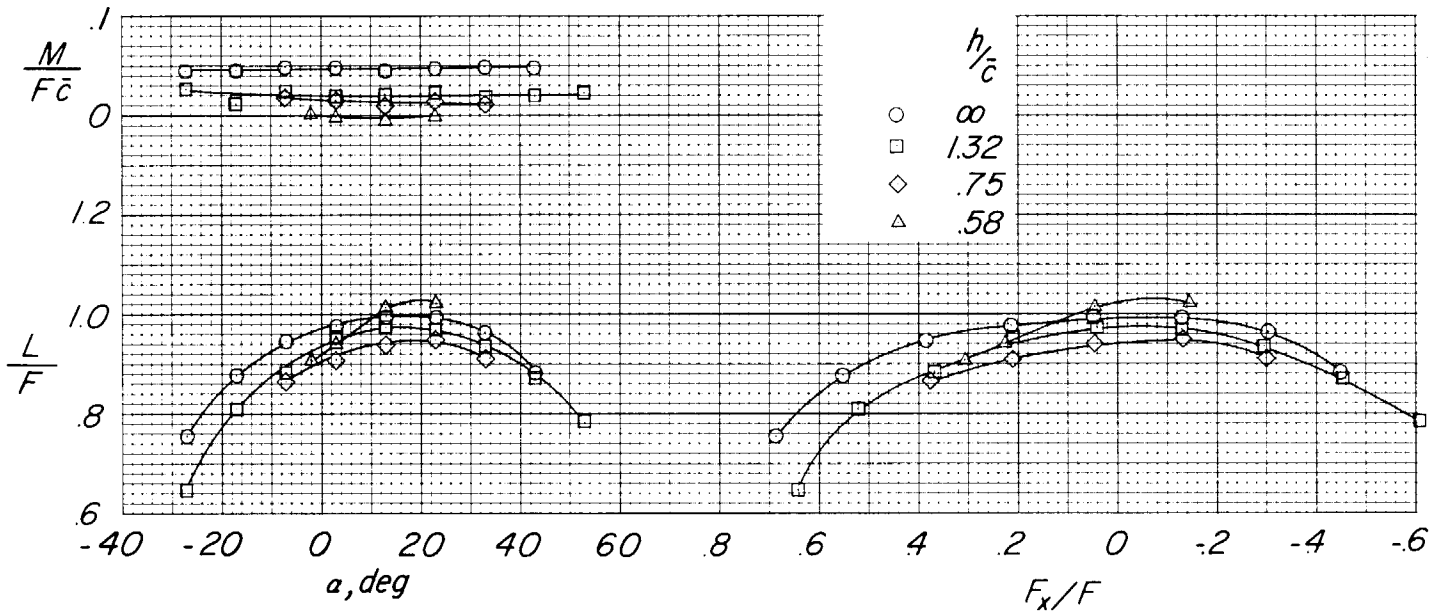

(a) $C_T = \infty$; $V_\infty/V_j = 0$.

Figure 14.- Effect of height above the ground for various thrust coefficients. A = 3.00; $\theta \approx 75^\circ$; c.g. at $0.35\bar{c}$. (×-marks indicate condition of thrust-drag equilibrium.)

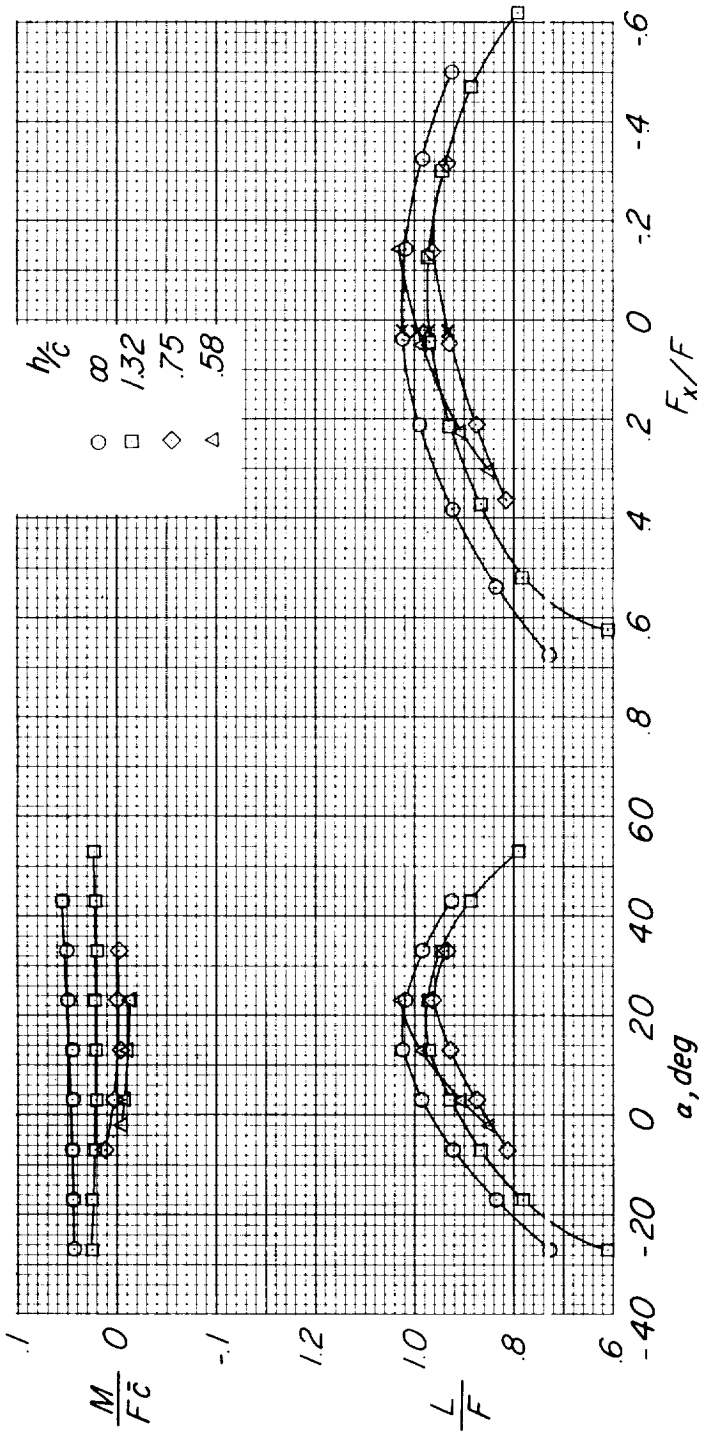

(b) C_T = 60.0; V_∞/V_j = 0.026.

Figure 14.- Continued.

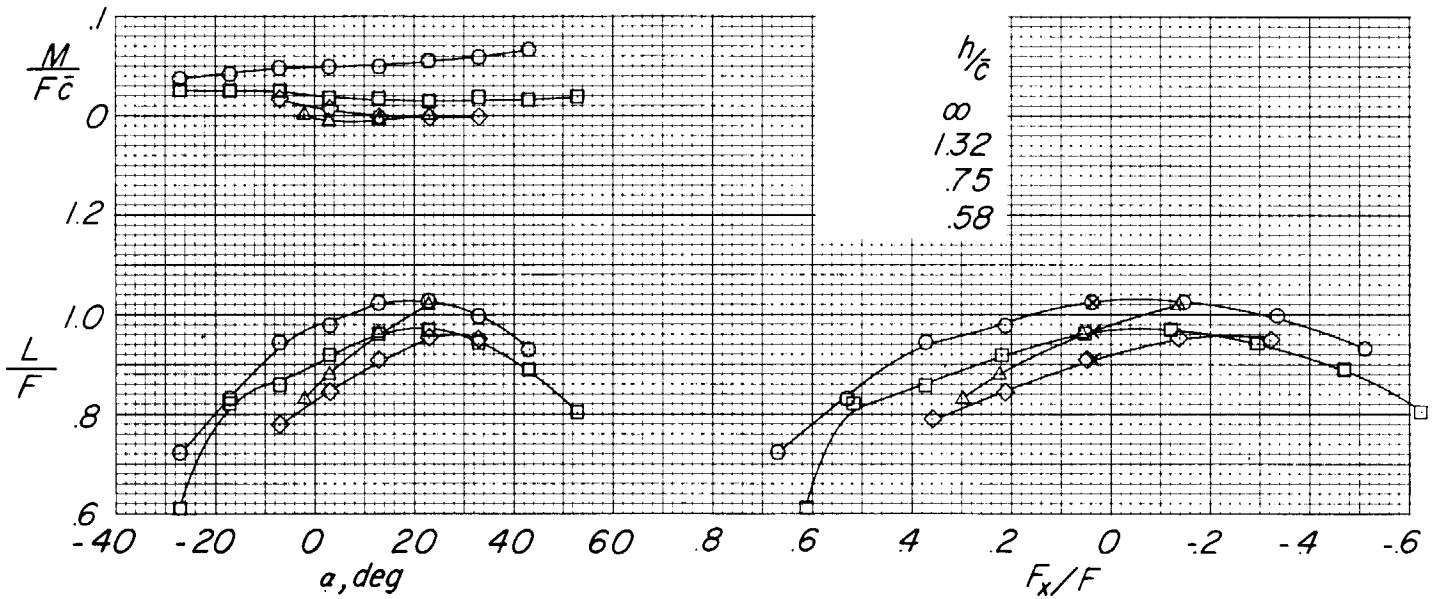

(c) $C_T = 27.2$; $V_\infty/V_j = 0.038$.

Figure 14.- Continued.

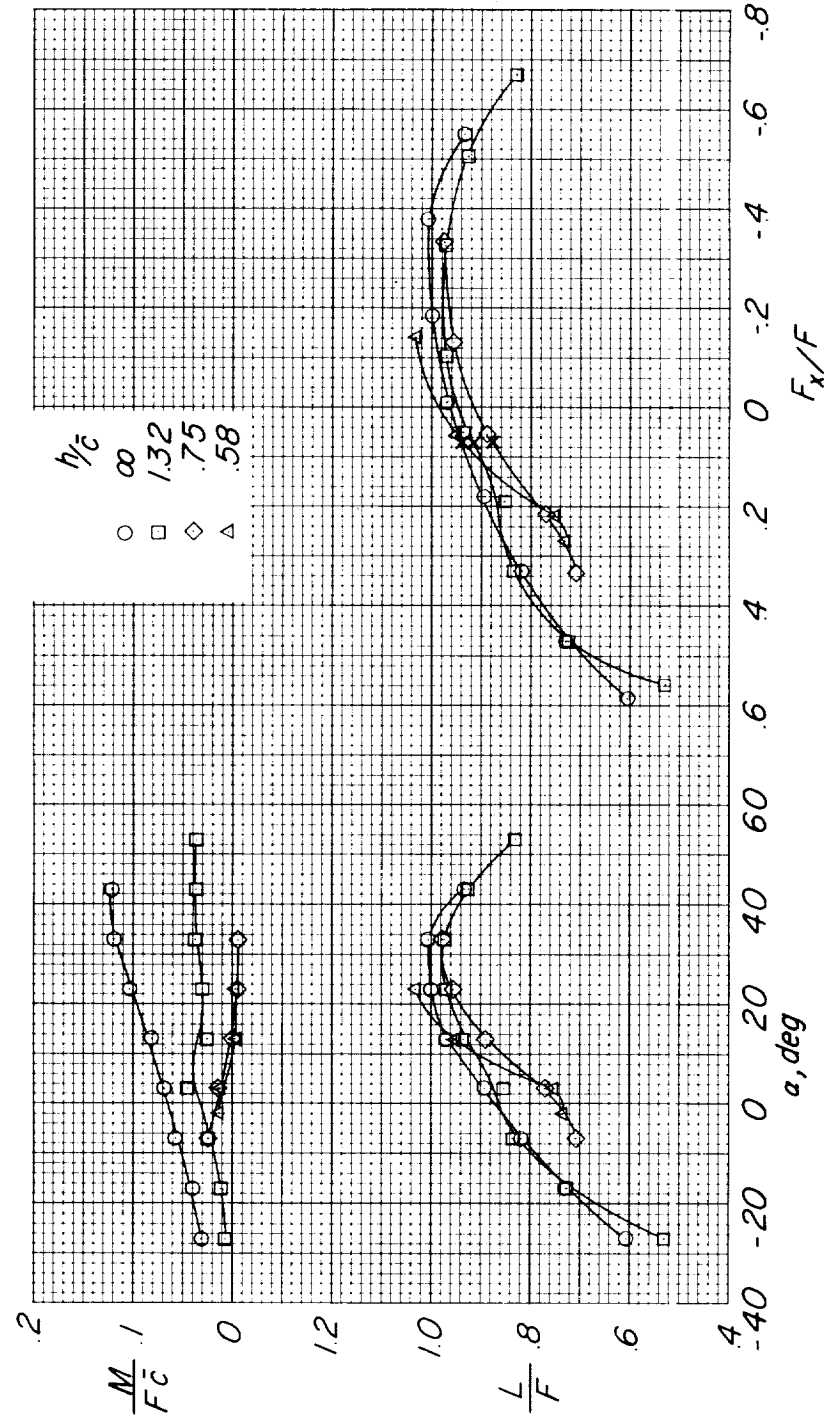

(d) $C_T = 7.5$; $V_\infty/V_j = 0.073$.

Figure 14.- Continued.

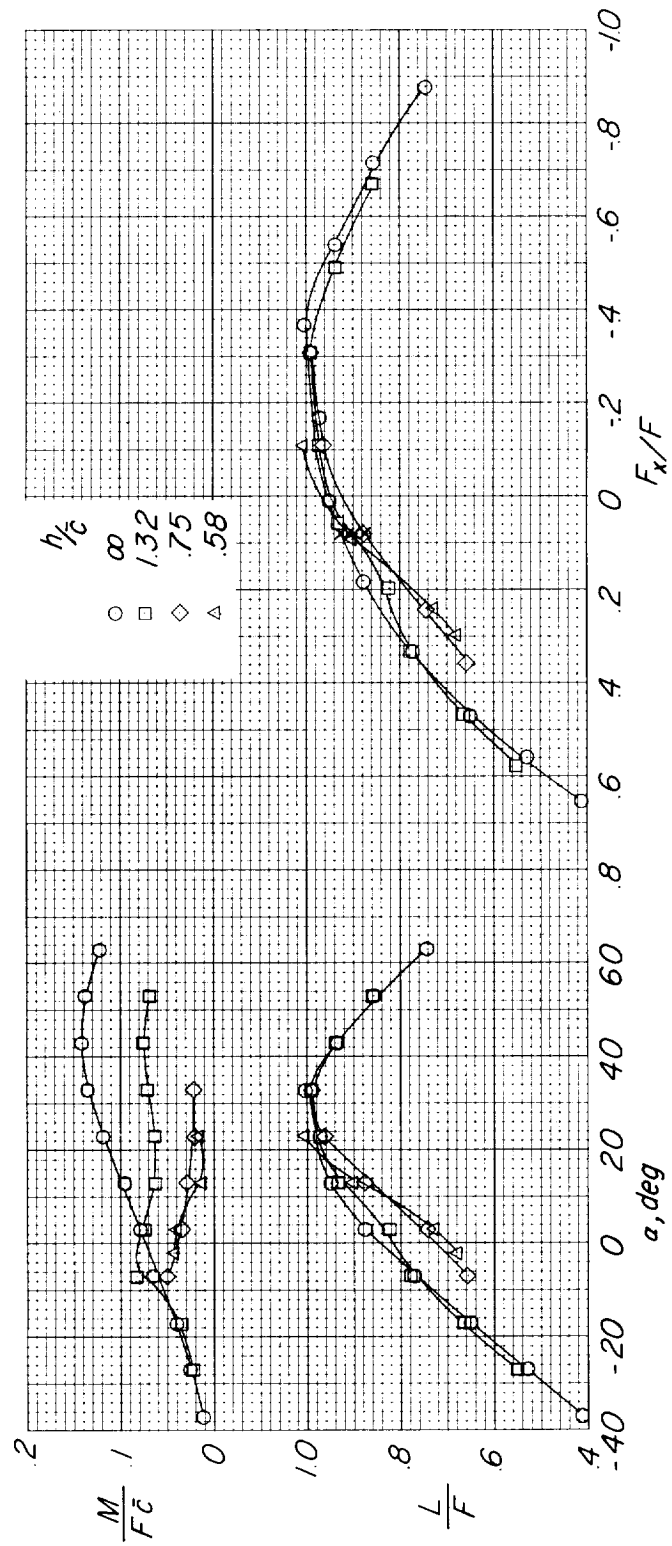

(e) $C_T = 6.0$; $V_\infty/V_j = 0.081$.

Figure 14.- Continued.

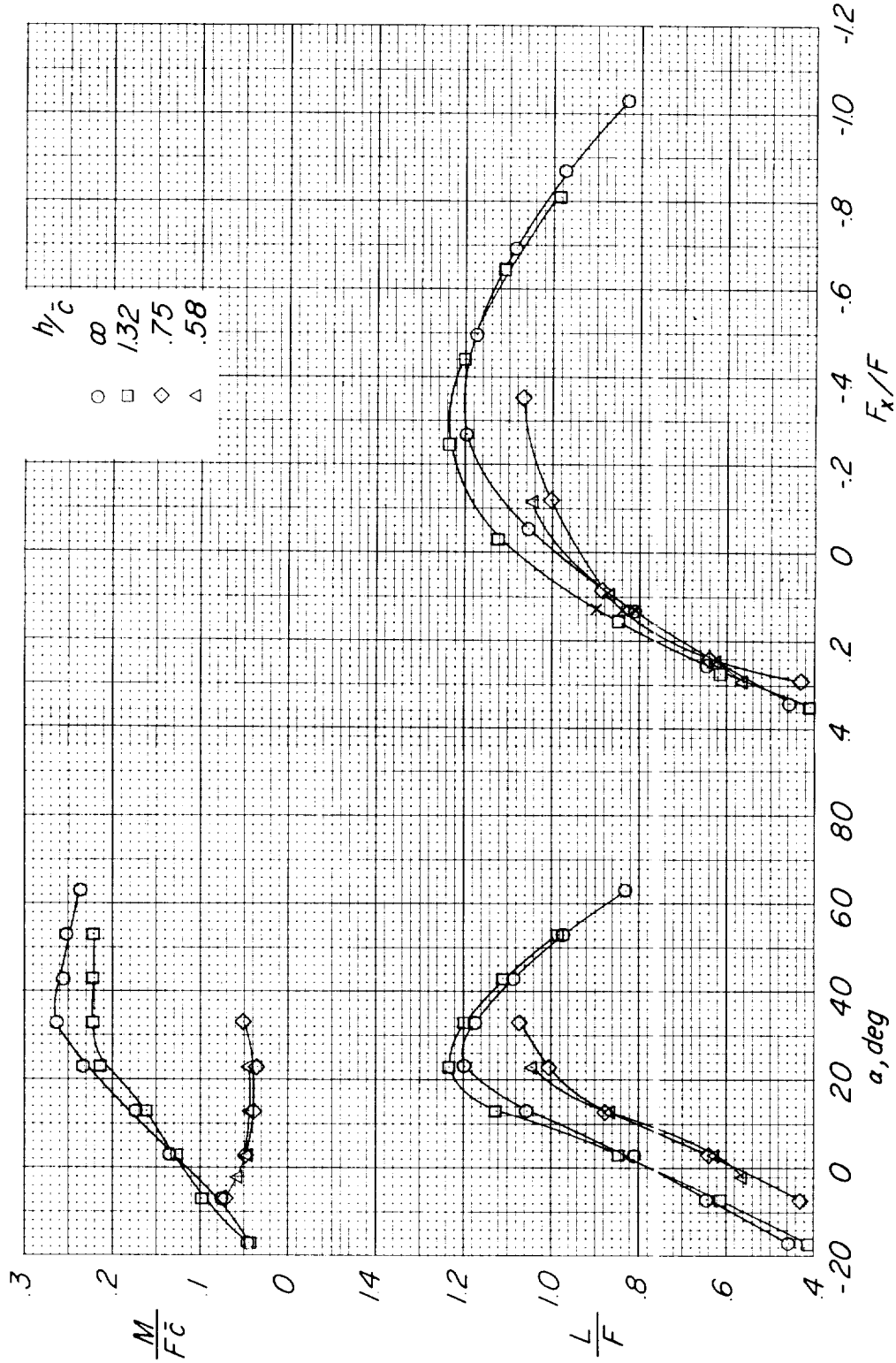

(f) $C_T = 2.2$; $V_\infty/V_j = 0.134$.

Figure 14.- Continued.

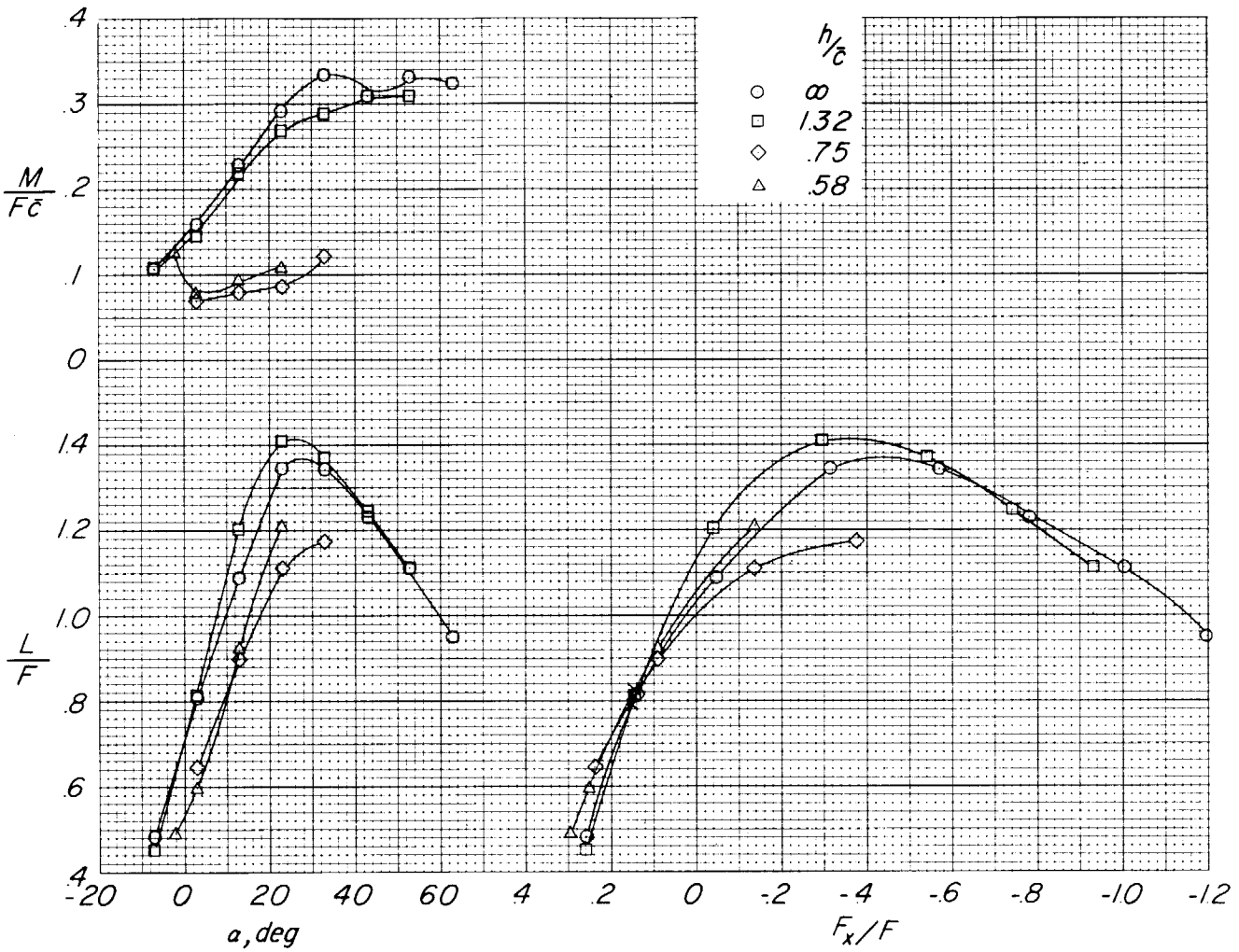

(g) $C_T = 1.6$; $V_\infty/V_j = 0.153$.

Figure 14.- Continued.

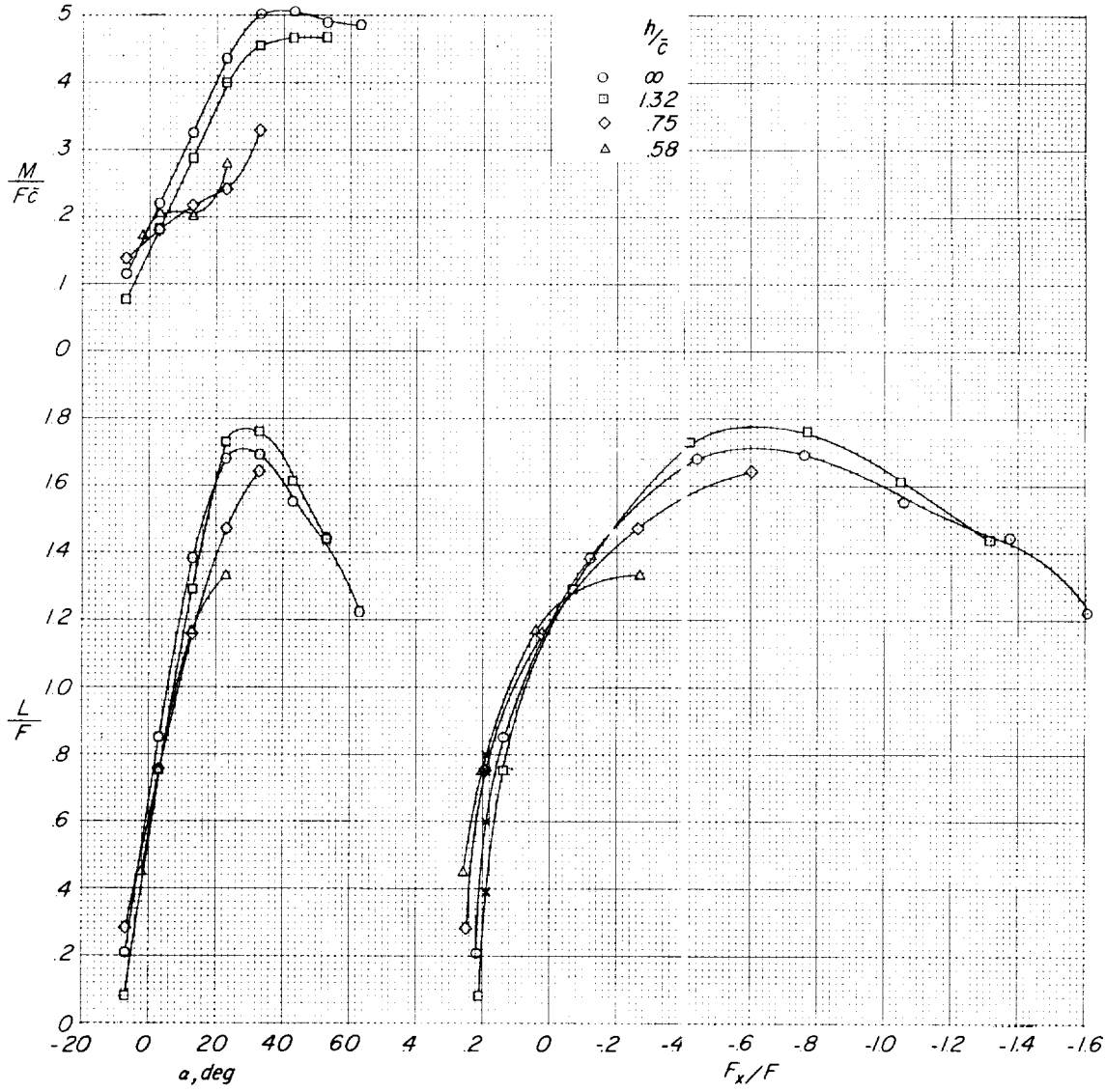

(h) $C_T = 0.9$; $V_\infty/V_j = 0.191$.

Figure 14.- Concluded.

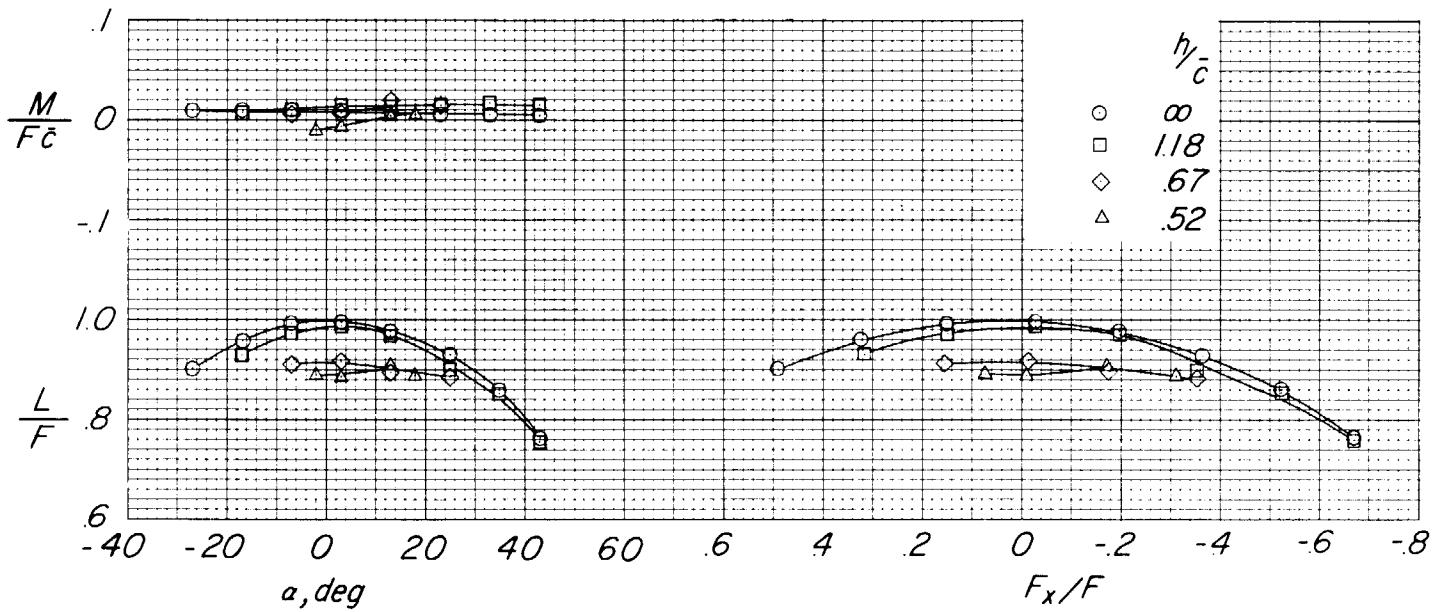

(a) $C_T = \infty$; $V_\infty/V_j = 0$.

Figure 15.- Effect of height above the ground for various thrust coefficients. A = 1.55; $\theta \approx 90^\circ$; c.g. at 0.20c̄. (×-marks indicate condition of thrust-drag equilibrium.)

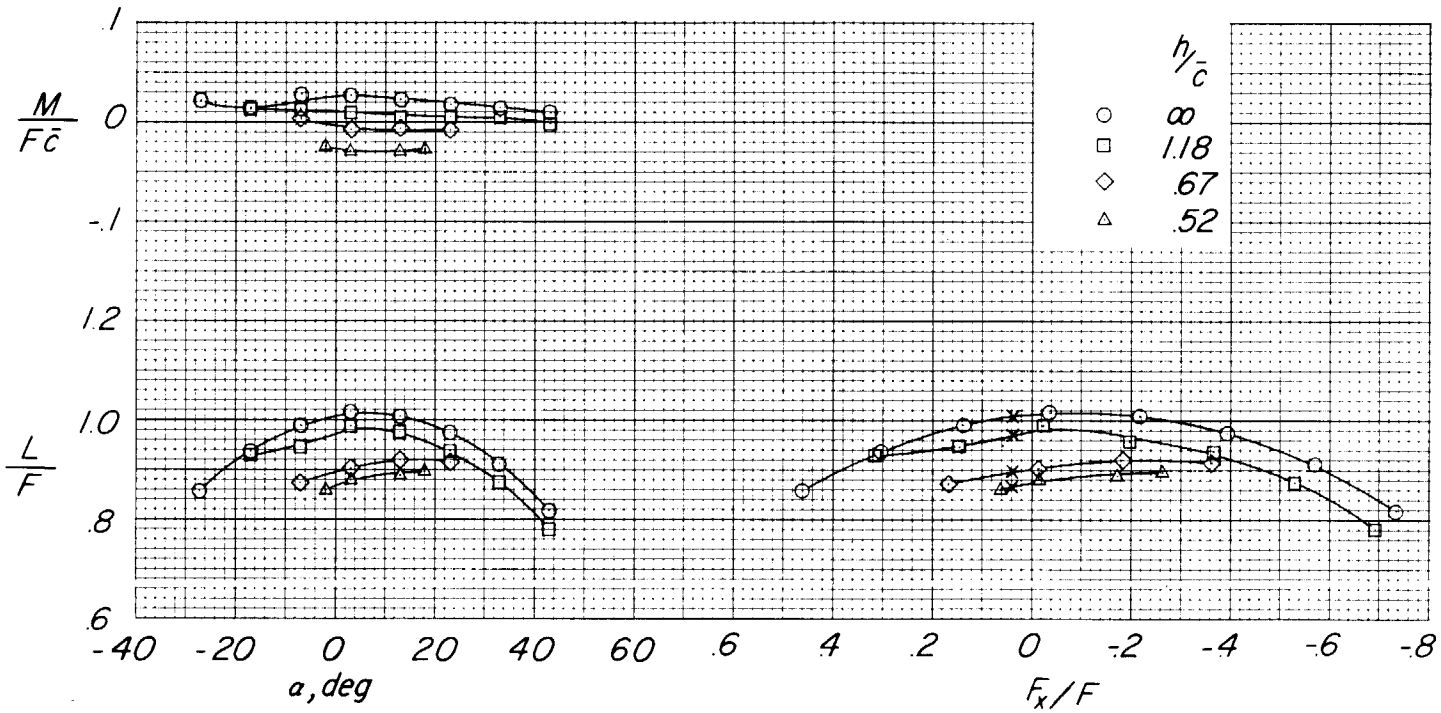

(b) $C_T = 32.7$; $V_\infty/V_j = 0.039$.

Figure 15.- Continued.

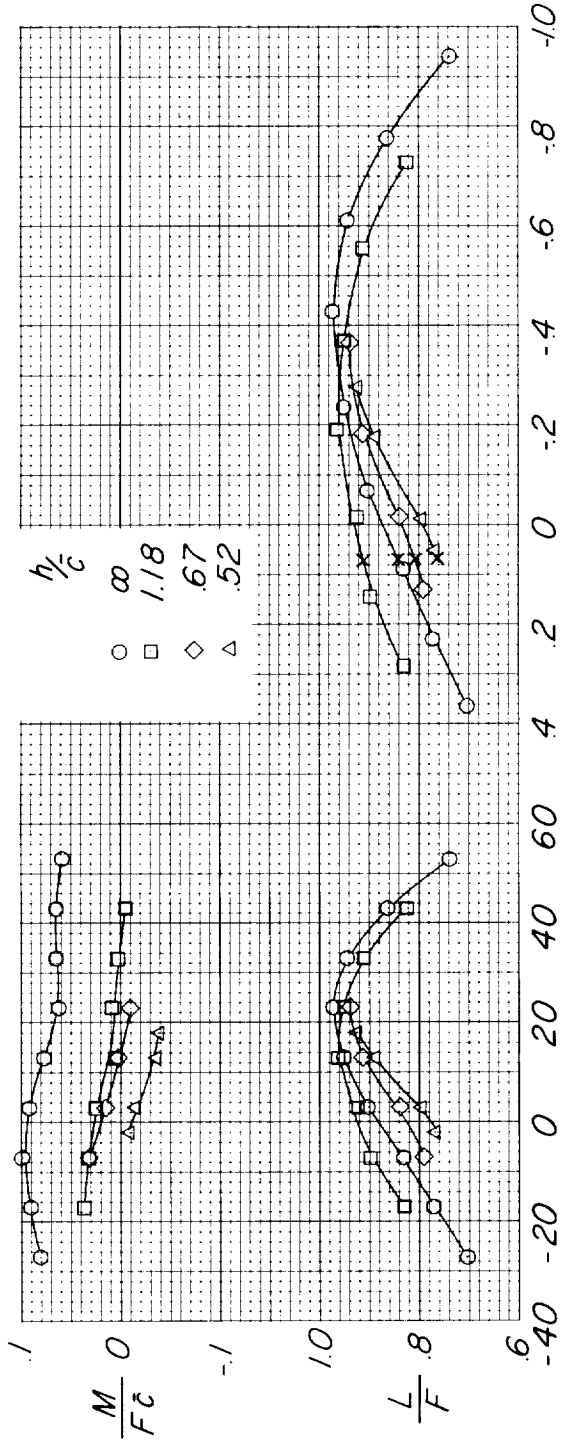

(c) $C_T = 9.0$; $V_\infty/V_j = 0.074$.

Figure 15.- Continued.

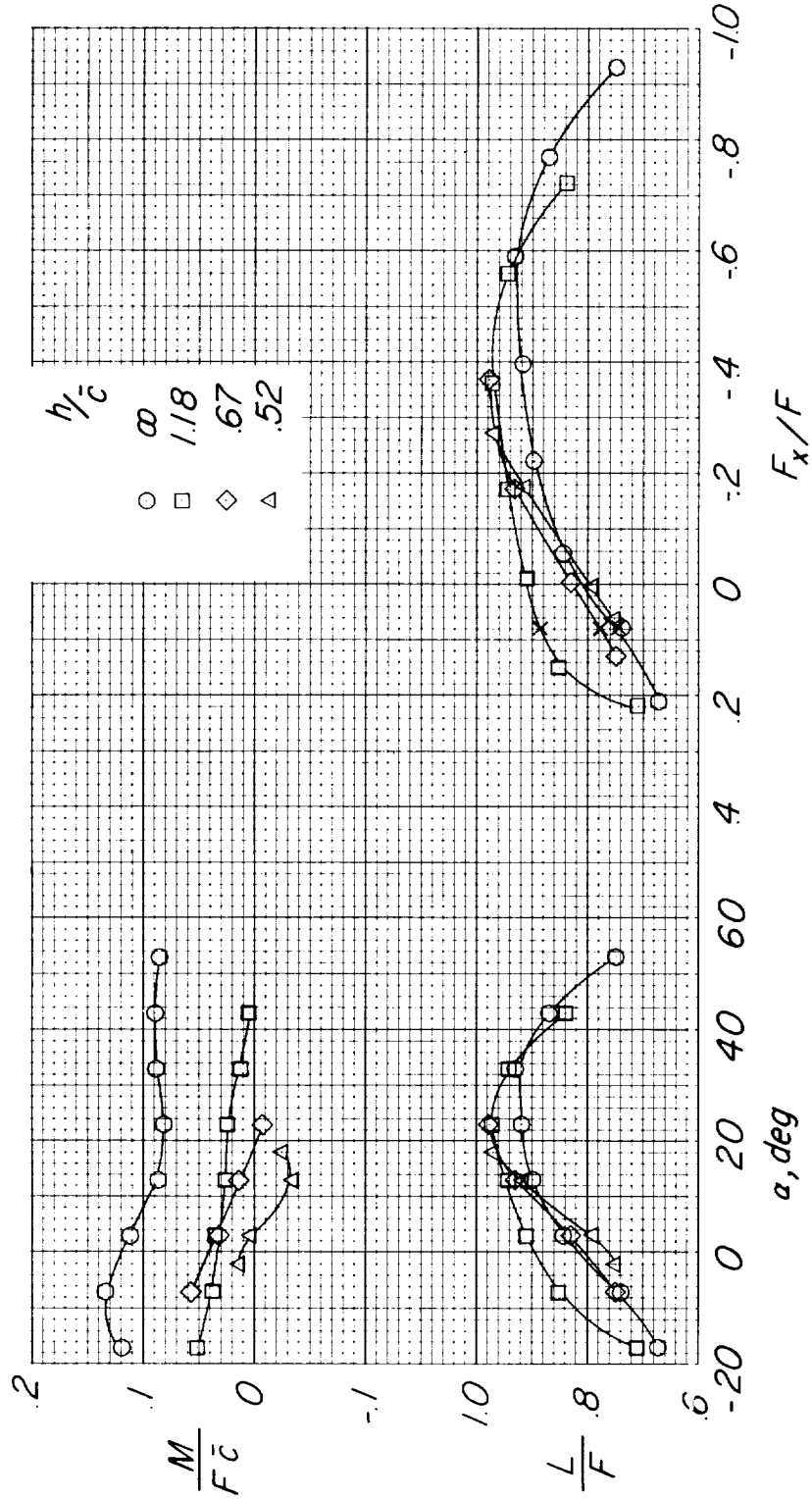

(d) $C_T = 7.0$; $V_\infty/V_j = 0.082$.

Figure 15.- Continued.

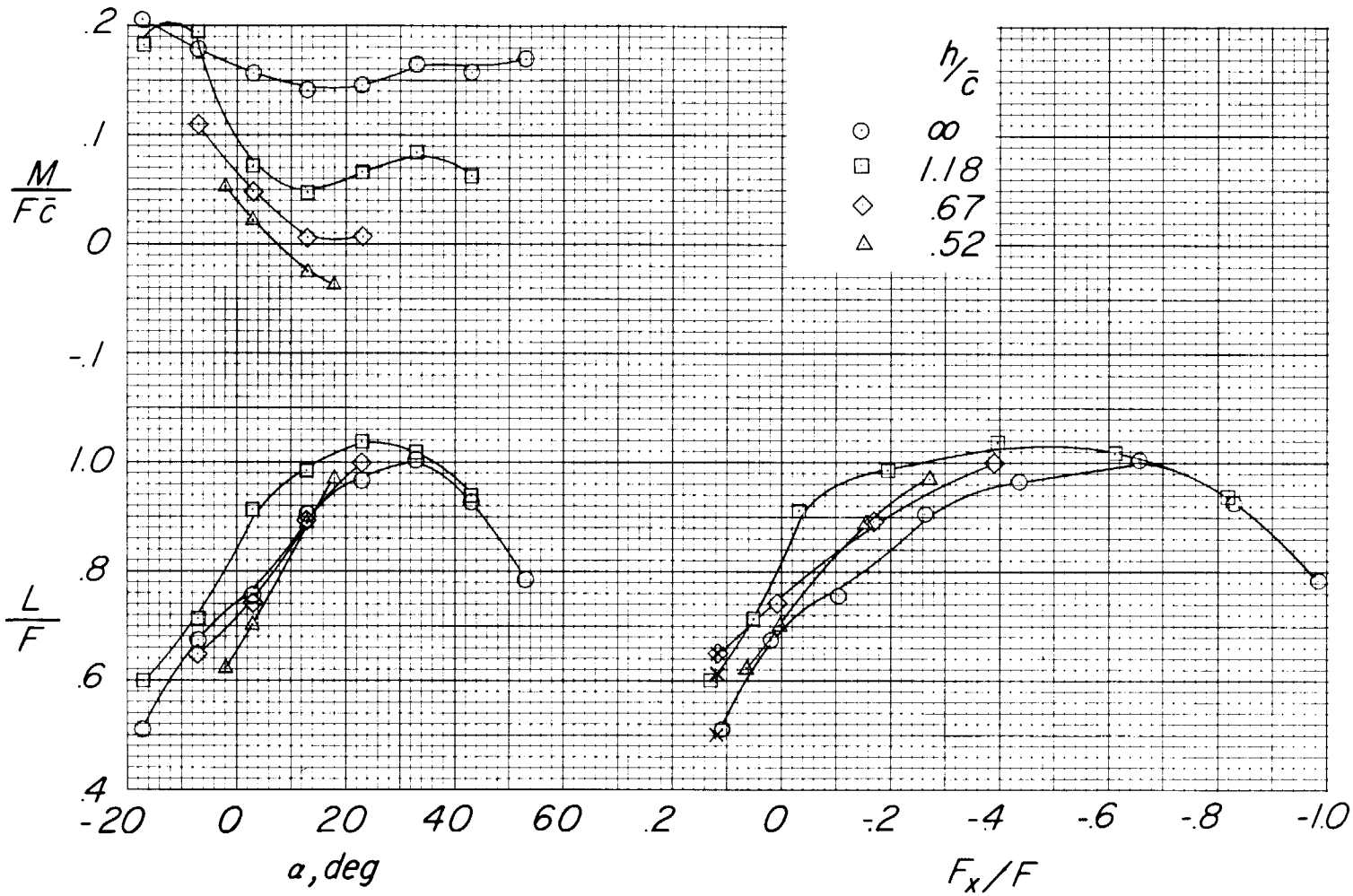

(e) $C_T = 3.3$; $V_\infty/V_j = 0.121$.

Figure 15.- Continued.

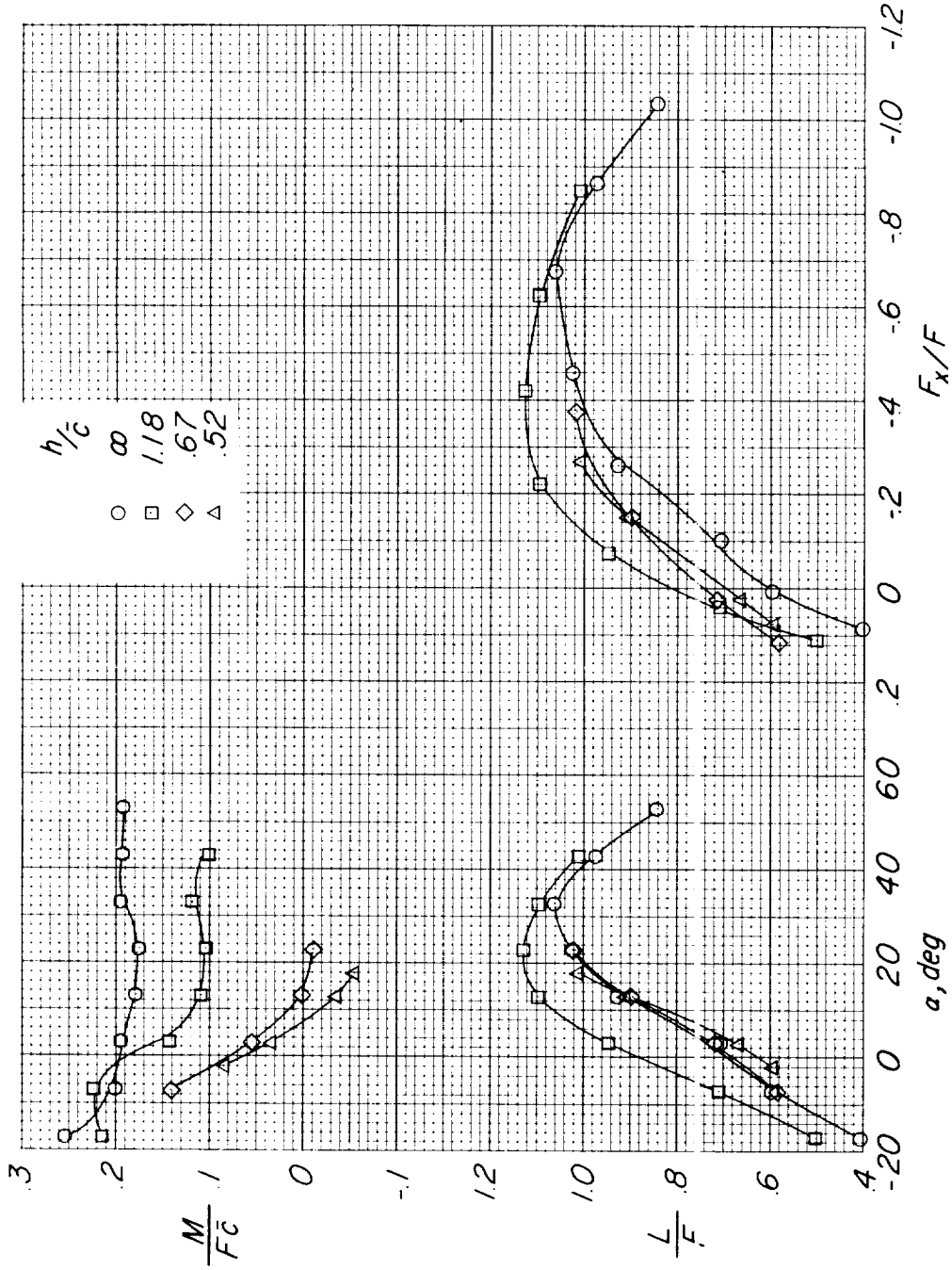

(f) $C_T = 2.5$; $V_\infty/V_j = 0.135$.

Figure 15.- Continued.

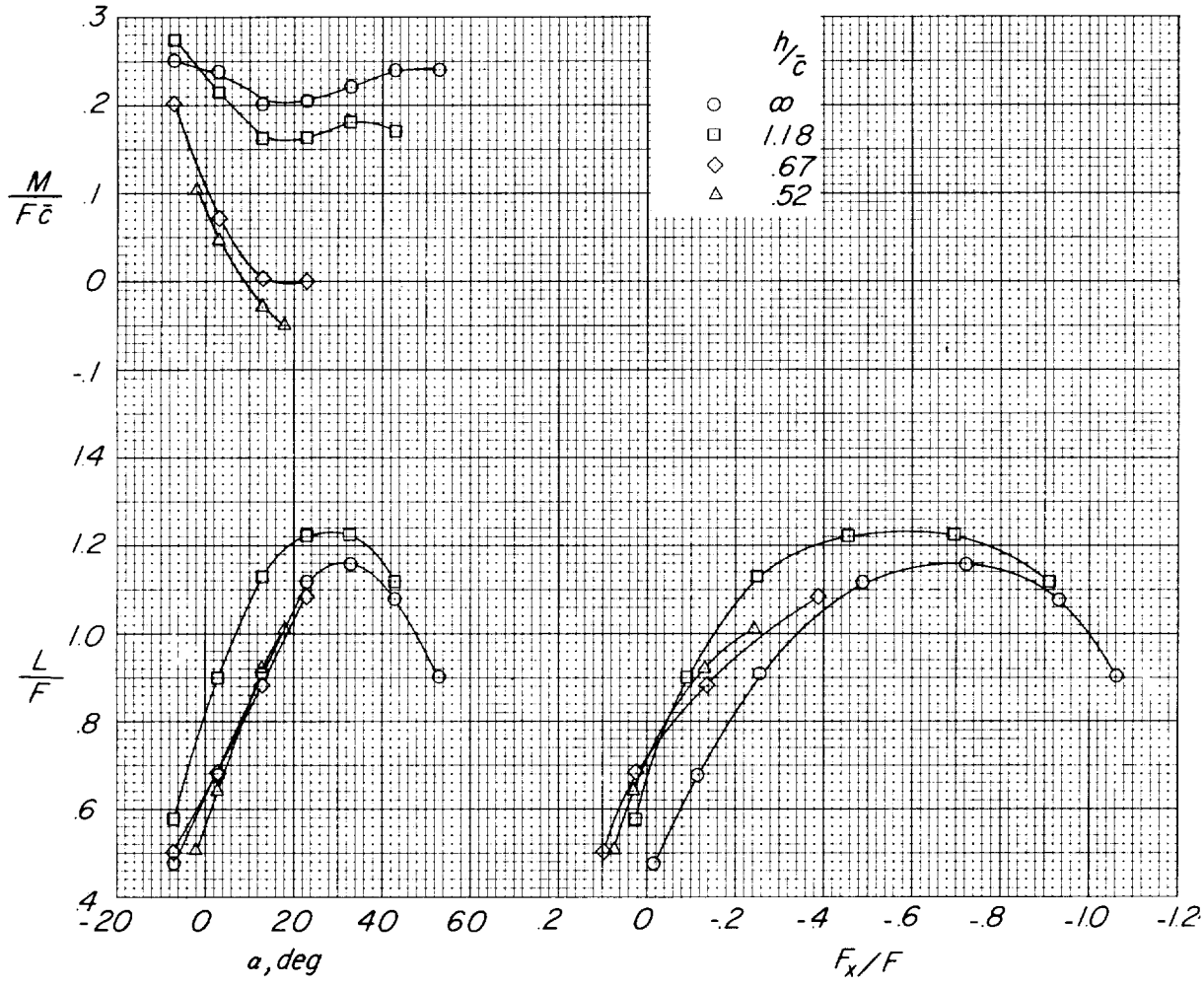

(g) $C_T = 1.9$; $V_\infty/V_j = 0.153$.

Figure 15.- Continued.

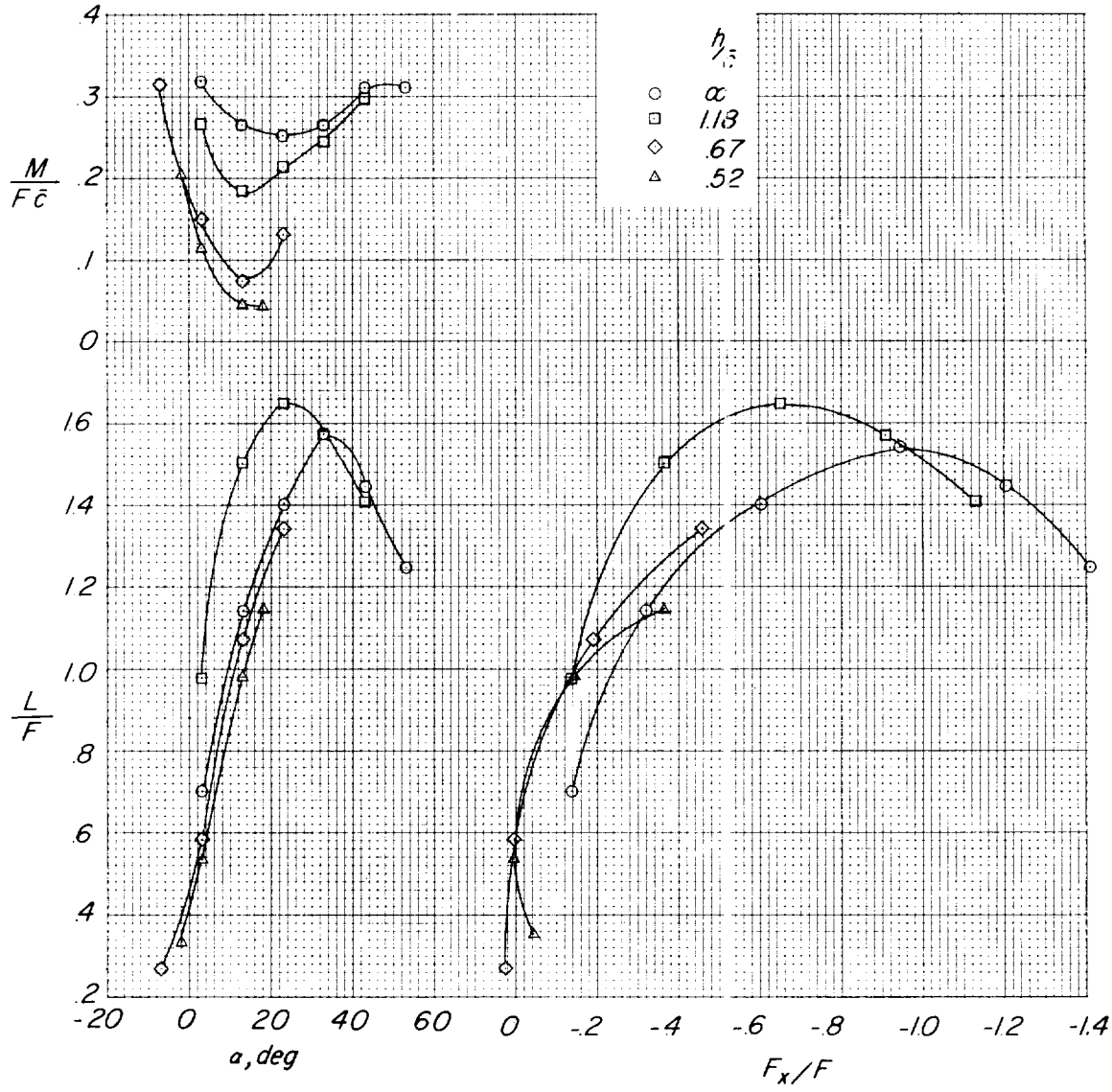

(h) $C_T = 1.1$; $V_\infty/V_j = 0.195$.

Figure 15.- Concluded.

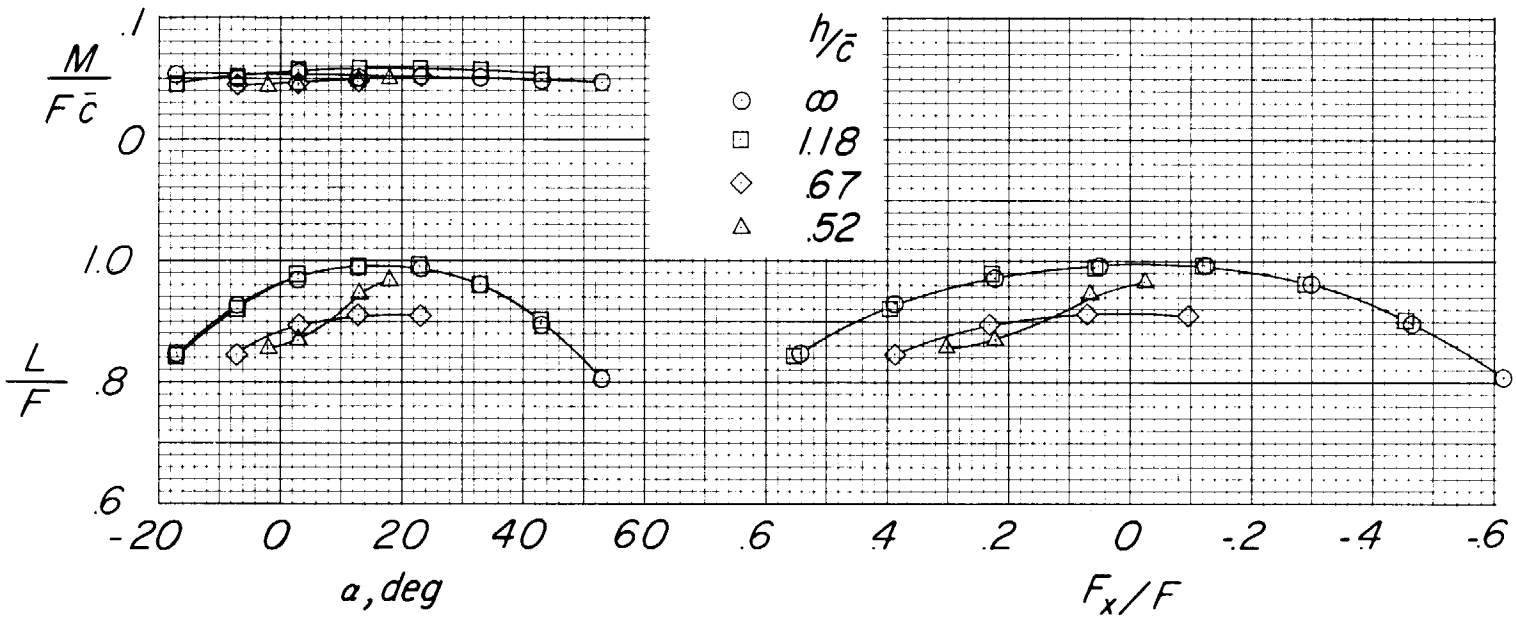

(a) $C_T = \infty$; $V_\infty/V_j = 0$.

Figure 16.- Effect of height above the ground for various thrust coefficients. A = 1.55; $\theta \approx 75^\circ$; c.g. at 0.20$\bar{c}$. (×-marks indicate condition of thrust-drag equilibrium.)

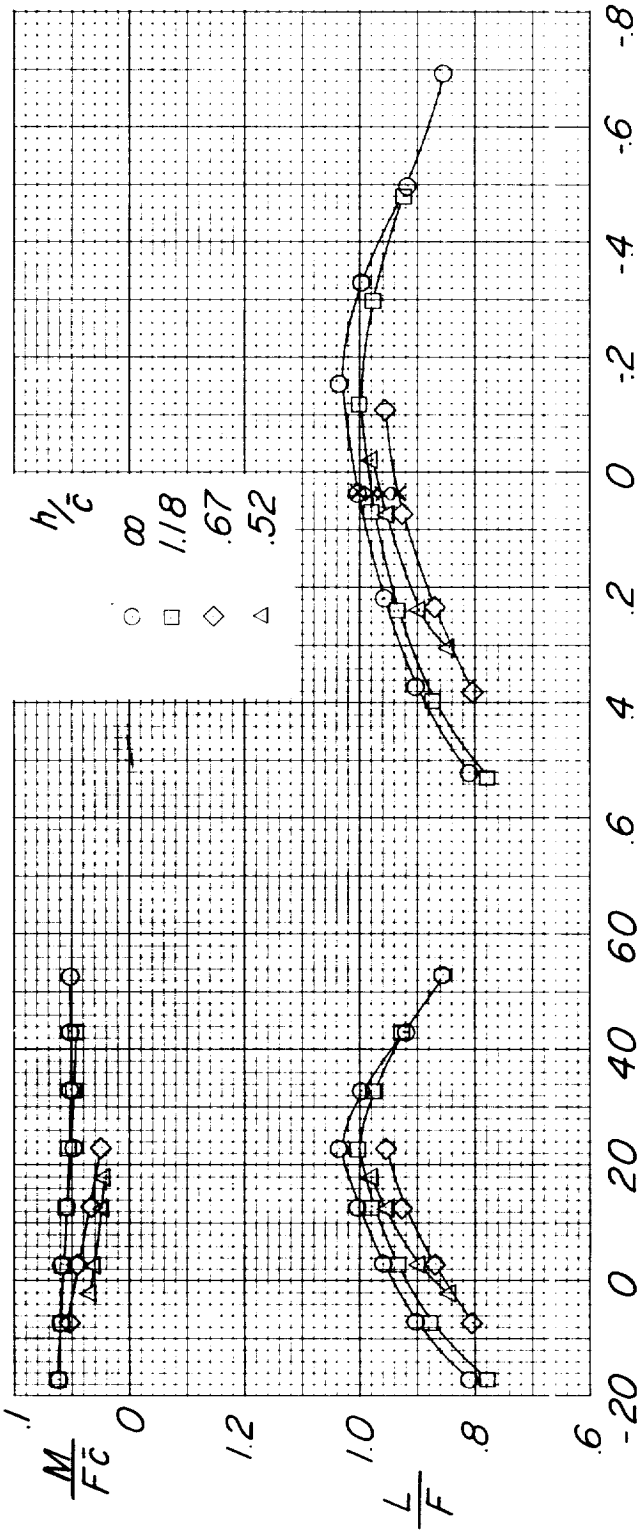

(b) $C_T = 33.5$; $V_\infty/V_j = 0.038$.

Figure 16.- Continued.

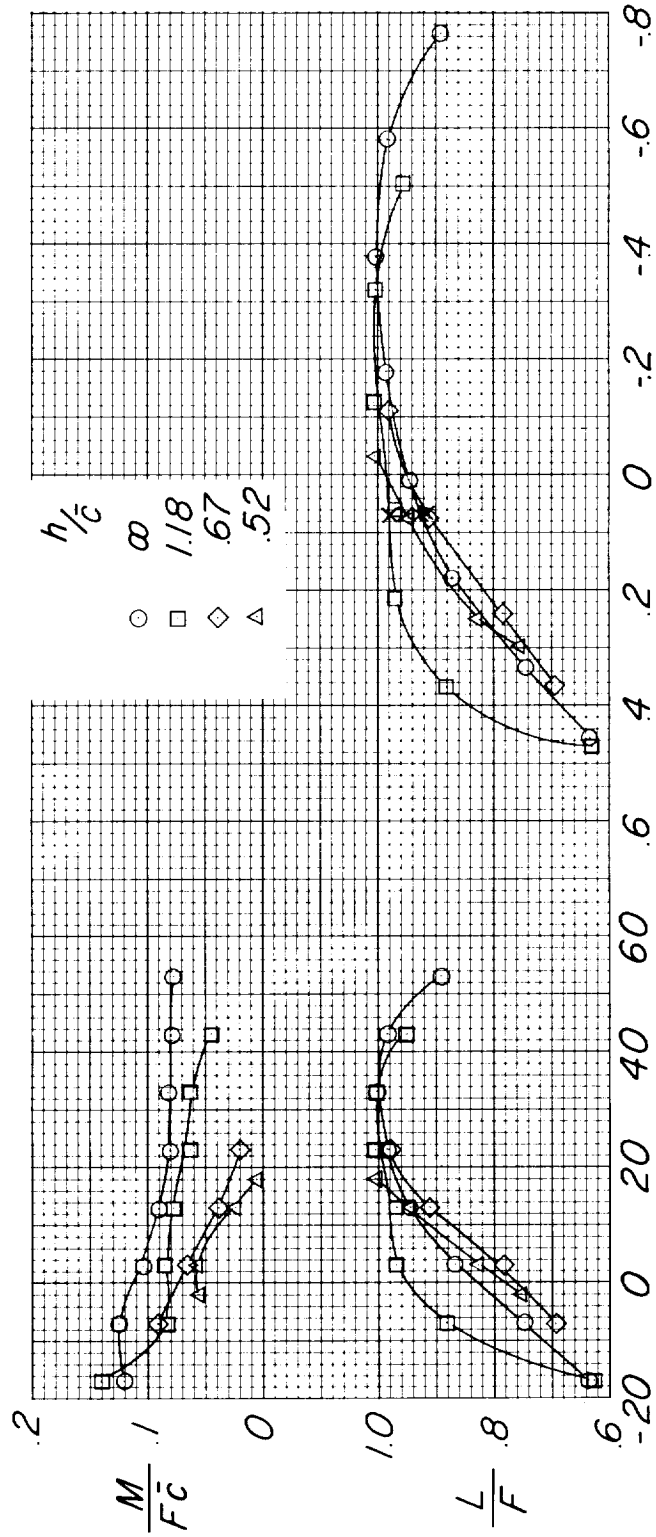

(c) $C_T = 9.3$; $V_\infty/V_j = 0.073$.

Figure 16.- Continued.

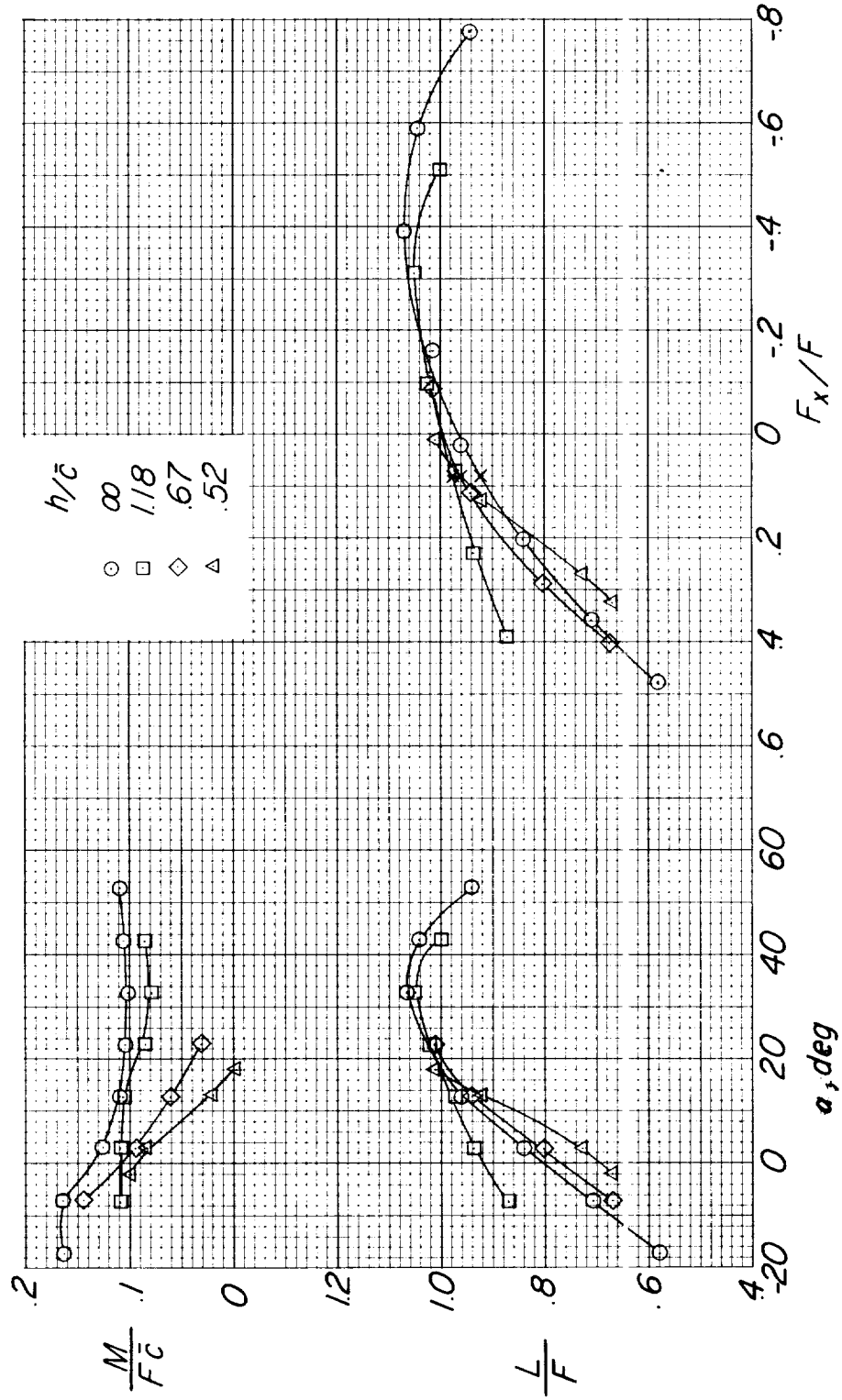

(d) $C_T = 7.0$; $V_\infty/V_j = 0.080$.

Figure 16.- Continued.

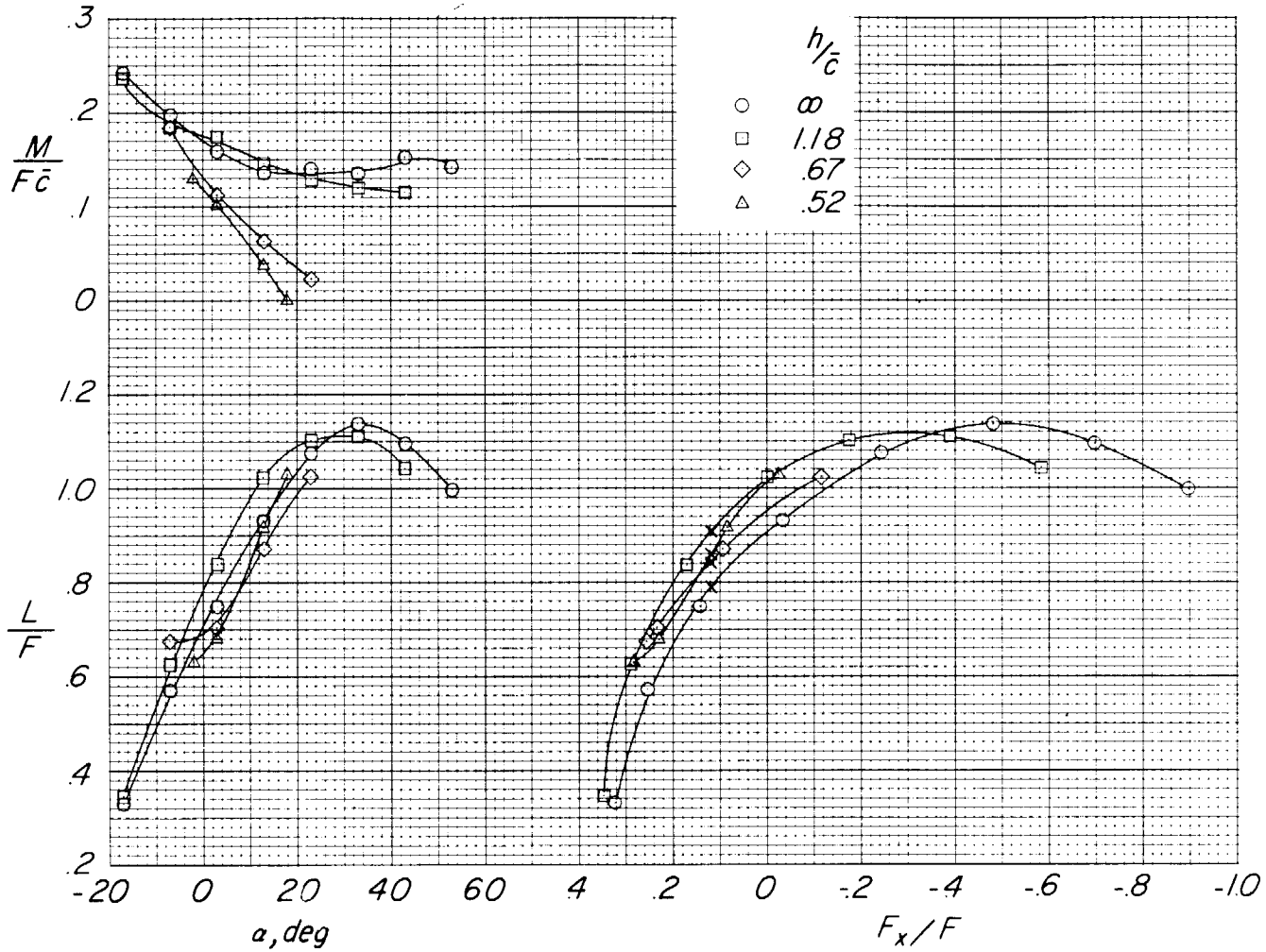

(e) $C_T = 3.4$; $V_\infty/V_j = 0.120$.

Figure 16.- Continued.

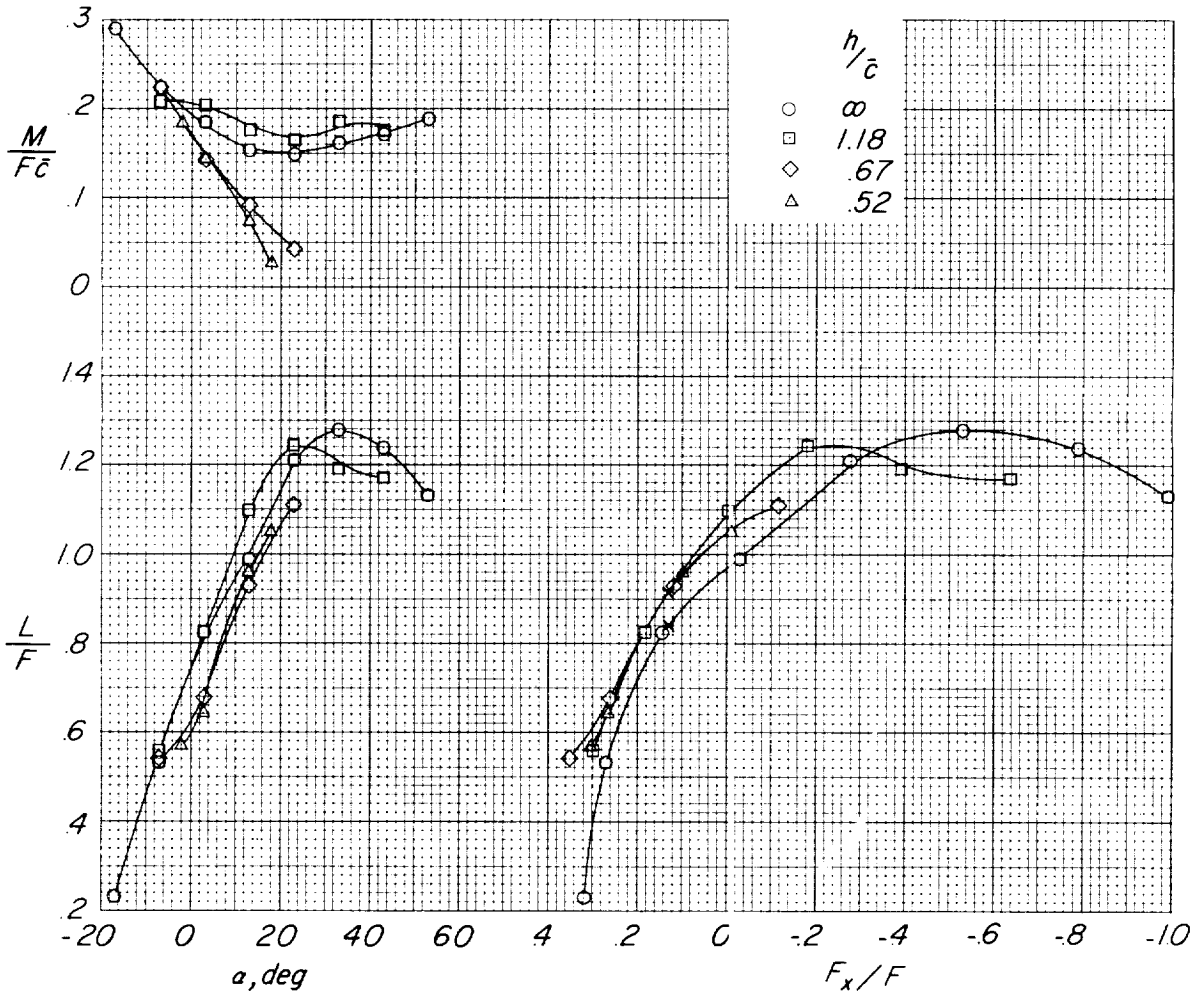

(f) $C_T = 2.5$; $V_\infty/V_j = 0.134$.

Figure 16.- Continued.

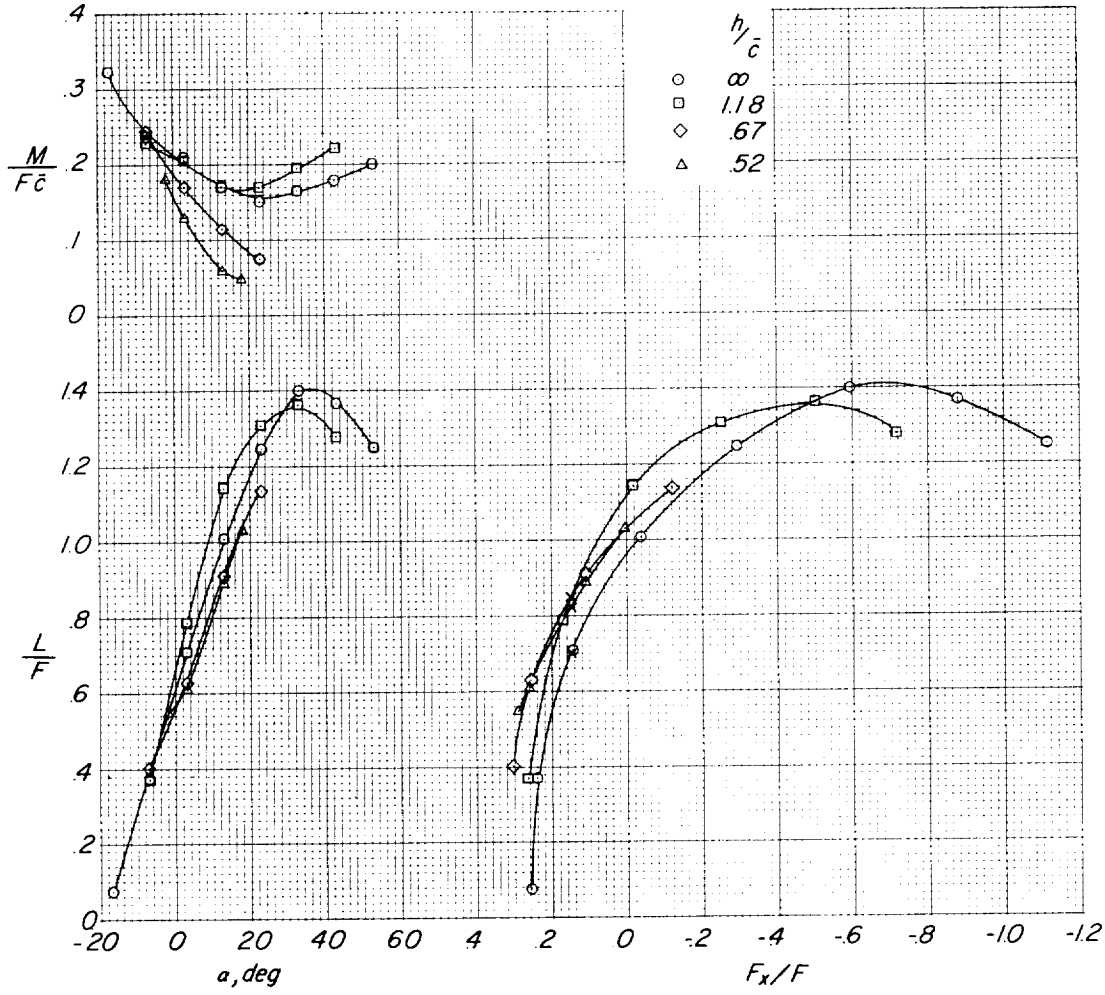

(g) $C_T = 1.9$; $V_\infty/V_j = 0.152$.

Figure 16.- Continued.

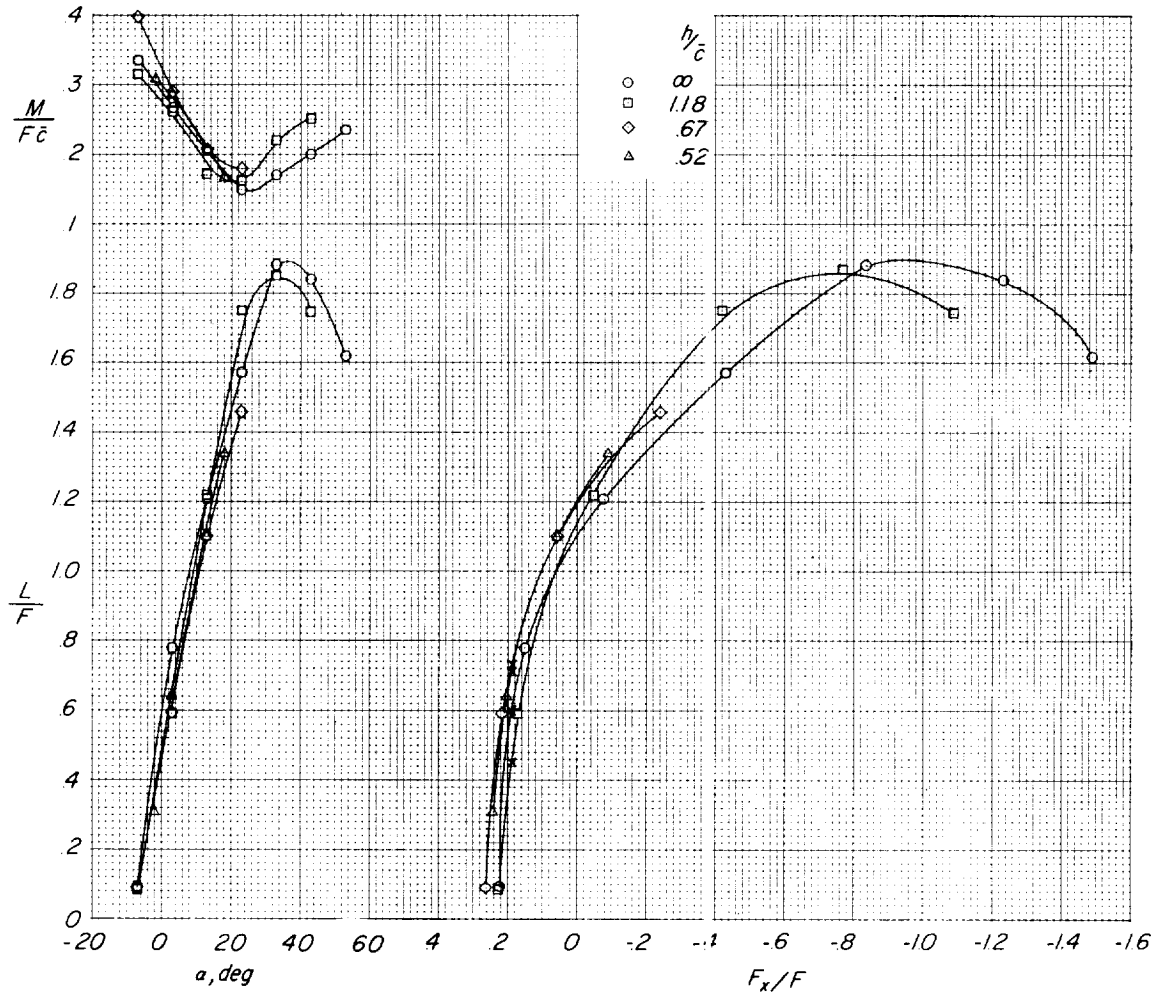

(h) $C_T = 1.1$; $V_\infty/V_j = 0.191$.

Figure 16.- Concluded.

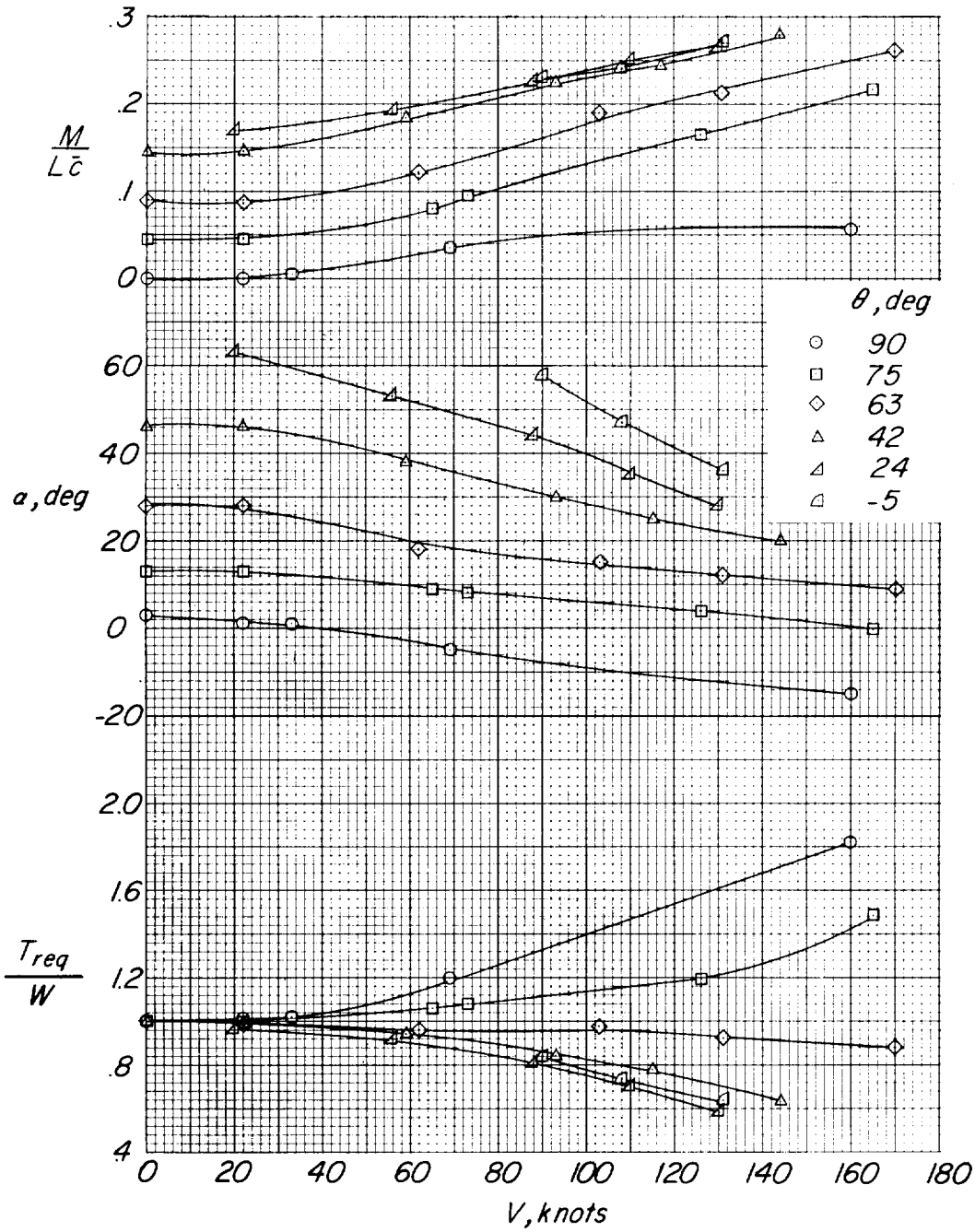

(a) A = 3.00; c.g. at 0.35c̄.

Figure 17.- Effect of static turning angle on ratio of thrust required to weight, angle of attack, and pitching moment in steady level flight. W/S = 100 lb/sq ft.

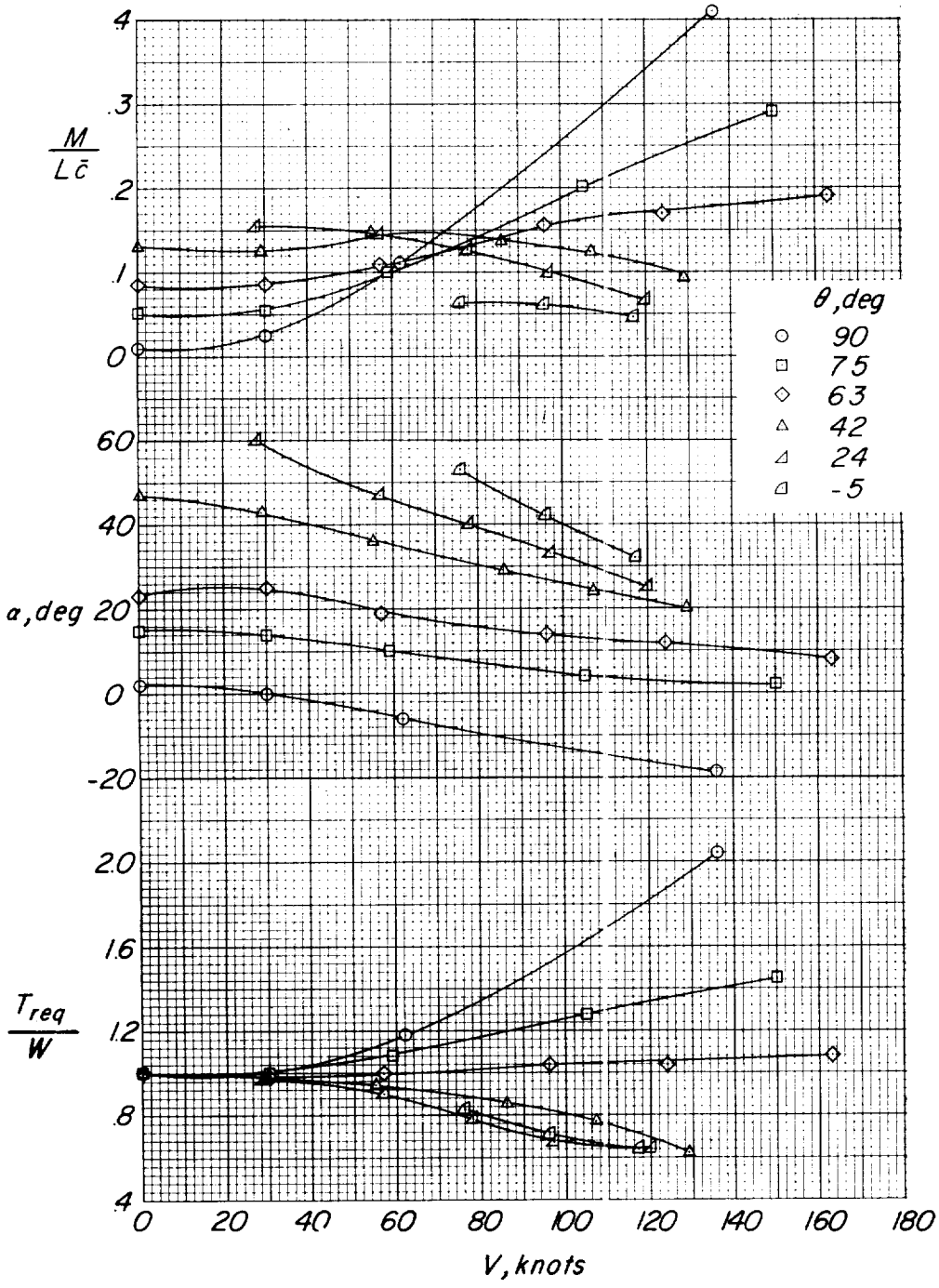

(b) A = 1.55; c.g. at 0.20$\bar{c}$.

Figure 17.- Concluded.

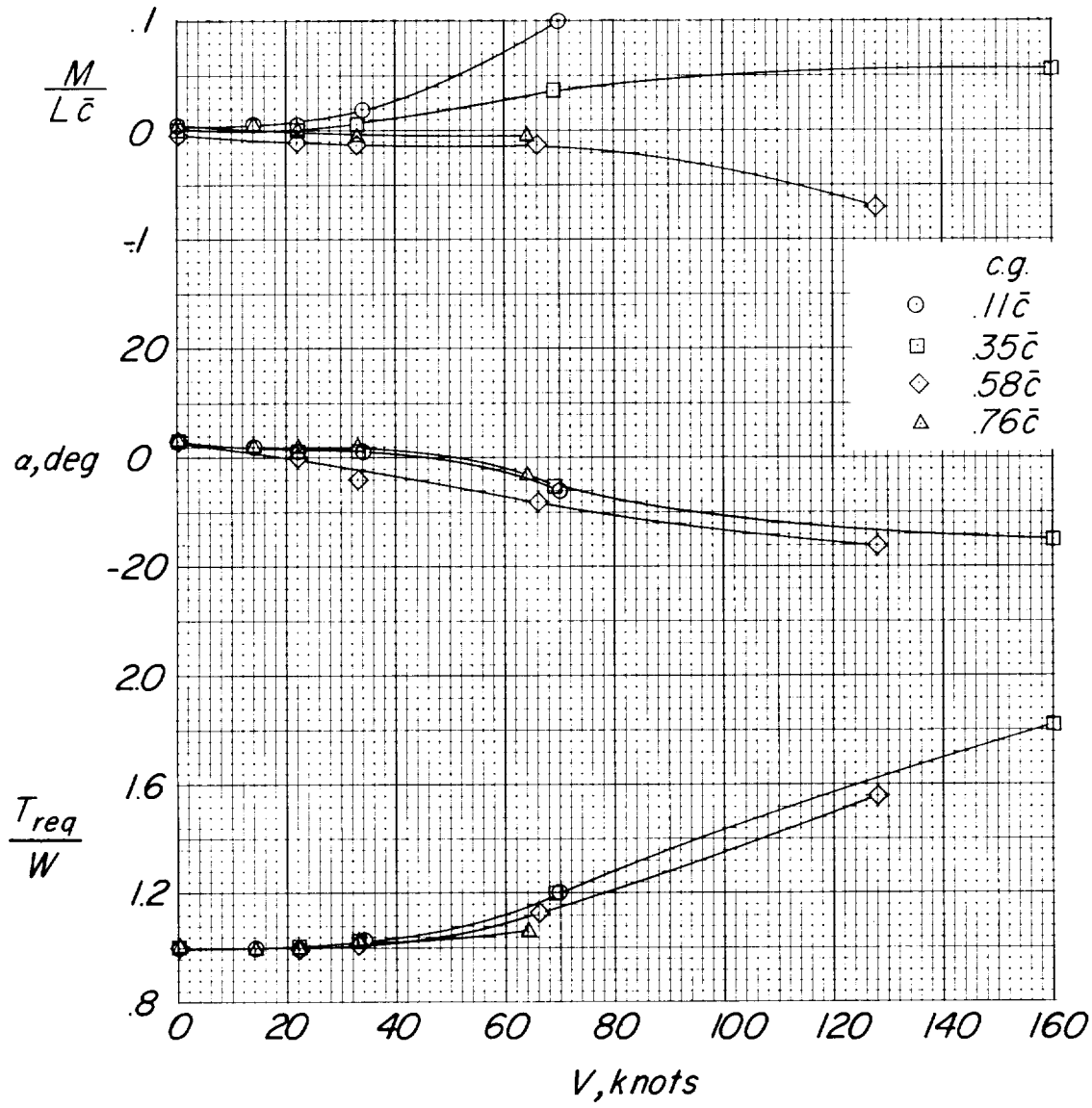

(a) $\theta \approx 90^{\circ}$.

Figure 18.- Effect of chordwise location of center of resultant force on ratio of thrust required to weight, angle of attack, and pitching moment in steady level flight. A = 3.00; W/S = 100 lb/sq ft.

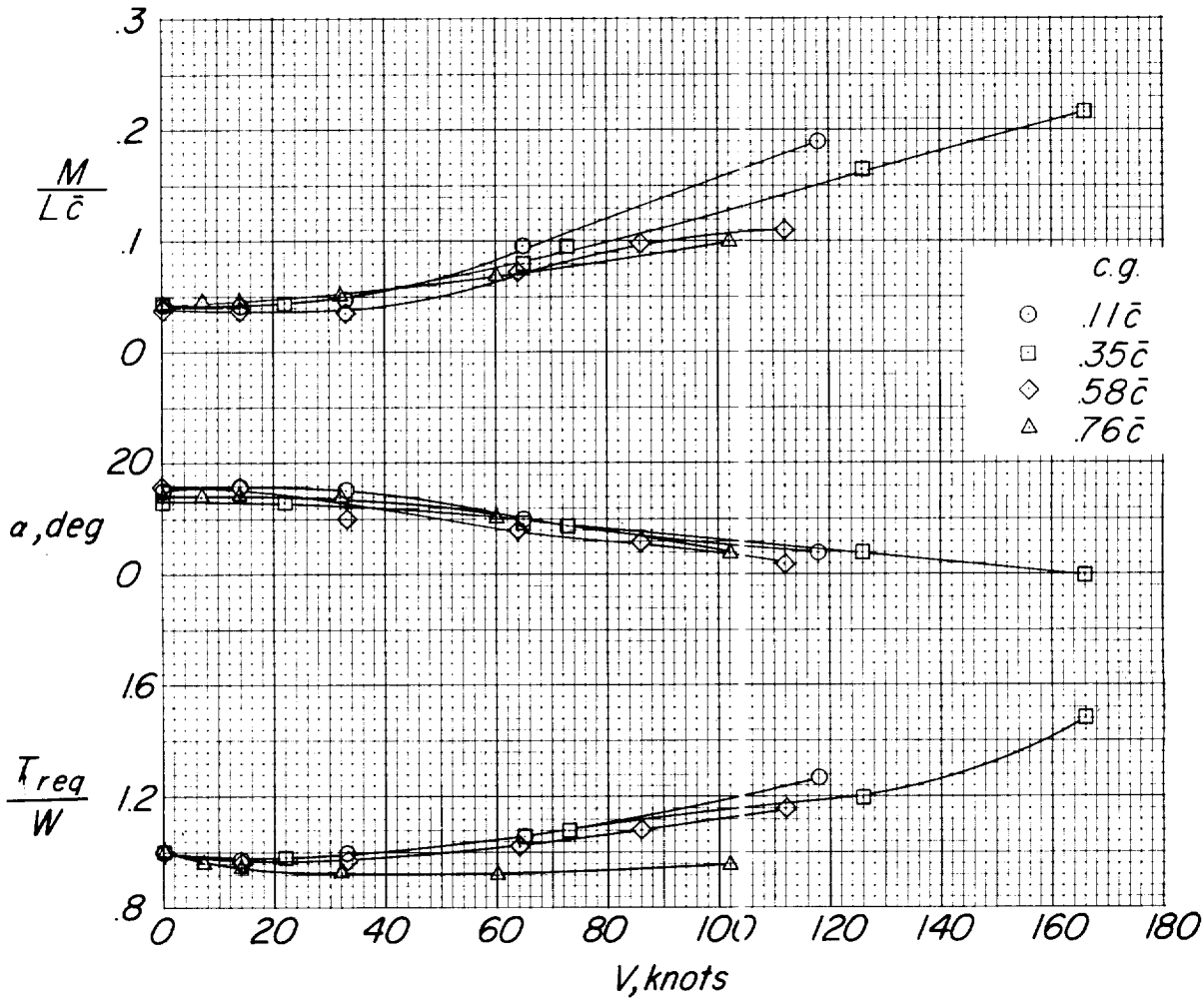

(b) $\theta \approx 75^{\circ}$.

Figure 18.- Concluded.

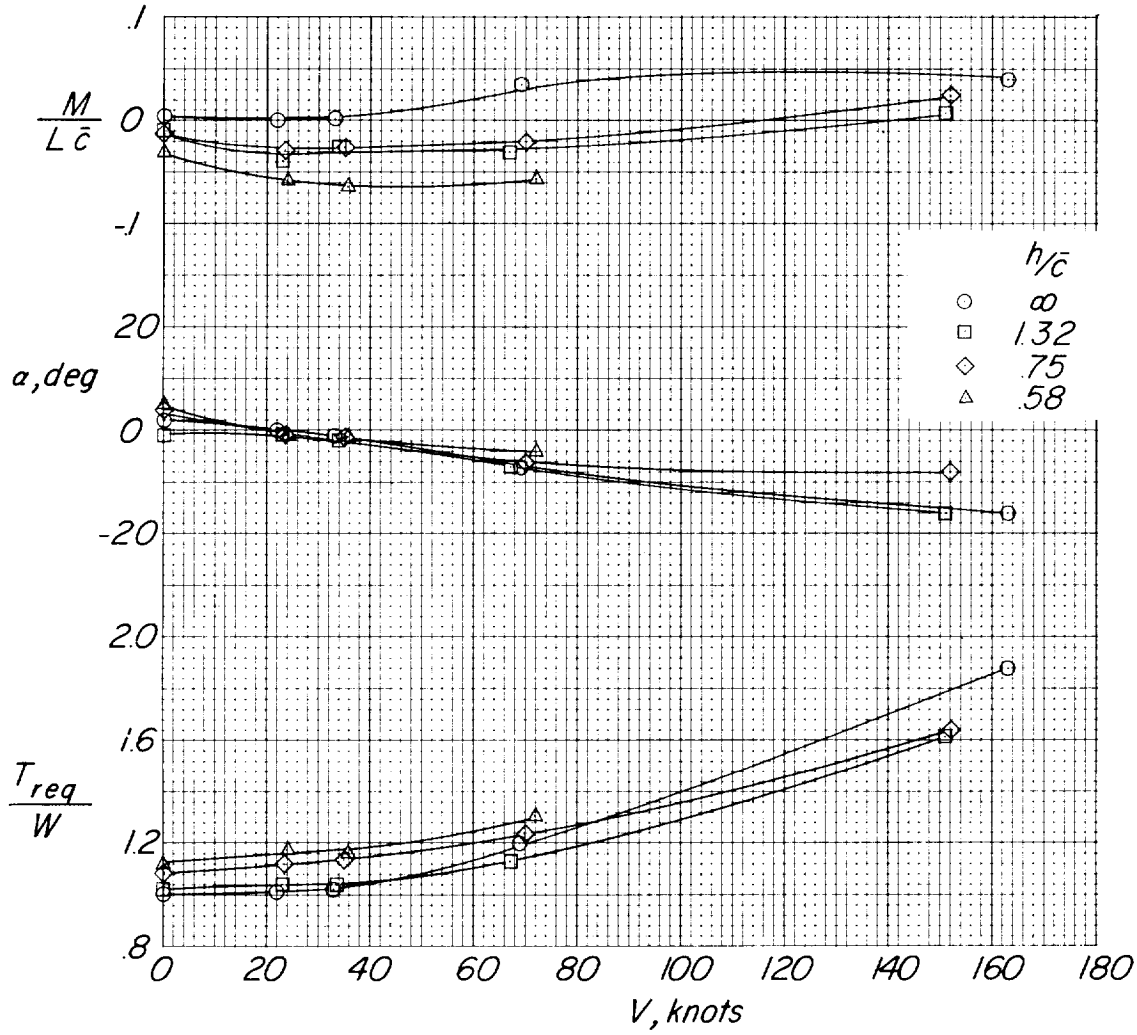

(a) $\theta \approx 90^{\circ}$.

Figure 19.- Effect of height above the ground on ratio of thrust required to weight, angle of attack, and pitching moment in steady level flight. A = 3.00; c.g. at 0.35$\bar{c}$; W/S = 100 lb/sq ft.

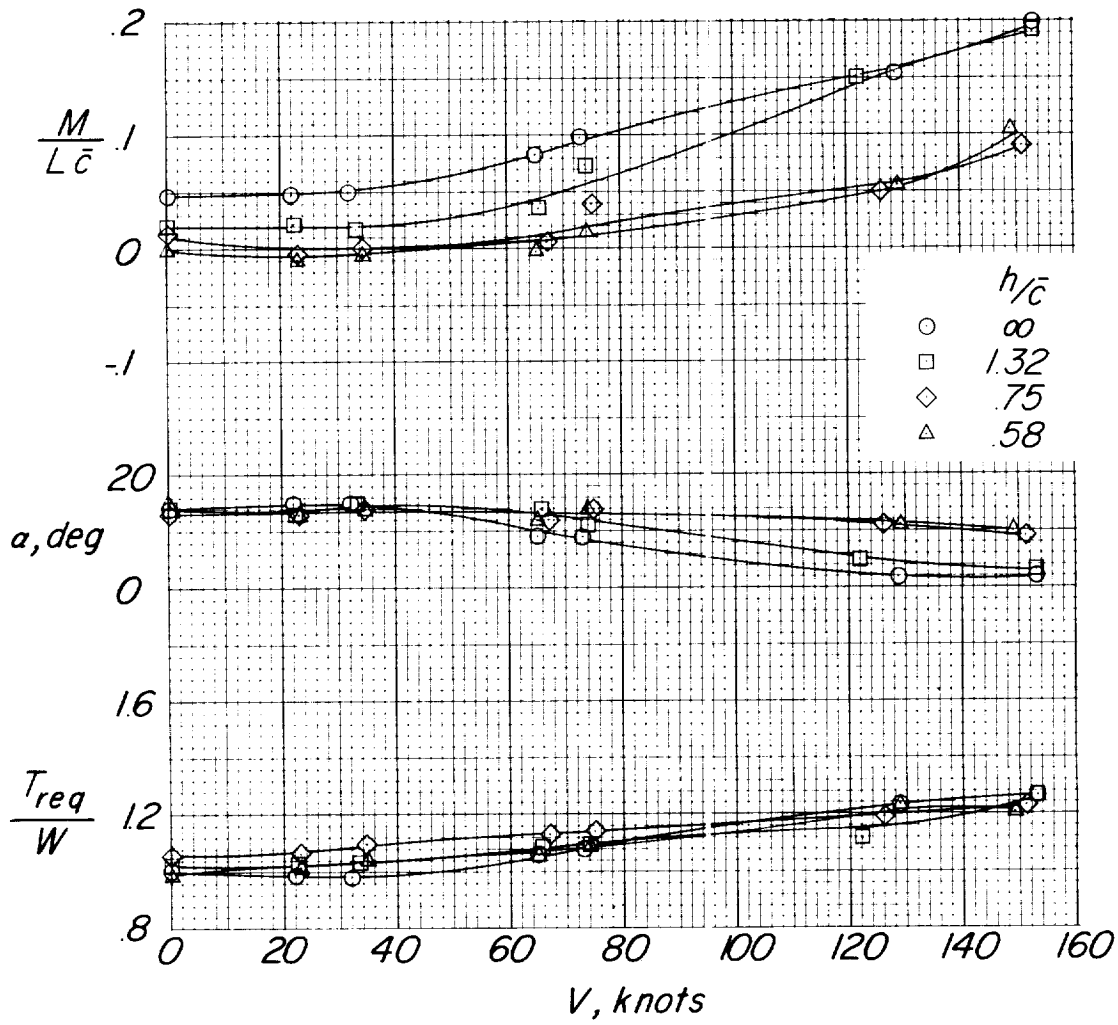

(b) $\theta \approx 75^{\circ}$.

Figure 19.- Concluded.

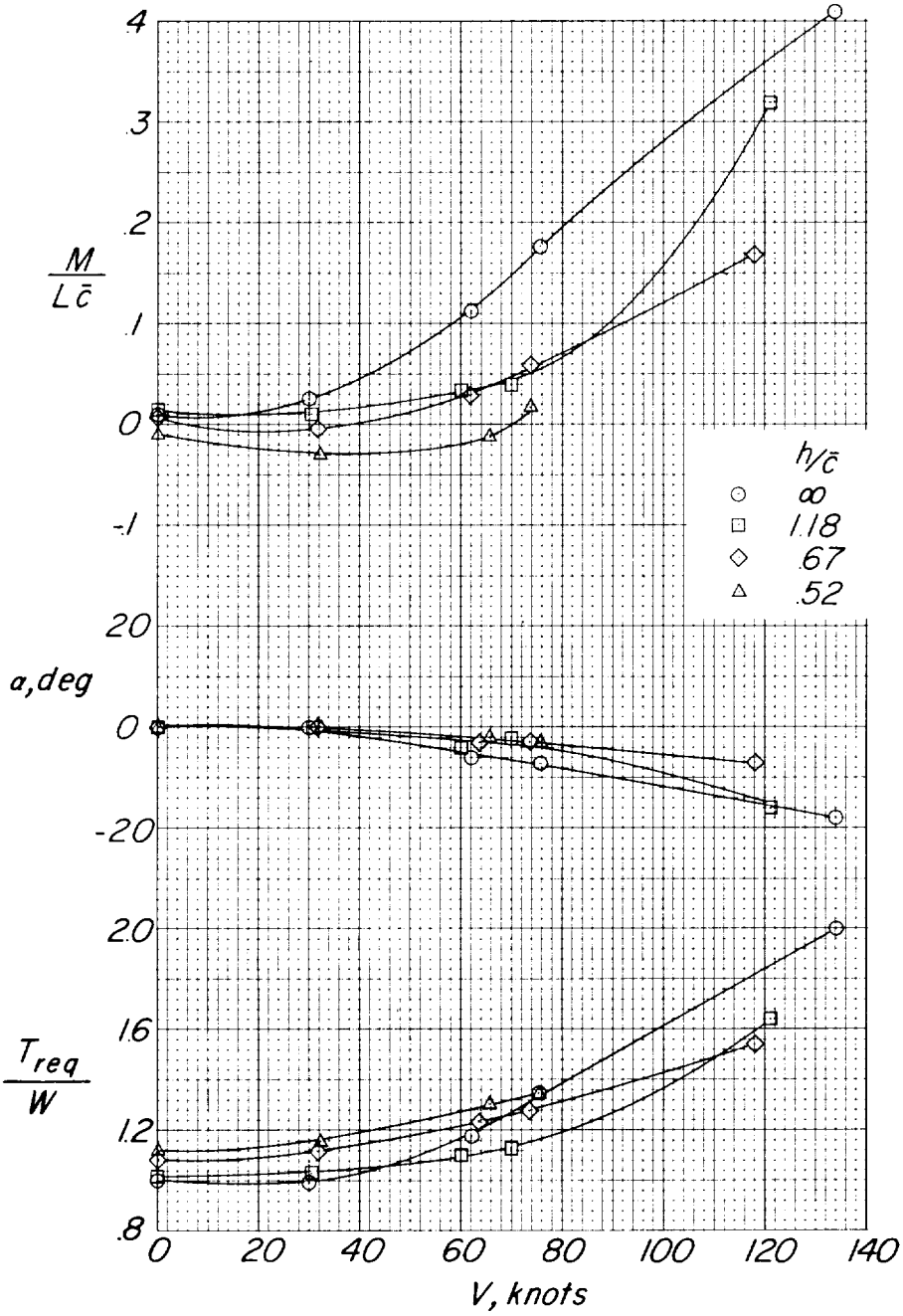

(a) $\theta \approx 90^{\circ}$.

Figure 20.- Effect of height above the ground on ratio of thrust required to weight, angle of attack, and pitching moment in steady level flight. A = 1.55; c.g. at $0.20\bar{c}$; W/S = 100 lb/sq ft.

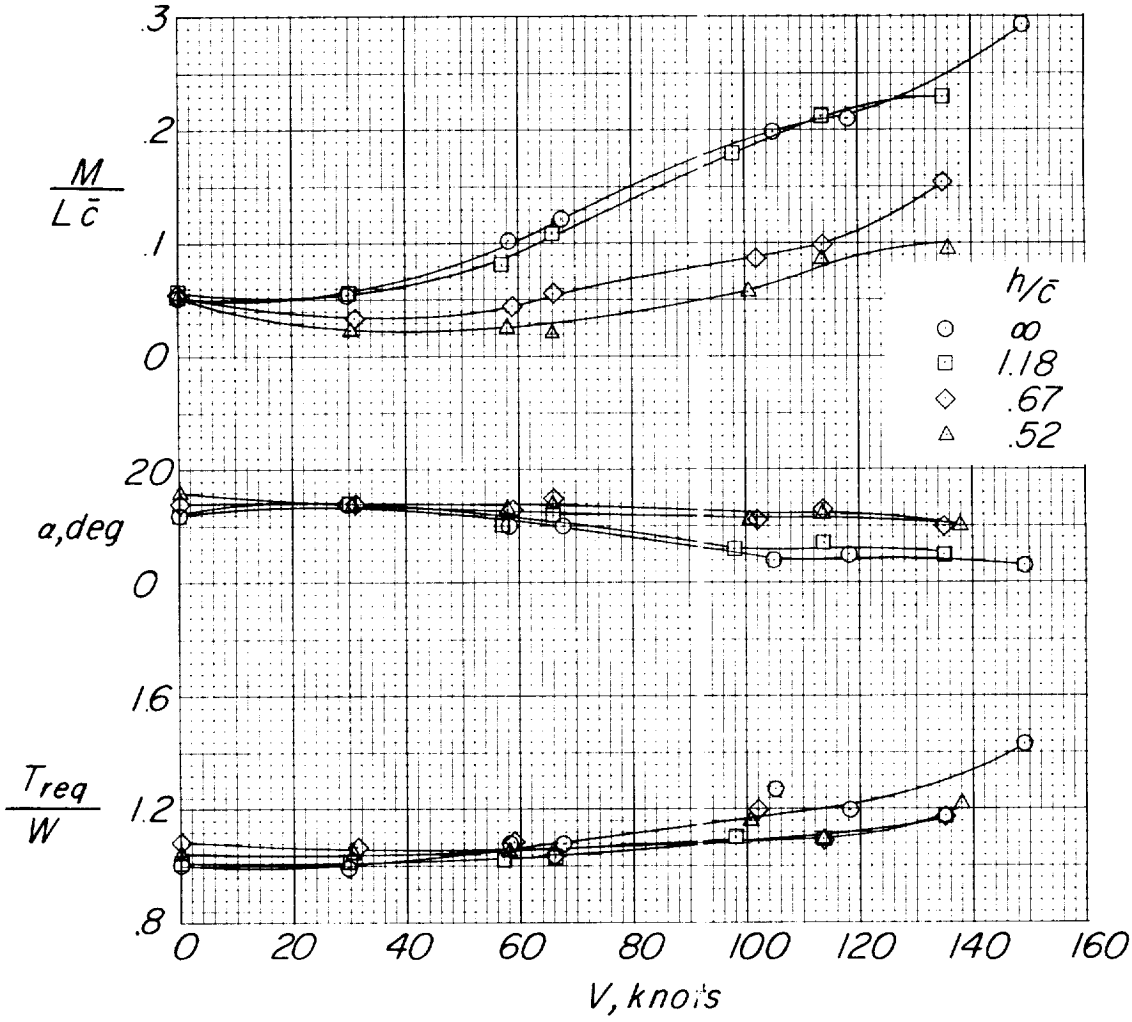

(b) $\theta \approx 75^{\circ}$.

Figure 20.- Concluded.

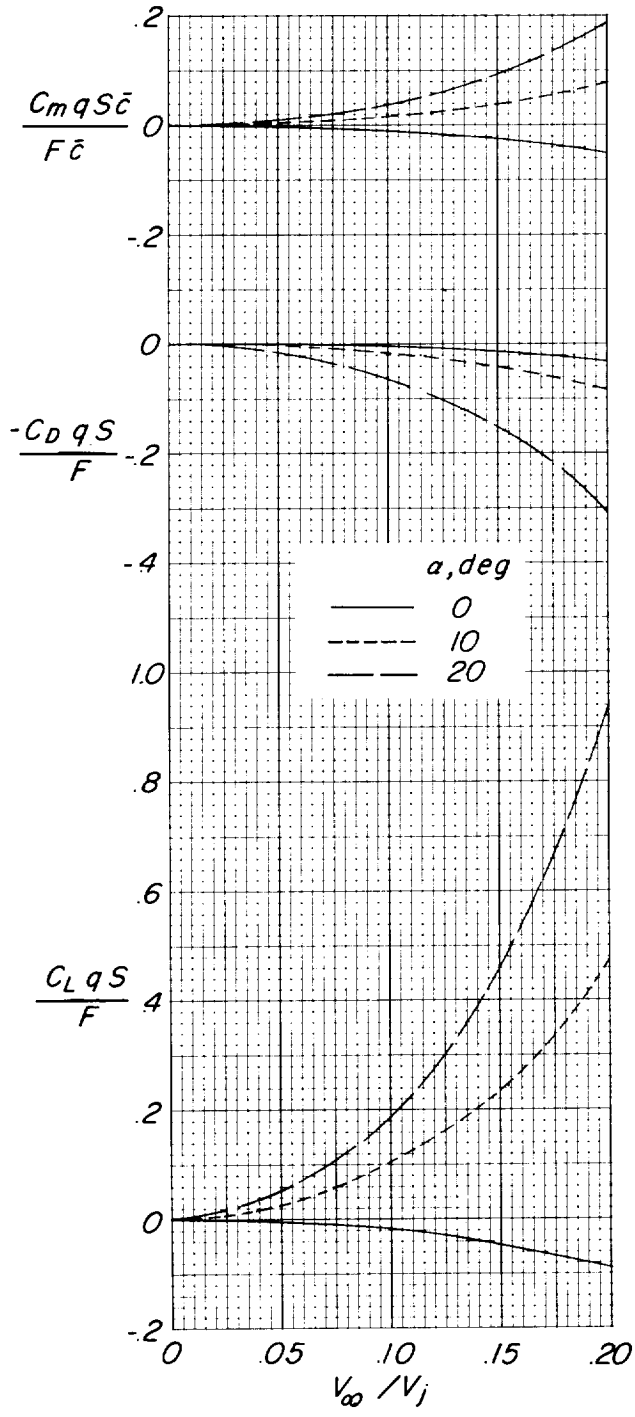

Figure 21.- Aerodynamic characteristics of the A = 3.00 model as calculated from power-off data. c.g. at 0.35$\bar{c}$.

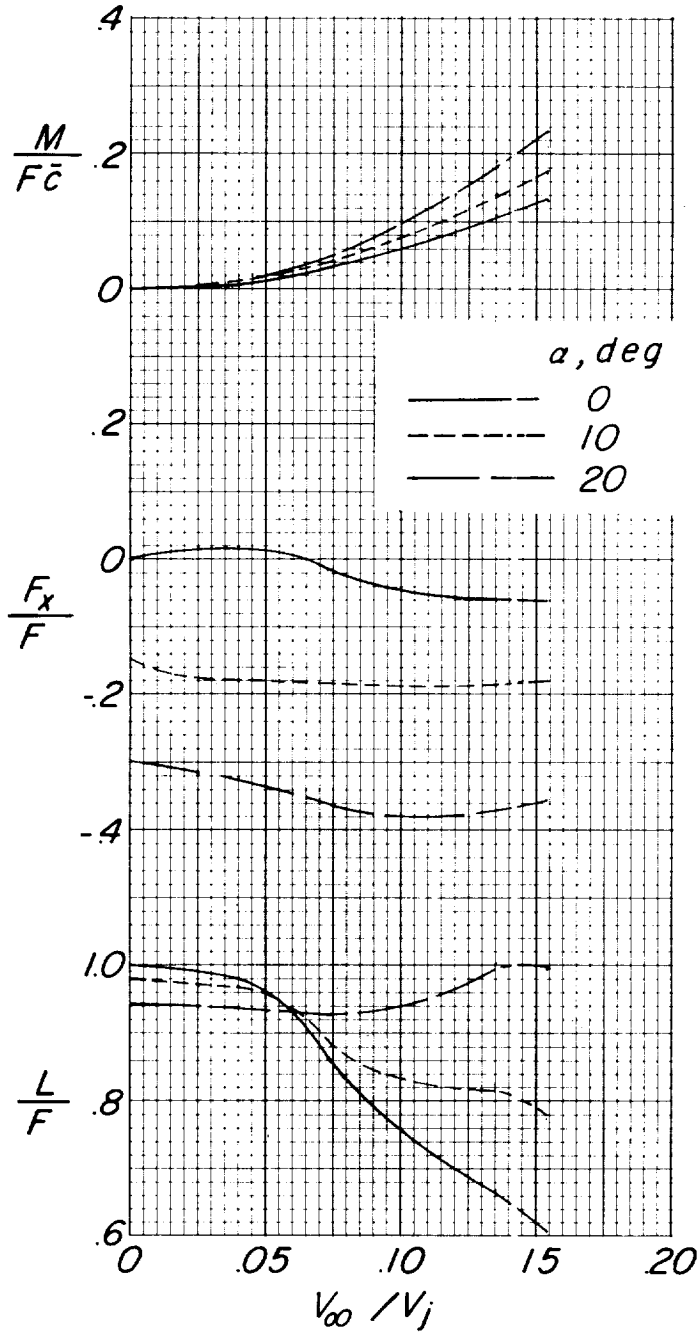

(a) $\theta \approx 90^{\circ}$.

Figure 22.- Effects of angle of attack and forward velocity on the power-on longitudinal characteristics of the A = 3.00 model. c.g. at 0.35c̄.

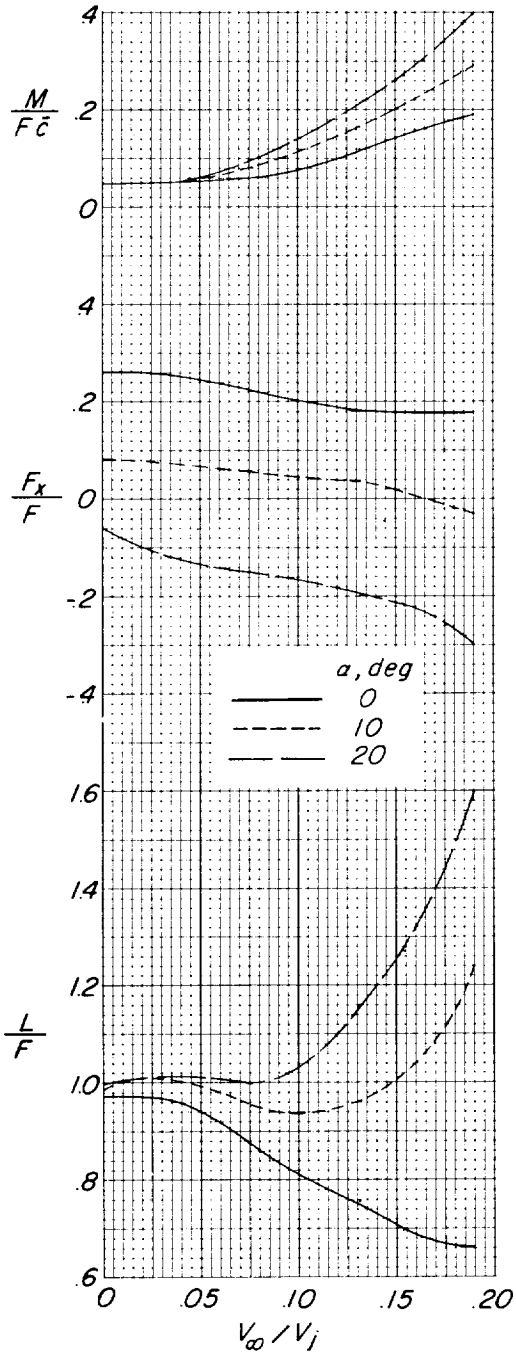

(b) $\theta \approx 75^{\circ}$.

Figure 22.- Continued.

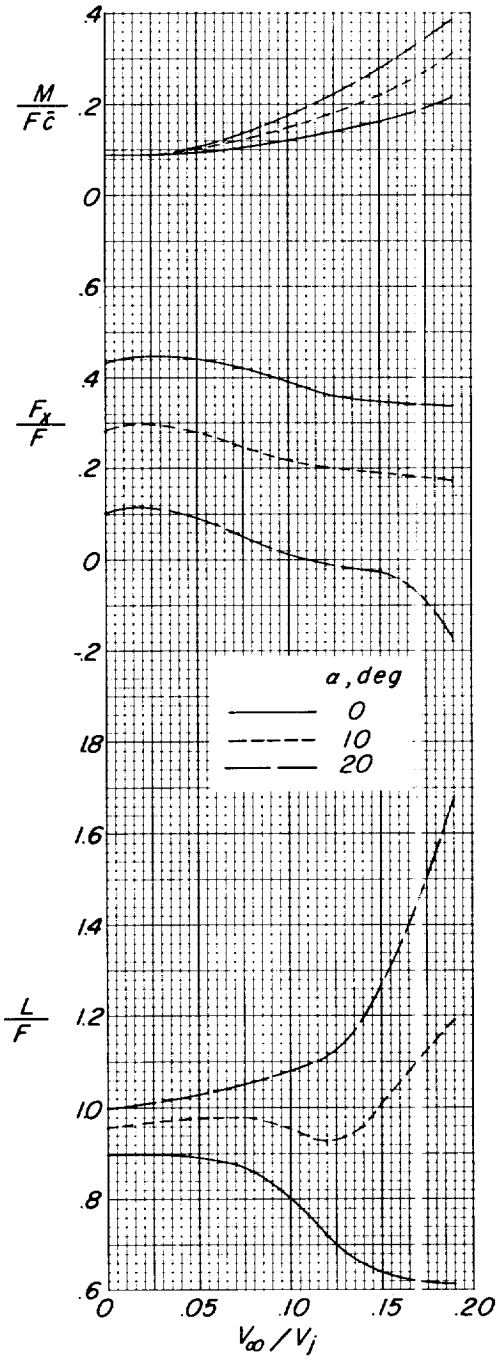

(c) $\theta \approx 63^{\circ}$.

Figure 22.- Continued.

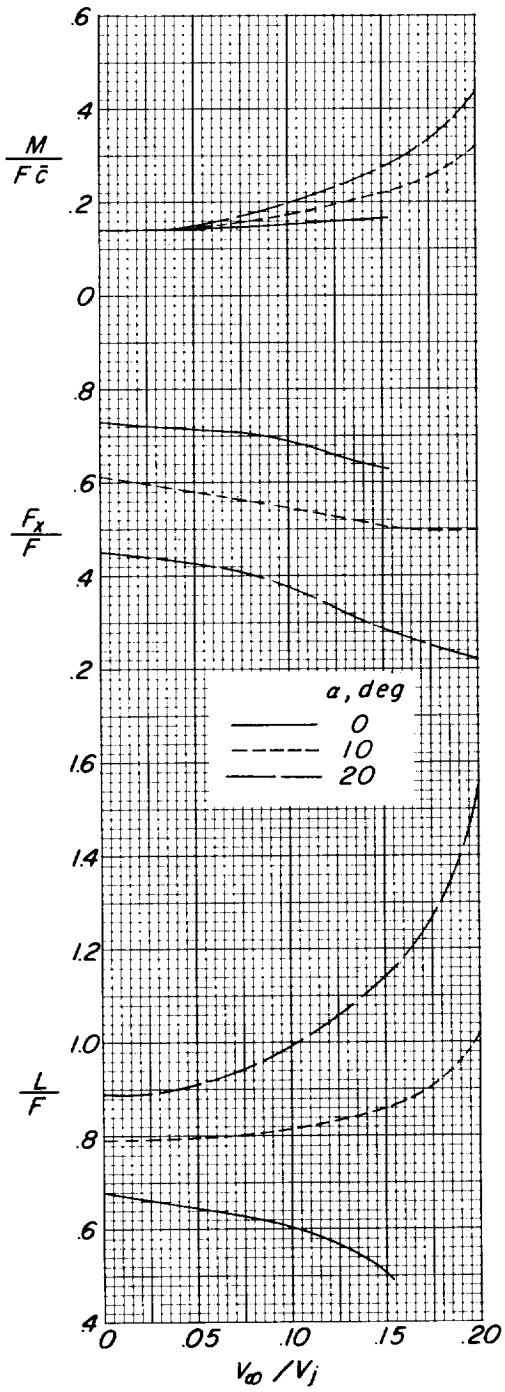

(d) $\theta \approx 42^{\circ}$.

Figure 22.- Continued.

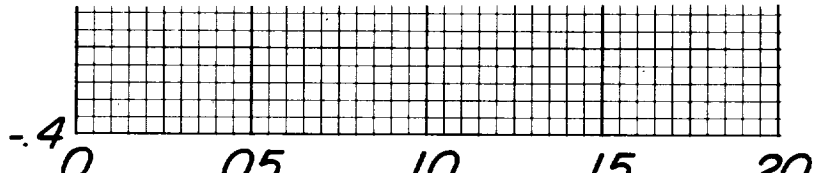

88

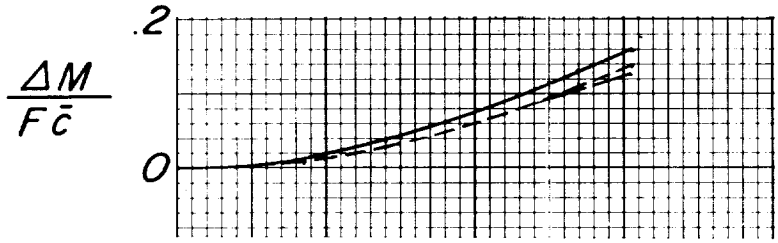

92

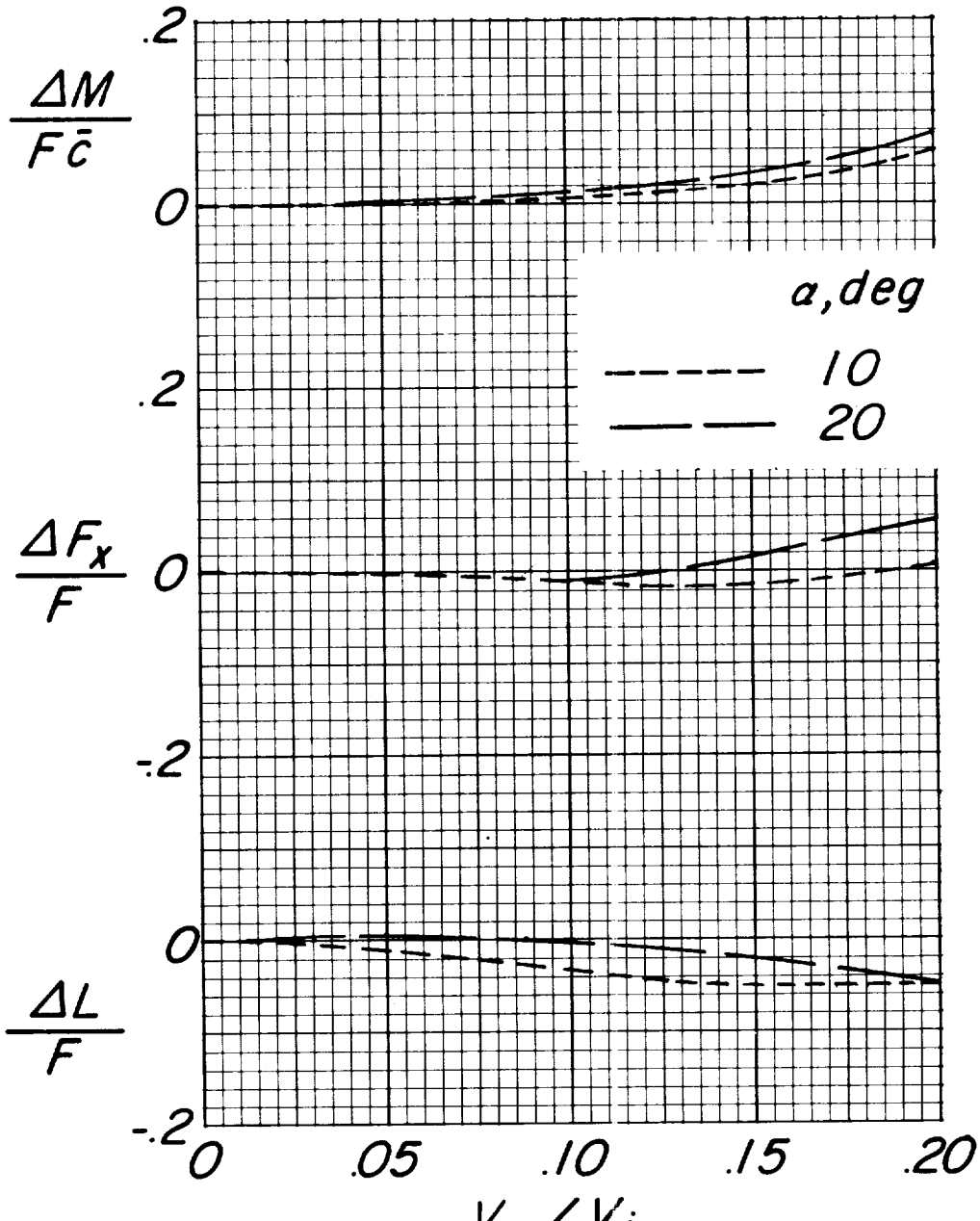

L-1466

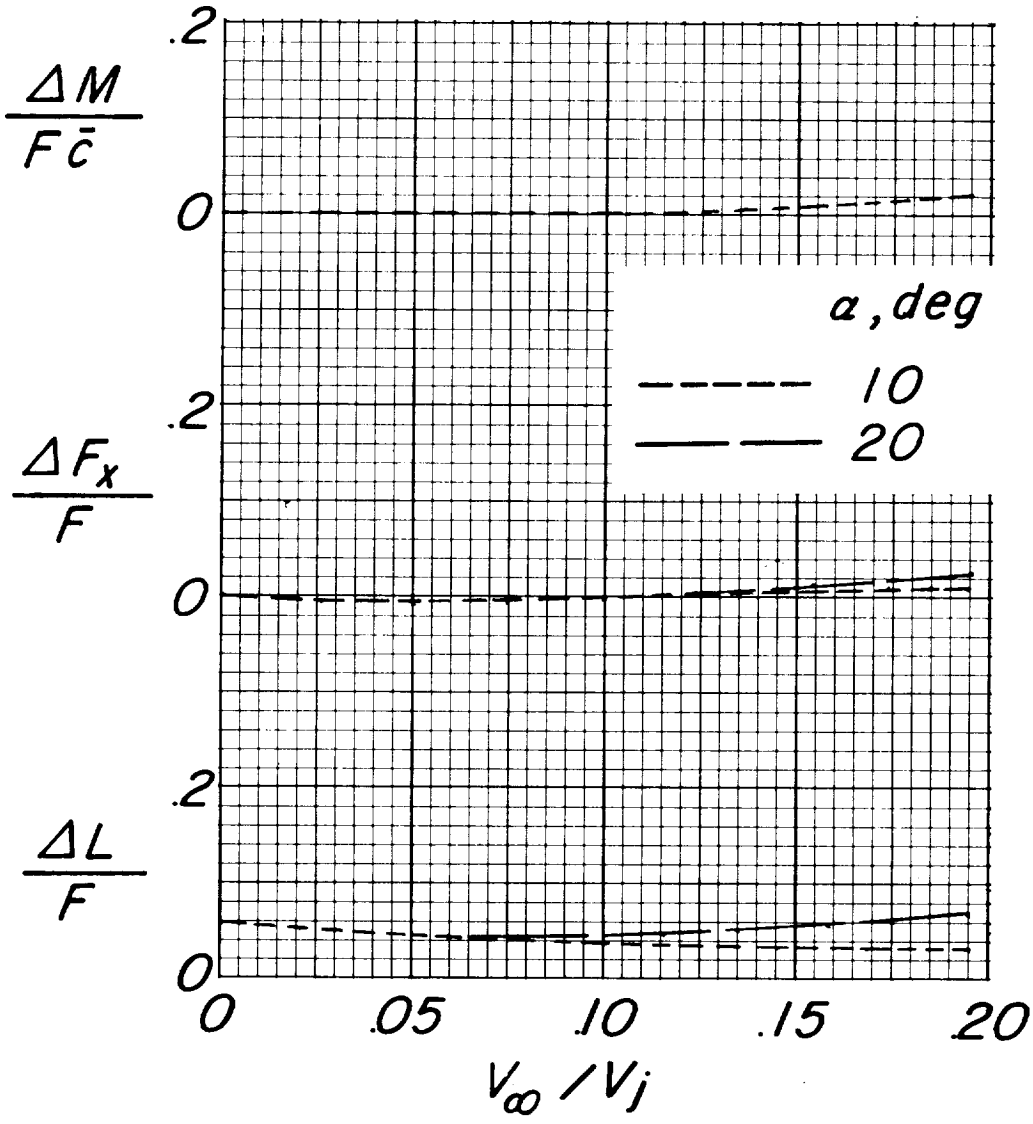

(f) $\theta \approx -5^{\circ}$.

Figure 23.- Concluded.

NASA - Langley Field, Va. L-1466